JAERI - M
88-045

JAPANESE CONTRIBUTIONS TO IAEA INTOR WORKSHOP PHASE TWO A, PART 3 CHAPTERIII : IMPURITY CONTROL

March 1988

Tadanori MIZOGUCHI[*1], Takashi OKAZAKI[*2], Noboru FUJISAWA
Tetsuya ABE , Toshio HIRAYAMA, Shigehisa HITOKI[*3]
Takashi KAWAMURA[*4], Yoshihiko KOIDE, Takashi MIZUUCHI[*5]
Akihiro MOHRI[*4], Hiroo NAKAMURA, Setsuo NIIKURA[*6]
Hiromasa NINOMIYA, Nobuaki NODA[*5], Hiroaki OGAWA
Masahiro SAIDOH, Katsuhiro SHIMIZU, Masayoshi SUGIHARA
Shuichi TAKAMURA[*4], Hiroshi TAKEUCHI, Tomonori TAKIZUKA
Noriaki UEDA[*5], Shin YAMAMOTO, Kozo YAMAZAKI[*4]
and Hidetoshi YOSHIDA

日 本 原 子 力 研 究 所
Japan Atomic Energy Research Institute

JAERI-Mレポートは，日本原子力研究所が不定期に公刊している研究報告書です。
入手の問合わせは，日本原子力研究所技術情報部情報資料課（〒319-11茨城県那珂郡東海村）あて，お申しこしください。なお，このほかに財団法人原子力弘済会資料センター（〒319-11 茨城県那珂郡東海村日本原子力研究所内）で複写による実費頒布をおこなっております。

JAERI-M reports are issued irregularly.
Inquiries about availability of the reports should be addressed to Information Division, Department of Technical Information, Japan Atomic Energy Research Institute, Tokai-mura, Naka-gun, Ibaraki-ken 319-11, Japan.

編集兼発行　日本原子力研究所
印　　刷　㈱原子力資料サービス

Japanese Contributions to IAEA INTOR Workshop Phase Two A, Part 3 Chapter III: Impurity Control

Tadanori MIZOGUCHI[*1], Takashi OKAZAKI[*2], Noboru FUJISAWA
Tetsuya ABE[+], Toshio HIRAYAMA, Shigehisa HITOKI[*3], Takashi KAWAMURA[*4]
Yoshihiko KOIDE, Takashi MIZUUCHI[*5], Akihiro MOHRI[*4], Hiroo NAKAMURA
Setsuo NIIKURA[*6], Hiromasa NINOMIYA, Nobuaki NODA[*5], Hiroaki OGAWA[+]
Masahiro SAIDOH, Katsuhiro SHIMIZU, Masayoshi SUGIHARA
Shuichi TAKAMURA[*4], Hiroshi TAKEUCHI, Tomonori TAKIZUKA[+]
Noriaki UEDA[*6], Shin YAMAMOTO, Kozo YAMAZAKI[*4] and Hidetoshi Yoshida

Department of Large Tokamak Research
Naka Fusion Research Establishment
Japan Atomic Energy Research Institute
Naka-machi, Naka-gun, Ibaraki-ken, Japan

(Received February 2, 1988)

This report corresponds to Chapter III of Japanese contribution report to IAEA INTOR Workshop, Phase Two A, Part 3. The major objectives of Impurity Control group during the Phase IIA Part 3 are (1) an assessment of the physics and engineering data base based on current experiments, (2) an evaluation of innovative ideas which would significantly improve the impurity control systems of INTOR-like design, and (3) design studies using sophisticated computational models to extrapolate at the operating parameters. The current data base from JT-60, JFT-2M, JIPPT-IIU and Heliotron E are reported and assessed for INTOR

+ Department of Thermonuclear Fusion Research
*1 On leave from Hitachi, Ltd.
*2 Energy Research Laboratory, Hitachi, Ltd.
*3 Mitsubishi electric Corporation
*4 Nagoya University
*5 Kyoto University
*6 Mitsubishi Atomic Power Industries, Inc.

impurity control system. Five innovations are evaluated. Newly developed two-dimensional fluid models are reported. The preliminary design studies found a reasonable divertor operation for the impurity control system of INTOR-like design.

Keywords: INTOR, Phase Two A Part 3, IAEA Impurity Control, Poloidal Divertor

IAEA INTORワークショップフェーズⅡAパート3報告書
第Ⅲ章 不純物制御

日本原子力研究所那珂研究所臨界プラズマ研究部
溝口忠憲[*1]・岡崎隆司[*2]・藤沢 登・阿部哲也[+]・平山俊雄
一木繁久[*3]・川村 孝[*4]・小出芳彦・水内 亨[*5]・毛利明博[*4]
中村博雄・新倉節夫[*6]・二宮博正・野田信明[*5]・小川宏明[+]
西堂雅博[+]・清水勝宏・杉原正芳・高村秀一[*4]・竹内 浩
滝塚知典[+]・上田憲照[*6]・山本 新・山崎耕造[*4]・吉田英俊

（1988年2月2日受理）

本報告書はＩＡＥＡ主催INTORワークショップ，フェーズⅡA，パート3における日本報告書の第3章に相当するものである。フェーズⅡA，パート3における不純物制御グループの主な作業目的は，(1)現状の実験に基づく物理及び工学データベースの評価，(2) INTOR設計における不純物制御システムを改善すると思われる先進的アイデアの検討及びその評価，(3)洗練された数値解析コードを用いて適切な運転パラメータを見い出す為の設計研究である。不純物制御の観点からJT－60，JFT－2M，JIPDT－ⅡU，Heliotron Eの最近のデータベースを紹介し検討を行った。新しく開発した2次元流体モデルを紹介し，そのコードの有効性ならびにＦＥＲ設計における不純物制御の成立性子を予備的検討結果ながら示した。

那珂研究所：〒311－01 茨城県那珂郡那珂町大字向山801－1
＋ 核融合研究部
＊1 外来研究員 日立（株）
＊2 日立・エネルギー研究所
＊3 三菱電機（株）
＊4 名古屋大学
＊5 京都大学
＊6 三菱原子力工業（株）

Contents

目　　次

1. Introduction and summary

The impurity control studies during the Phase IIA Part 3 [5] have mainly carried out (1) an assessment of the experimental and engineering data base for impurity control system based on current experiments, (2) an evaluation of five innovations brought up at the specialist meeting on Jan. 1986 [9], and (3) design studies using sophisticated computational models to extrapolate to the operating parameters and performance of INTOR-like designs. The Impurity Control Physics group have preliminary concluded and recommended the followings for a potential update of the INTOR design:

1) retain the poloidal divertor (single or double null) as the reference impurity control system.
2) retain a pumping speed in the 200,000 ℓ/sec range,
3) consider the impact of operation with Z_{eff} in the range of 2,
4) consider the use of first wall armor in the physics phase of INTOR operation for protection of the first wall against disruptions,
5) retain the consideration of high Z materials with high sputtering threshold energies for divertor plate materials because these still appear to be advantageous for reducing sputtering with high recycling, low temperature divertor operation, and
6) encourage research and development (primarily physics experiments and modelling studies) to resolve the present uncertainties associated with impurity control systems based on poloidal divertors.

Present experiments indicate that low Z_{eff} operation in the 1.2-1.5 range will be very difficult especially allowing for $n_{He}/n_e \sim 5\%$. A more realistic value would be in the range around 2. This change could reduce the fusion yield up to 30% compared to Z_{eff}=1.5, so it will have a considerable impact on the rest of the design. The pumped limiter concept would remain as a back-up option of the impurity and particle control system for INTOR if this concept could be demonstrated successfully in experiments.

Five innovations were proposed for the INTOR impurity control system [9], 1) impurity flow reversal, 2) radiatively cooled edge, 3) ergodic limiter, 4) helieum burial, and 5) liquid metal divertor target. It is recommended that further studies for helium burial and liquid

metal divertor plates be pursued because of the possibility of near-term applications of those materials. Further studies for other three are encouraged, but required to demonstrate their advantages sufficiently clear before justifing their inclusion in the INTOR design.

As Japanese contributions, recent experimental results from JT-60, JFT-2M, JIPPT-IIU and Heliotron-E are presented during INTOR workshop. Experimental results in JT-60 show that a poloidal divertor configuration is very effective for impurity and particle control in a large tokamak. The diffusion coefficient of D = (0.6-1.0) m^2/s observed at JT-60 core plasma is good agreement with those observed at JET and TFTR. JFT-2M tokamak found H-like transitions not only in the open divertor configuration but also in D-shaped limiter bounded plasmas. They also found that H-transition does not depend on heating methods. H-mode discharge, however, are often terminated by the impurity radiation losses. These observations suggest that the compatibility of improved particle confinement and impurity removal from core plasma may be a problem with H-mode discharges.

For design studies, refinement of the model being implemented is the most important task. It has been newly developed two types of two-dimensional fluid code: the one solved by the finite element method and the other solved by the Partice In Cell (PIC) method for numerical treatments. Validation of the latter code is reported by simulating the boundary plasma conditions in Doublet III divertor experiments. The simulation is in satisfactory agreement with the experimental data from DIII. With this code, the preliminary calculation for the INTOR-like divertor plasma revealed that divertor operation of high density and low temperature divertor plasma is possible at a real geometry of open divertor configuration. The electrostatic particle model for divertor plasma is also developed. Several suggestions were made to the fluid model from the particle simulation studies.

2. Assessment of experimental data base for impurity studies

2.1 JT-60

The major impurities in JT-60 were oxygen, carbon and titanium which were the coating materials of the first wall. A slight amount of nickel, iron and chronium which are constituents of Inconel vessel and limiter substrates are observed in divertor discharges. Figure 1 shows the typical VUV spectrum in the hydrogen divertor discharge [11]. The molibdenum which is TiC coated limiter substrates are also identified in limiter discharges. In ohmically heated discharges the amount of titanium was around 1×10^{-3}% and 8×10^{-3}% at $\bar{n}_e=2\times10^{19}$ m^{-3} in hydrogen and helium discharges, respectively. For NB heated hydrogen plasmas the titanium concentration is about two time higher than that in ohmically heated plasmas. And the quantities of nickel, iron and chronium were below 1/10-1/100 of that of titanium.

The ratio of the light impurity density to proton density is 1.2% or 2.4% if the species are assumed to be totally oxygen or carbon, respectively. The averaged Z_{eff} falls smoothly with the increase of the electron density and minimum Z_{eff} is about 1.5 at $\bar{n}_e \simeq 5\times10^{19}$ m^{-3} as shown in Fig. 2 [12]. Z_{eff} of 1.5 is also obtained from the visible bremsstrahlung measurement assuming the simple spitzer resistivity. These observations were suggested that the light ions were the dominant impurities in JT-60 [11]. The value of Z_{eff} for NB heated plasmas were slightly larger than that of ohmically heated plasmas.

The anomarous diffusion coefficient of impurity transport were estimated to $D_A \simeq 1$ m^2/sec in ohmically heated plasma and $D_A \simeq 0.8$ m^2/sec and 0.6 m^2/sec in discharges with co- and counter- NB injection, respectively. Fig. 3 shows time evolutions of soft x-ray diode array signals and TiXXI line intensity of a NB heated plasma with co- and counter-injection [11]. Fig. 4 shows similar time evolution of TiXXI line intensity of a ohmically heated plasma [13]. The TiXXI line intensity simulated by 1-D impurity transport code are also shown in both figures. There was no significant difference in the impurity transport among those cases, and typically $D_A \simeq 0.6$-1.0 m/sec. In addition, it was suggested that the impurity transport was not affected by a toroidal rotation of $\sim4\times10^4$ m/sec and $\sim8\times10^4$ m/sec for 8.4 MW co- and 7.7 MW counter injection, respectively. In JET and TFTR, the diffusion coefficient of $D_A \simeq 1$ m^2/sec is observed for impurity

transport. This good agreement for the diffusion coefficient between three large tokamaks offers a reasonable data base on impurity transport for of INTOR-like design.

Divertor experiments have been successfully performed in JT-60. In ohmically heated plasma with divertor operation, radiation loss in main plasma saturates with the increase of plasma current as shown in Fig. 5(b) and its ratio to the input power is about 20% [14]. Fig. 6 shows global energy balance including the heat depositions in the divertor plates. About 70% of input power is exhausted into the divertor chamber and a half of it is dissipated as the radiation loss. Similar global energy balance of the NB-heated plasma is shown in Fig. 7. Fig. 8 also demonstrates a dramatic effect of the diverotr in reducing the radiation loss in the NB-heated and ohmically heated plasmas [12]. The radiation loss from the main plasma is typically 5-10% of the absorbed power in divertor discharges. The diverotr is particularly effective in reducing the radiation loss of the NB-heated plasmas and keeps the ratio of the radiation power and the absorved power below that of the ohmically heated plasmas.

Disruption characteristics of JT-60, as shown in Table 1[10], are divided into three types by their causes, namely, 1) disruptions triggered by enhanced MHD activities induced at q_{eff} =2 and 3, 2) disruptions due to a critical density limit, and 3) disruptions caused by impurity introduction. NB heated discharges have suffered only from the type of disruptions caused by impurity introduction. A density limit in NB heated discharge has not yet been observed in JT-60 divertor operation. Most of disruptions in NB-heated plasmas caused by impurity introduction from divertor plates. A time behaviour seems to be characterized by a sequence of metal impurity introduction, growth of MHD activities, thermal collapses, and disruptions. Impurities from divertor plates is probably introduced by evaporation of target materials due to a localized high heat flux. The control of this type of disruptions has been demonstrated by swinging the separatrix on the plates and by reducing time averaged heat flux on them. When a heat spot is moved gradually by changing the separatrix in a divertor region during NB heating, evaporation of target material is drastically suppressed and impurity radiation can be reduced. As a result, disruptions are successfully avoided. Plasmas heated by ICRF and LH

(for current drive and electron heating) have also suffered from disruptions mainly caused by impurities. ICRF heated plasmas are quite susceptible to disruptions, even after an adequate conditioning. However, the addition of NB heating completely suppresses the occurrence of disruptions. Probably the additional NB heating power may compensate for the radiation loss induced by impurities.

The maximum current decay rate tends to increase with increase of a plasma current. All data measured so far are below the design value of 380 MA/s as shown in Fig. 9. The decay rate for limiter plasmas tends to be larger than that for divertor plasmas.

Based on soft X-ray and PIN diode signals, the decay time for the central PIN diode signals is around 10-100 ms and a characteristic time which is the fastest decay rate at the start of decay is around 1-10 ms as shown in Fig. 10. They are summarized in Table 2. The energy decay rate is expected to be in a same order as the decay rate of a PIN diode signal through a central plasma region. In TFTR and JET, the energy decay rate of ~0.1 ms, one order faster than that in JT-60, is observed [6,7]. The difference between JT-60 and the other two is not clear. Further studies are required since the faster energy decay rate give a significant impact on the first wall and divertor designs of INTOR-like devices.

2.2 JFT-2M

Recent additional heating experiments in JFT-2M have achieved the H-mode in the open divertor configuration with NBI heating. Furthermore, H-like transitions were observed not only in ICRF heated open divertor discharges but also in D-shaped limiter bounded plasma [15]. Improved energy confinement in the limiter plasma reveals that a diverted magnetic configuration is not the necessary condition for an H-transition. As the H-transition, temperature and density pedestals are suddenly formed before the total stored energy increases. This fact suggests that the energy and particle transport near the plasma edge are evidently improved at the H-transition. According to these observations it can say that the transport effects in the edge region of the plasma will determine the energy confinement property of the tokamak plasma. In JFT-2M experiments, H-mode discharges are often terminated by the radiation losses as discussed in Appendix 2.2.1. The emission of FeX, lower ionization state, is rather depressed like the H_α signal but the

emission of FeXV and FeXVIII increases exponentially during H-mode discharge as shown in Fig. 11. The large increase of the emission from higher ionized ion are due to the large increase of the higher ionized impurity ion densities. Impurity injection (Ar) experiments suggest that the increase in the density of these ions is due not to an increase in the impurity influx but to improved particle confinement during the H-mode phase.

2.3 JIPPT-II U

The preliminary ergodic magnetic limiter experiments with the m=3/n=1 helical field perturbation are reported [16]. They observed that application of the local helical field perturbation result in the ergodization of the edge confinement region and favorable effect of suppressing impurity influx as shown in Fig. 12. The existance of the threshold of the ergodization was suggested from the dependence of the ergodization on the pulse hight and width of herical perturbations.

It is also shown the effectiveness of weak external helical field perturbation for stability, especiallyf for disruption control. Fig. 13 shows time evolution of electron temperature profile with and without the application of hilical field pulse. It is demonstrated that the m=3/n=2 dominant helical field perturbation induces one or two mini-disruptions and that the 2/1 magnetic island is ergodized by these mini-disruptions. As a results, the temperature flatterning process is interrupted and major disruption is avoided.

2.4 Heliotron E

Particle control with conventionals, pumped limiter is demonstrated [17]. About 2-4% of the particles lost from the plasma are removed if the pump limiter is located inside the last closed magnetic flux surface. Little or no particle control is observed if the pump limiter is placed outside the last closed surface.

3. Innovations

As Japanese contributions [9], three innovations were proposed, (1) ergodic magnetic limiter, (2) radiatively cooled edge, and (3) liquid metal divertor plates.

3.1 Ergodic magnetic limiter

Ergodic magnetic limiter (EML) has been considered one of possible impurity control systems in tokamaks for long time. Some concepts of EML had already been proposed in Phase One INTOR [2]. Recently, experimental efforts have been carried out at JIPPT-IIU and CSTN-II at the Nagoya University as shown in [17], [18] and Appendix 3.1.1-3.1.3. In CSTN-II experiments, they show that a set of local helical coils can produce the helical field of mode index around m/n, typically 10/1, specified by the structure of helical coils and the direction of herical coil current. A drastic change in the plasma potential was observed with the application of helical field perturbation. The increse in the plasma potential was accompanied by the decrease in the local electron density. That is, when the helical field applied the edge plasma contacts with the wall through the magnetic field lines in relatively short connection length. A rapid loss of electrons to the wall should be reduced to generate a positive plasma potential with respect to the wall because of the ambipolarity.

The wall loading was found to be extremely nonuniform along the poloidal direction. A rotating helical field was succeeded in making a time averaged loading to the wall uniform along the poloidal and toroidal direction.

In JIPPT-IIU as already discribed, the ergodization of the edge confinement region with the local helical field perturbation brought a favorable effect of suppressing impurity influx and decreasing edge plasma temperature. Theoretical calculations predict that the radial diffusion in the effectively ergodized magnetic field seems to be comparable with an anomalous diffusion coefficient. Further studies are encouraged at CNTS-II and JIPPT-IIU (also TEXT, TEXTOR and TORE-SUPRA).

3.2 Radiatively cooled edge

The reactor potential of a radiatively cooled edge had been considered during INTOR Phase IIA part 1 workshop [3]. However the subject was raised again at the innovation specialist meeting [9]. An interesting operation region called 'detached plasma' in which most of input power was radiated at a narrow edge plasma boundary was found in TFTR [7]. Various model calculations showed that the thickness of the radiating layer was sensitive to assumptions made regarding cross field transport. Also, the radiative loss powers strongly depend on materials of limiter and first wall which are primary impurity sources. Using INTOR-like parameters and assuming carbon graphite as limiter and first wall materials, the possibility of the self-limited impurity production with radiatively cooled edge plasma are analysed intensively as shown in [19]. Cross field transport is, for example assumed to be anomarous, $\chi_e \simeq 2\times10^{19}/n_e$ cm^2/s, D^A=0.4 for plasma and $D_K^A = -0.4\times(2r/r_p^2)$ for impurities. It is assumed that $\chi_i = 5\times\chi_i^{NC}$, neo-classical. In scrape-off layer, it is assumed that $\chi_e = \chi_i = D^A = D_A^K = D_B$, Bohn diffusion. These assumptions are based on recent experimental results in JT-60, JET and TFTR. The 70% of input power (or magic alpha power) are radiated at boundary region and 30% of that goes to limiter and first wall directely as shown in Fig. 14. The radiation losses due to carbon impurity are rather small and the radiative layer are somehow restricted to the narrow region of the limiter shadow as shown in Fig. 15. As a results edge plasma temperature at a limiter head is still about 80-100 eV at which erosion of the limiter due to physical sputtering is very serious. Nevertheless, self-limited impurity production can be achieved with the carbon concentration of 1.2% and the averaged Z_{eff} of 1.5. For the reactor application, the thickness of the radiating layer must be taken into account by an increase in the size of the confinement vessel Besides, the impact of a radiating edge layer upon improved confinement issues should be examined.

3.3 Others

The concept of liquid metal divertor was proposed at a Specialists Meeting on Tokamak Concept Innovations [9]. However, further investigations were not intended. Several innovative ideas associated with materials are also proposed at the meeting from the other delegations. Some comments for them are shown in Appendix 3.3.1-3.3.3.

3.4 Conclusion of innovative concepts

As the assessment of innovative concepts for the impurity control at the INTOR workshop[5], it is recommended that the concepts of self-pumping by mean of helium burial and liquid metal divertor plates should be actively pursued. It is planed the self-pumping experiments at TEXTOR[7]. Some preliminary experiments of liquid divertor have been performed at T3-M[8], and found that many of the percieved difficulties were not as severe as first thought. However, the schemes will require extensive demonstrations and further tests on experiments before it can be adopted for INTOR or INTOR-like devices.

The other three innovations, flow reversl, radiative edge, and ergodic limiters, are somewhat less certain. Flow reversal would require the use of neutral beams which are not part of the present design and would increase the total power load. They would be a natural feature of current drive with neutral beams, however. The use of a radiative edge would require a fairly large edge radiating layer. Detached plasma experiments on TFTR and DITE indicate that such radiating layers can exist, but attempts to maintain them with high heating powers have not been successful. The concept is not sufficiently well developed to warrant inclusion in the INTOR design at this time. The case of the ergodic limiter is similar. While preliminary experiments on TEXT have demonstrated that an ergodic layer can be formed, it appears to offer no clear advantage to a poloidal divertor. Continued reserch in each of these three areas is encouraged, but they are not yet sufficiently well developed nor are their advantages sufficiently clear to warrant their inclusion in the INTOR design at this time.

4. Design studies

4.1 Benchmark calculation of neutral code

At the INTOR Experts Meeting on Impurity Control Modelling (IAEA, Vienna, 16-18 September 1985), it was proposed benchmark calculation of neutral transport code treated by Monte-Carlo method. A highly simplified divertor geometry and plasma parameters were used. Benchmark calculation was carried out by using DEGAS code development by D.B. Heifetz et al. Good qualitative agreement were obtained.

4.2 Refinement of the code being implemented

The reference design of the INTOR impurity control system is a single null poloidal divertor. For modeling of a diverted plasma, it had been used one dimensional fluid code with two dimentional neutral code. Assuming rather simple divertor geometry, the divertor operation with high density and low temperature divertor plasmas was found with an appropriate heat and particle flux to the region. However, it is necessary to include the radial diffusion process in the scrape-off layer for accurate estimation of particle and energy deposition on a divertor plate. Besides, it is important to analize the behavior of neutral particles in real divertor geometry. As critical issues during Phase IIA part 3, refinement of the model being implemented became a main subject.

Two types of two-dimensional time dependent fluid code have been developed. The first one is the complete two-dimensional fluid code solved by the finite elements method in the plasma equilibrium and real geometry including the scrape-off plasma, the periphery of the main plasma and the divertor plasma. This code being under development is assumed the toroidal axisymmetry under the rectangular toroidal coordinates (Appendix 4.2.1).

The second one is also the two-dimensional fluid code but employs Particle In Cell (PIC) method for numerical treatments [20]. The fluid flow channels in the scrape-off and divertor region can be applied from poloidal magnetic flux tubes obtained by equilibrium calculation. By the PIC method with a proper geometry, fluid behavior in the computational region is easily solved with free boundary conditions. Free boundary condition means that the energy flux to the vacant cell across

the boundary must vanish at the initial step of the PIC scheme. Transport of the core plasma, however, is not solved in the code. The appropriate particle flux Γ, energy flux Qe for electron and Qi for ion must be assumed at the boundary of the core plasma.

Coupled with two dimensional neutral transport code using Monte-Carlo method, the fluid equation and neutral gas transport are solved in the scrap-off and divertor plasma region. In the vacuum region, only neutral gas transport is solved. The neutral transport package in called every several tenth of the fluid calculation time cycle.

Two dimensional neutral transport code has been developed using the Monte-Carlo techniques (Appendix 4.2.2). The code can handle any number of hydrogen species including two type of neutral sources, which is enough for studies of neutral behaviors in JT-60.

4.3 Model validation and divertor modeling

The characteristics of the divertor plasma in JT-60 has been analyzed with a conventional divertor model of which the scrape-off plasma transport is described by one-dimensional fluid model and neutral particle transport is simulated by two-dimensional Monte-Carlo method [21]. In ohmically heated plasma, the calculated radiation loss power is somehow smaller than the experimental values measured by bolometers in the divertor chamber as shown in Fig. 16. The radiation loss by impurity such as oxygen and carbon is regarded as the reason for the above difference because only hydrogen line radiation by the collisional-radiative model is included in the model. If hydrogen line radiation is enhanced by a factor of three, H_α intensity and radiation loss power agree with the numerical results.

In neutral beam heated plasma, on the other hand, the calculated loss power is larger than the experimental value measured by bolometer. The difference may be explained by the ambiguity of the main and scrape-off plasma parameters in the auxiliary heated plasma and the effects of fast ions.

The neutral pressure in the divertor chamber is well simulated the experimental observation as shown in Fig. 17. The averaged neutral density in the divertor chamber is proportional to the square of the main plasma density. Assuming that global particle confinement time during NBI heating is about a half of that in Ohmically heated plasmas,

it can be explained that pressure during NBI heating is two to three times higher than that in Ohmic heating.

Validation of the newly developed divertor code (PIC treatments) is shown by simulating the boundary plasma conditions in Doublet III divertor experiments [20]. The distribution of plasma temperature and density in the divertor region were calculated using prescribed values of the cross field transport coefficients (i.e. D=0.5 Bohm and $\chi_e = \chi_i$=4D) and the input power (1MW) for various values of the plasma particle flow across the separatrix. The results of this calculation are in satisfactory agreement with the experimental data from DIII as shown in Fig. 18.

In this model validation study, they found that an important parameter besides transport coefficients is the pitch angle of the field line B_θ/B_T, where B_θ and B_T are poloidal and toroidal magnetic field, respectively. Fig. 19 shows the pitch angle distribution along the poloidal flux tubes in the Doublet-III divertor configulation in use. As shown in Fig. 20, the peak shift of the electron temperature and ion saturation current profiles obserbed at the mid-plane of the device experimentally can be simulated with the effect of the distributed pitch angle. The shift cannot occur with spatially uniform B_θ/B_T. The peak shift can be explained by the deceleration of the poloidal flow velocity, as shown in Fig. 21, and decrease of the poloidal heat conduction near the null point because of the smaller pitch angle.

For modeling of divertor plasmas, the fluid model has usually been applied. However, it is not clear that the usual fluid equations can describe accurately the scrape-off layer and divertor plasma. By this means, it has been developed the electrostatic particle model which can express correctly the velocity distribution function and the self-consistent electrostatic field. The simulation model is based on a one-dimensional system parallel to the magnetic field [22] (Appendix 4.2.2).

As simulation results, it is found that Coulomb collisions play a very important role in supplying electrons with large velocities. The pre-sheath with the scale length of the system size is formed by the collisional relaxation of the velocity distribution as well as by the particle source. The ion heat conduction flux becomes important in a high-recycling plasma. This value is found to be much larger than that estimated by the ion temperature gradient.

Several suggestions were made to the fluid model from these studies. In usual analyses by fluid model, the boundary condition for the parallel flow velocity at the divertor plate is given by $V_{\parallel} = C_s$. where C_s is the sound speed. In a low recycling plasma, however, $V_{\parallel}$ exceeds C_s in the divertor region, while in a high-recycling plasma $V_{\parallel}$ is equal to C_s at the understream just behind the recycling region. It is usually assumed in fluid equations that both electron and ion temperatures are isotropic. The isotropy in the electron temperature is almost realized in high collisionality, $\nu_* > 1$, which is defined by the ratio of the collion frequency to the bounce frequency of an electron, because of effects of the trapping due to the sheath potential. On the contrary, anisotropy in the ion temperature is large, even when $\nu_* >> 1$. Therefore the parallel temperature of ions, $T_{i\parallel}$, and perpendicular one, $T_{i\perp}$, should be treated separately in fluid equations. When particles are highly recycled near the plate and $V_{\parallel} << C_s$ in the divertor region, the ion heat conduction flux, q_i, becomes very important in the total heat flux.

The preliminary calculation of the FER divertor plasma is carried out by the newly developed two dimensional fluid code (solved by PIC method). Fig. 2.22 shows the model geometry. In the simulation studies, the impurity flow equations are added, but the behavior of only He^+ ion is included. Assuming $Q_T = Q_e + Q_i = 60$ MW, $\Gamma_p = 1\times10^{22}$ s^{-1} or 3×10^{22} s^{-1}, and $\Gamma_{He} = 0.05\ \Gamma_p$, the maximum temperature T_e in the scrape-off layer is approximately 210 eV. T_e decreases to approximately 20 eV at the divertor plate as shown in Fig. 23. Electron density near the divertor plate builds up to $n_e \simeq 2\times10^{20}$ m^{-3} for $\Gamma_p = 1\times10^{22}$ s^{-1} and $n_e \simeq 6\times10^{20}$ m^{-3} for $\Gamma_p = 3\times10^{22}$ s^{-1}. Fig. 24 shows the distribution of deposited energy flux on the inner and outer divertor plate. It seems that the total heat load on the inner divertor plate is quite equal to that on the outer divertor plate. In EC analysis of single null divertor configuration, however, the heat load on the outer divertor plate is about two times larger than that on the inner divertor plate because of non-symmetric heat conduction along the diverted flux tube. Further studies are encouraged with this code including impurity materials of divertor target and appropriate impurity production mechanism.

4.4 Operation scenario issues

The reference operation scenario of INTOR is a pulsed operation with full inductive current ramp up. A pulse length of plasma burning is about 200 sec. It has been shown that a divertor operation of high density and low temperature divertor plasma is accomplished with appropriate particle and heat flux at divertor throat entrance.

If optional operation scenarios such as non-inductive current ramp-up or transformar recharging of quasi-steady state operation is considered, it is questionable to obtain proper boundary conditions to so as to perform cold and dense divertor plasmas. For instance, LHCD has not yet been established for high density plasma so that the main plasma density during LHCD phase is one order lower than that in burning phase. That means less particle flux diffused out from main plasma to scrape-off layer. Besides, the heat flux could be small because the absorbed power of lower hybrid wave would not be so large, based on resent experiments for current drive efficiency. In FER operation scenario, the absorbed power of LH is only 20 MW. In these conditions of particle and heat flux, the temperature of divertor plasmas become 30-50 eV [23]. Concerning a effect of sheath potential, a release rate of impurities from a tungsten target is high enough to shorten a lifetime of the plate. Thus in order to accompalish high recycling divertor plasma, it is necessary to maintain a reasonable balance between the input power and plasma density. One possibility to enhance the particle flux to divertor throat is to increase the bulk plasma density. Based on the recent experimental results in JT-60, the efficiency for current drive is improved as the average bulk temperature is increased. The resultant higher plasma density may balance a particle flux on its heat flux. It was shown that the divertor plasma temperature decreased below 10 eV under the condition of improved efficiency for current drive.

The efficiency for current drive by means of NBI is, in general, smaller than that by LH. That means lower bulk density and less particle flux to divertor chamber during the current ramp-up or transformar recharging phase by NBI-CD. Hence, the operational range is somehow restricted in a case of NBI-CD.

References

[1] INTOR GROUP, International Tokamak Reactor: Zero Phase (Rep. Int. Tokamak Reactor Workshop Vienna, 1979), International Atomic Energy Agency, Vienna (1980); see also Summary in Nucl. Fusion 20 (1980) 349.

[2] INTOR GROUP, International Tokamak Reactor: Phase One (Rep. Int. Tokamak Reactor Workshop Vienna, 1980-81), International Atomic Energy Agency, Vienna (1982); see also Summary in Nucl. Fusion 22 (1982) 135.

[3] INTOR GROUP, International Tokamak Reactor: Phase Two A Part 1 (Rep. Int. Tokamak Reactor Workshop Vienna, 1981-83), International Atomic Energy Agency, Vienna (1983); see also Summary in Nucl. Fusion 23 (1983) 1513.

[4] INTOR GROUP, International Tokamak Reactor: Phase Two A Part 2 (Rep. Int. Tokamak Reactor Workshop Vienna, 1984-85), International Atomic Energy Agency, Vienna (1986); see also Summary in Nucl. Fusion 25 (1985) 1719.

[5] INTOR GROUP, International Tokamak Reactor: Phase Two A Part 3 (Rep. Int. Tokamak Reactor Workshop Vienna, 1985-87), International Atomic Energy Agency, Vienna (1988) (to be published).

[6] INTOR GROUP, EC Report of INTOR Phase IIA Part 3 (INTOR Workshop, Vienna, 1987).

[7] INTOR GROUP, USA Report of INTOR Phase IIA Part 3 (INTOR Workshop, Vienna, 1987).

[8] INTOR GROUP, USSR Report of INTOR Phase IIA Part 3 (INTOR Workshop, Vienna, 1987).

[9] Report of INTOR-Related IAEA Specialist Meeting on Tokamak Concept Innovations, (January 1986) IAEA-TECDO-373.

[10] Report of INTOR-Related IAEA Specialists' Meeting on Plasma Disruptions, which is included in Ref. [5].

[11] JT-60 Team (presented by H. Takeuchi), "Impurity and MHD Behavior in JT-60 Divertor Discharge", in the 11th International Conference on Plasma Physics and Controlled Nuclear Fusion Research. IAEA-CN-47/A-IV-3, Kyoto, Japan, 13-20 Nov. 1986.

[12] JT-60 Team (Presented by M. Yoshikawa) "Recent Experiments in JT-60", in the 11th International Conference on Plasma Physics and Controlled Nuclear Fusion Research, IAEA-CN-47/A-I-1, Kyoto, Japan, 13-20 Nov. 1986.

[13] T. Hirayama, T. Sugie, A. Sakasai, H. Kubo, Y. Koide, N. Akaoka, H. Takeuchi, and M. Nagami, "Impurity Transport in Ohmically Heated JT-60 Plasma", JAERI-M 86-161, 1986.

[14] Y. Koide, K. Yamada, H. Yoshida, H. Nakamura, S. Niikura and S. Tsuji, "Radiation Loss and Global Energy Balance of Ohmically Heated Divertor Discharge in JT-60 Tokamak", JAERI-M 86-056, 1986.

[15] K. Odajima, et al., "Confinement Studies of Additionally Heated Plasma in JFT-2M Tokamak", in the 11th International Conference on Plasma Physics and Controlled Nuclear Fusion Research, IAEA-CN-47/A-III-2, Kyoto, Japan, 13-20 Nov. 1986.

[16] K. Yamazaki et al., "Disruption Control Experiments using Local Modular Multipole-field Coils", in the 11th International Conference on Plasma.

[17] D.L. Hillis, et al., and O. Motojima, T. Mizuuchi, et al., "Pump Limiter Studies on the Heliotron-E Device", J. of Nuclear Materials, 145-147 (1987) 496-500.

[18] S. Takamura, N. Ohnishi, H. Yamada and T. Okuda, "Electric and Magnetic Structure of Edge Plasma in A Tokamak with Helical Magnetic Limiter", printed in Phys. Fluids [1987].

[19] T. Mizoguchi, M. Sugihara, S. Yamamoto, N. Fujisawa and FER design team "Characteristics of Radiatively Cooled Edge Plasma for Fusion Experimental Reactor - Conceptual Design Study of FY 86 FER" to be published in JAERI report.

[20] N. Ueda, M. Kasai, M. Tanaka, M. Sugihara and S. Sengoku, "Development of a Two-Dimensional Fluid Code and Its Application to the Doublet III Divertor Experiment", to be submitted to Nuclear Fusion, 1987.

[21] H. Yoshida, "Divertor Analysis of JT-60", presented at TRIPARTITE IEA meeting, Naka, Japan, Nov. 21-22, 1986.

[22] T. Kakizuka, K. Tani and M. Azumi, "Particle Simulation of Divertor Plasma", presented at U.S.-Japan Workshop on Advanced Plasma. Modeling Sep. 24-27, 1985 and to be published in IPP Research Report.

[23] S. Hitoki, M. Sugihara and S. Yamamoto "Cold and Dense Divertor Plasma in Phase of Current Drive", to submit to Journal of Japanese Applied Physics, 1987.

Table 1 Disruption classification, characteristics and its control method in JT-60 experiments.

	Classification	characteristics	control method	controlled
OH	$q_{eff} \lesssim 2$	large m=2	$q_{eff} > 2.1$	yes
	$q_{eff} \sim 3$	large m=3	$q_{eff} > 3$ or $q_{eff} < 3$ ramp-up phase: gas puff, $\dot{I}_p$, position	yes
	density limit	large MHD, $P_R \sim P_{OH}$	divertor and gas puff $\bar{n}_e < 25B_T/Rq_a$ and $7B_T/R$ ($10^{19}m^{-3}$)	yes
	impurity	large MHD, $P_R \sim P_{OH}$	discharge cleaning, limiter material or divertor with high current	yes
NB	density limit (not yet obserbed in JT-60 divertor operation)			
	impurity (evaporation)	large MHD, $P_R \sim P_{NB}$	limiter material or divertor	yes
	(high beta [JFT-2M] large MHD with $q_{eff} \sim 2$ and $G^{Troyon} \sim 2.3$)			?
ICRF LH	impurity	simple impurity increase	antenna cleaning, additional heating power of NB and position control	yes
		A small minor disruption induces antenna breakdown and a major disruption	?	?

Table 2 Examples of time decay rates of a PIN diode signal from a plasma center. This decay rates is expected in same order of thermal energy quench time during disruptions.

Heating	Shot No.	t_D(ms)	t_D^*(ms)	I_p(MA)	Configuration
OH	2289	27	11	2.0	Div.
	2319	40	2	2.0	
IC	2466	16	1	1.5	Div.
LH	3747	26	2	1.5	Div.
LH + NBI	3938	8	2	1.0	Lim.

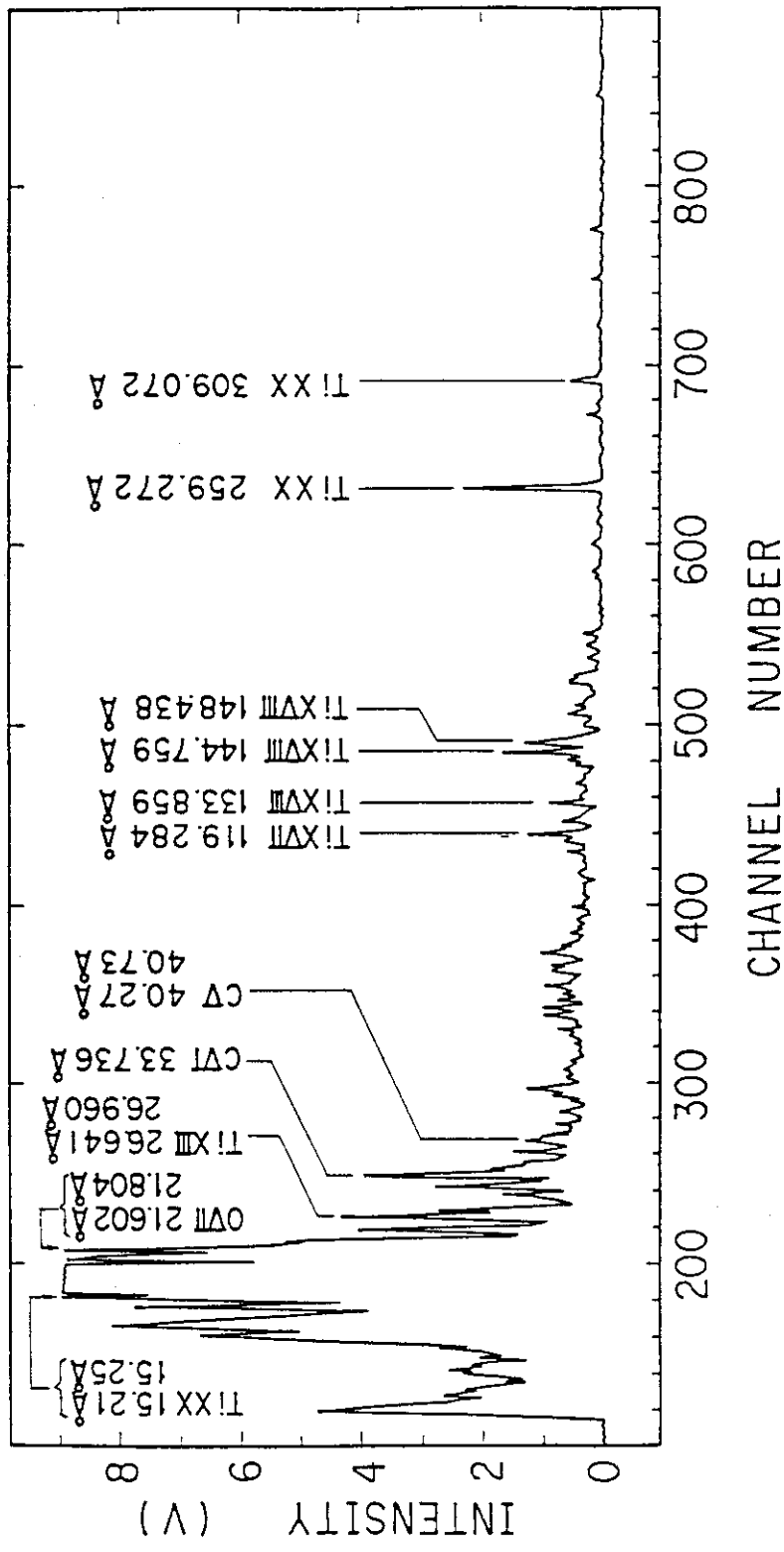

Fig. 1 Typical VUV spectrum recorded by unit type spectrometer, integrated over 20 ms on the condition of B_T=4.5 T, I_p=2 MA in divertor discharge. Carbon, oxygen and titanium are major impurities in JT-60 divertor operation.

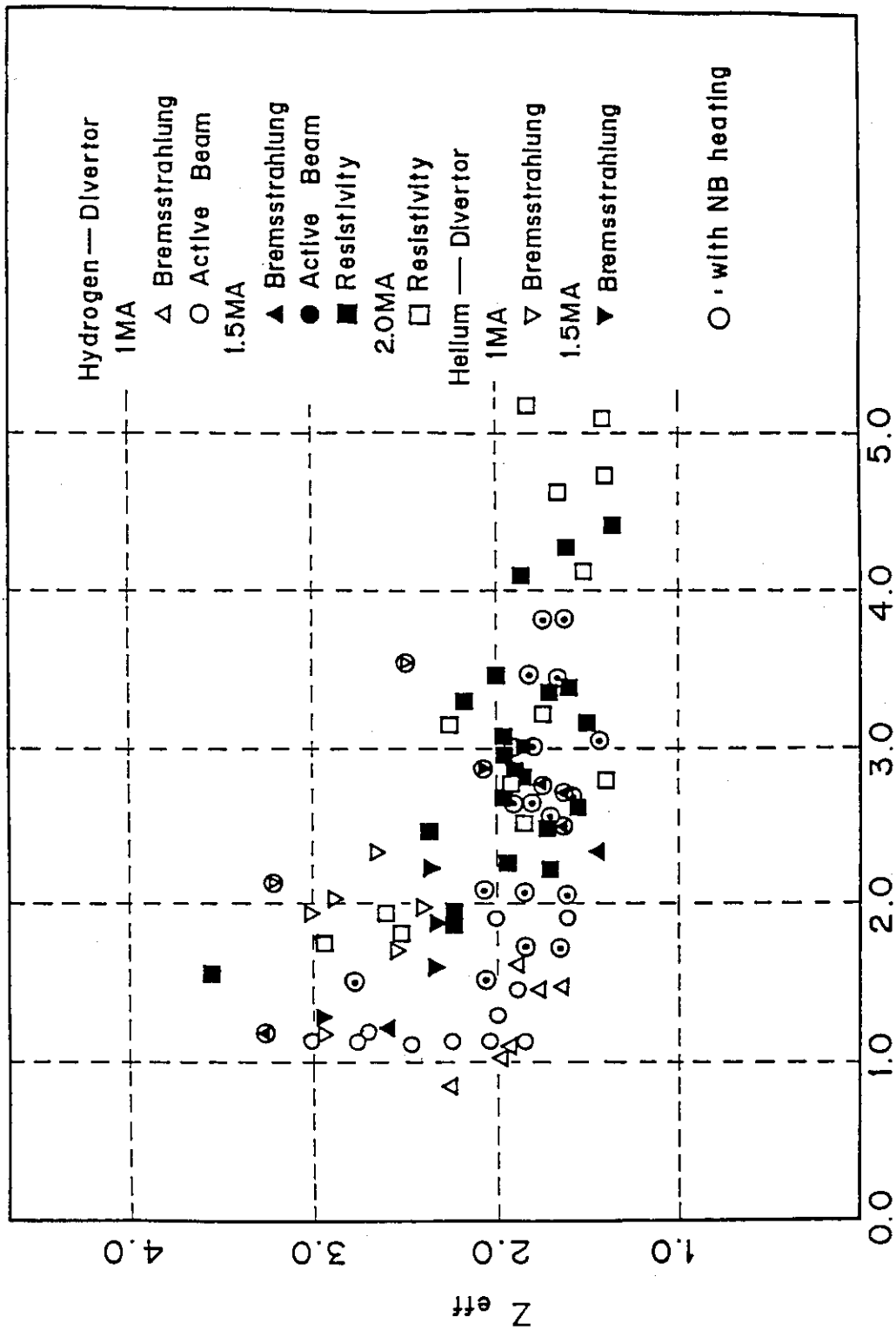

Fig. 2 Z_{eff} vs. $\bar{n}_e$ for ohmically heated and NB-heated plasma in JT-60. The relatively low Z_{eff}, less than 1.5, can be achieved with high electron density even in NB-heated plasmas.

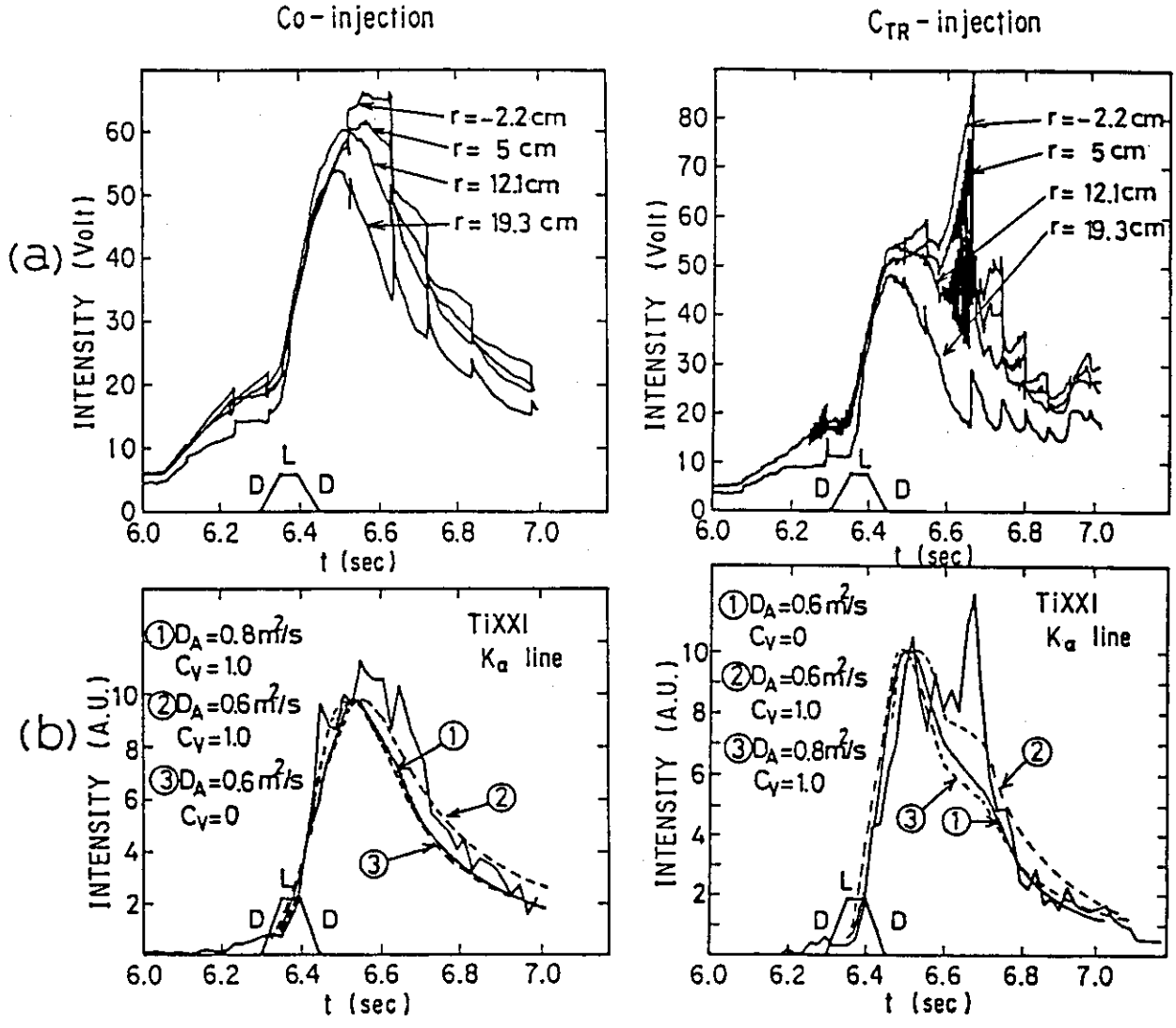

Fig. 3 The comparison of time evolution of (a) soft X-ray, (b) TiXXI resonance line with co- and counter-NB injection. Titanium was intentionally injected by switching the configuration from divertor to limiter one, and back to divertor as shown in the figure. The fitting results of diffusion coefficient simulated by 1-D transport code are D_A=0.6 m²/s and D_A=0.8 m²/s with C_V=1.0 for counter- and Co- NB injected plasma.

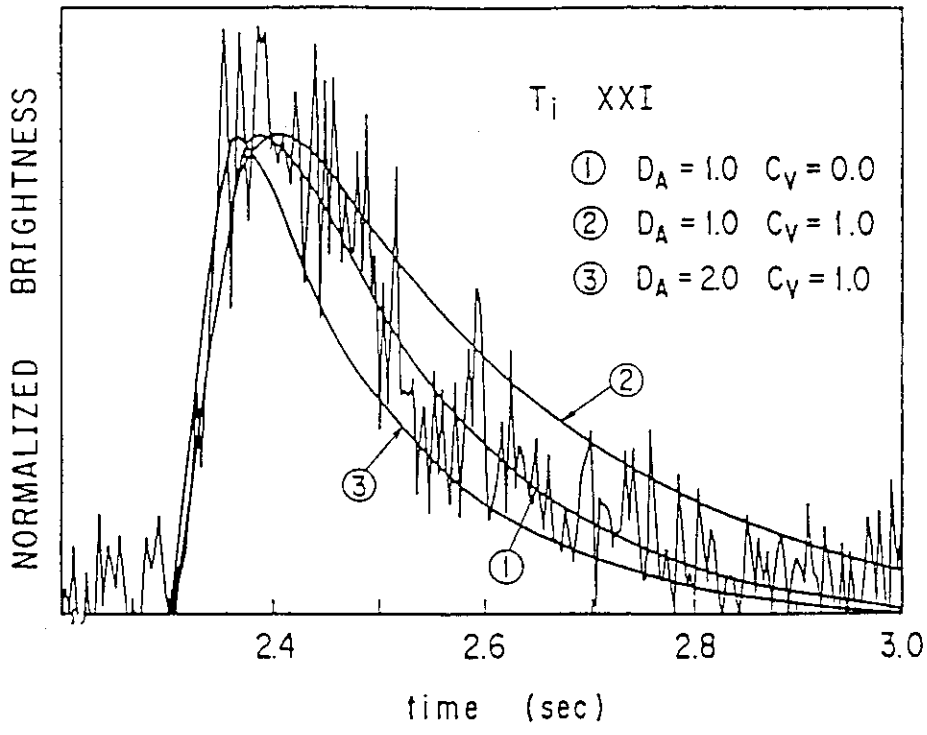

Fig. 4 The time evolution of TiXXI resonance line in the ohmically heated plasma. In this case, the best fitting results is D_A=1.0 m^2/s with C_V=0.

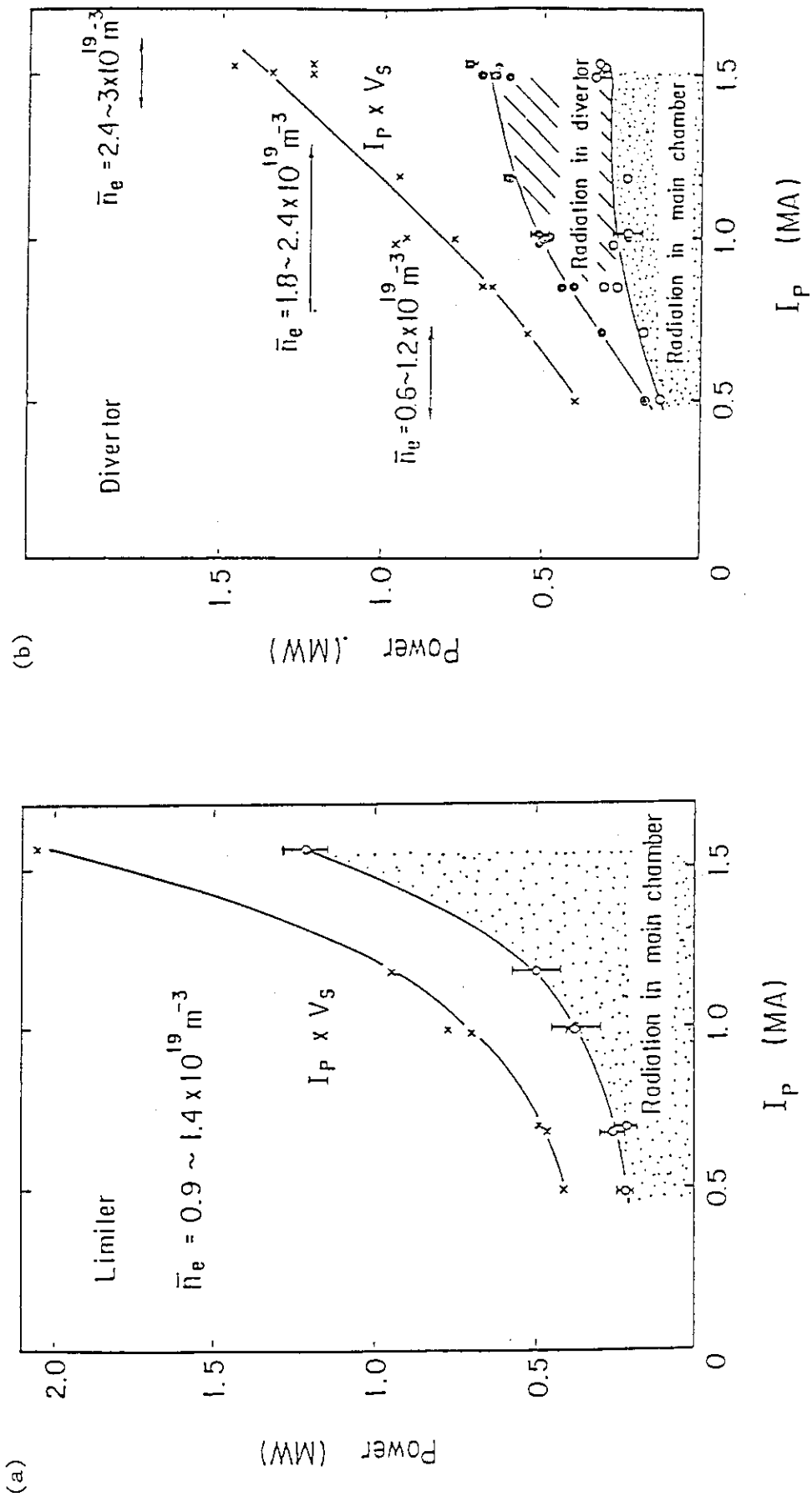

Fig. 5 Comparison of radiation power in main plasma chamber with (a) limiter discharges and (b) divertor discharges. The product of I_p and V_s ($I_p \times V_s$), radiation power in main and divertor plasma are shown as a function of plasma current I_p. In divertor discharge, radiation power in main chamber seems to be saturated as plasma current and ohmic input power increase.

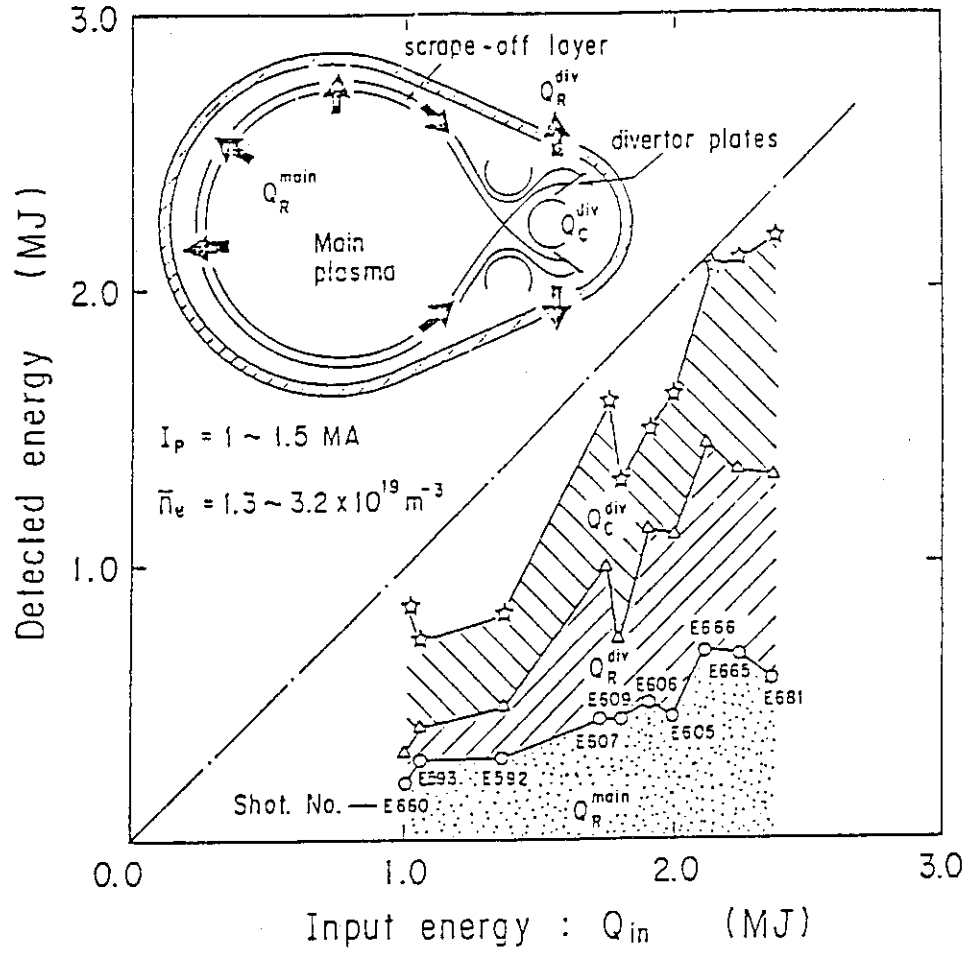

Fig. 6 Energy balance of diverted discharges, about 70% of input energy are exhausted into divertor chamber, and fair amount of this energy is dissipated by radiation loss. These observations are shown that impurity and particle control is successfully performed with the poloidal divertor in JT-60.

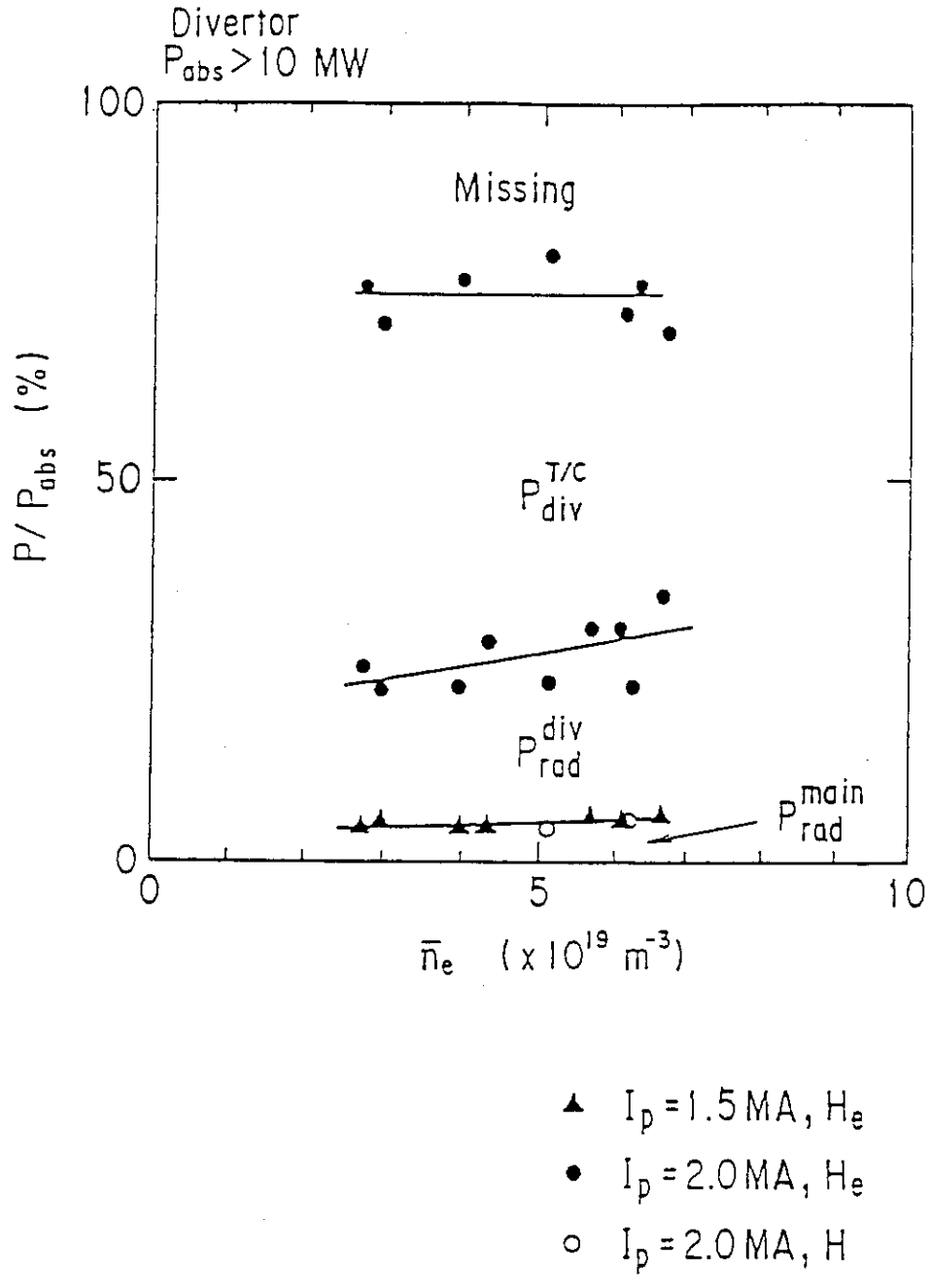

Fig. 7 $\bar{n}_e$ vs. radiation power fraction in main and divertor chamber with NB-heated plasma. The fraction of radiation power loss in main plasma over the input power is only 5-10%.

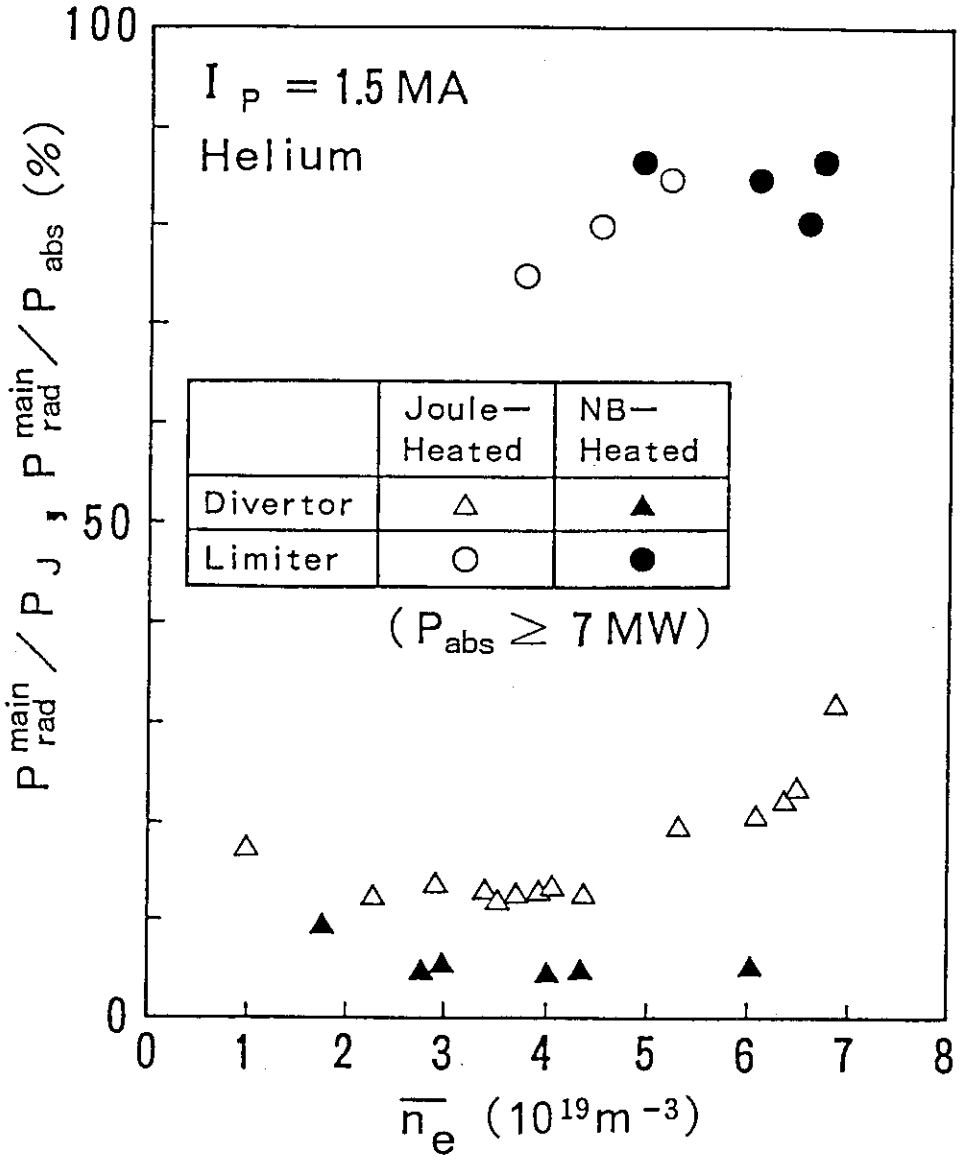

Fig. 8 Comparison of radiation power fraction in main chamber between ohmically heated and in NB-heated plasma.

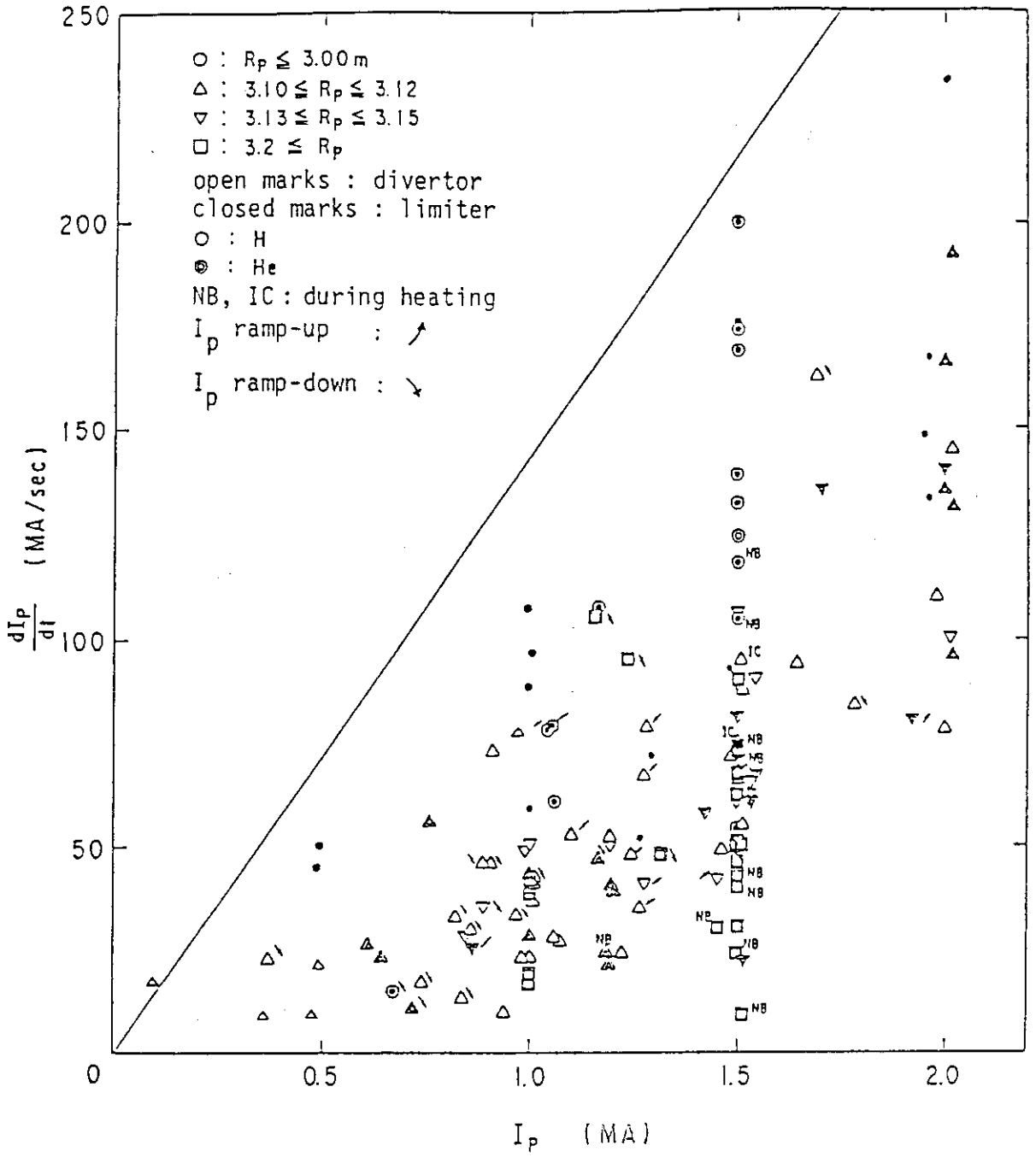

Fig. 9 Relations between a plasma current and current decay rate at disruptions. The solid line indicates the design value of 380 MA/s at I_p=2.7 MA for JT-60. The current decay faster than the design value has not been observed yet in any disruptions of JT-60.

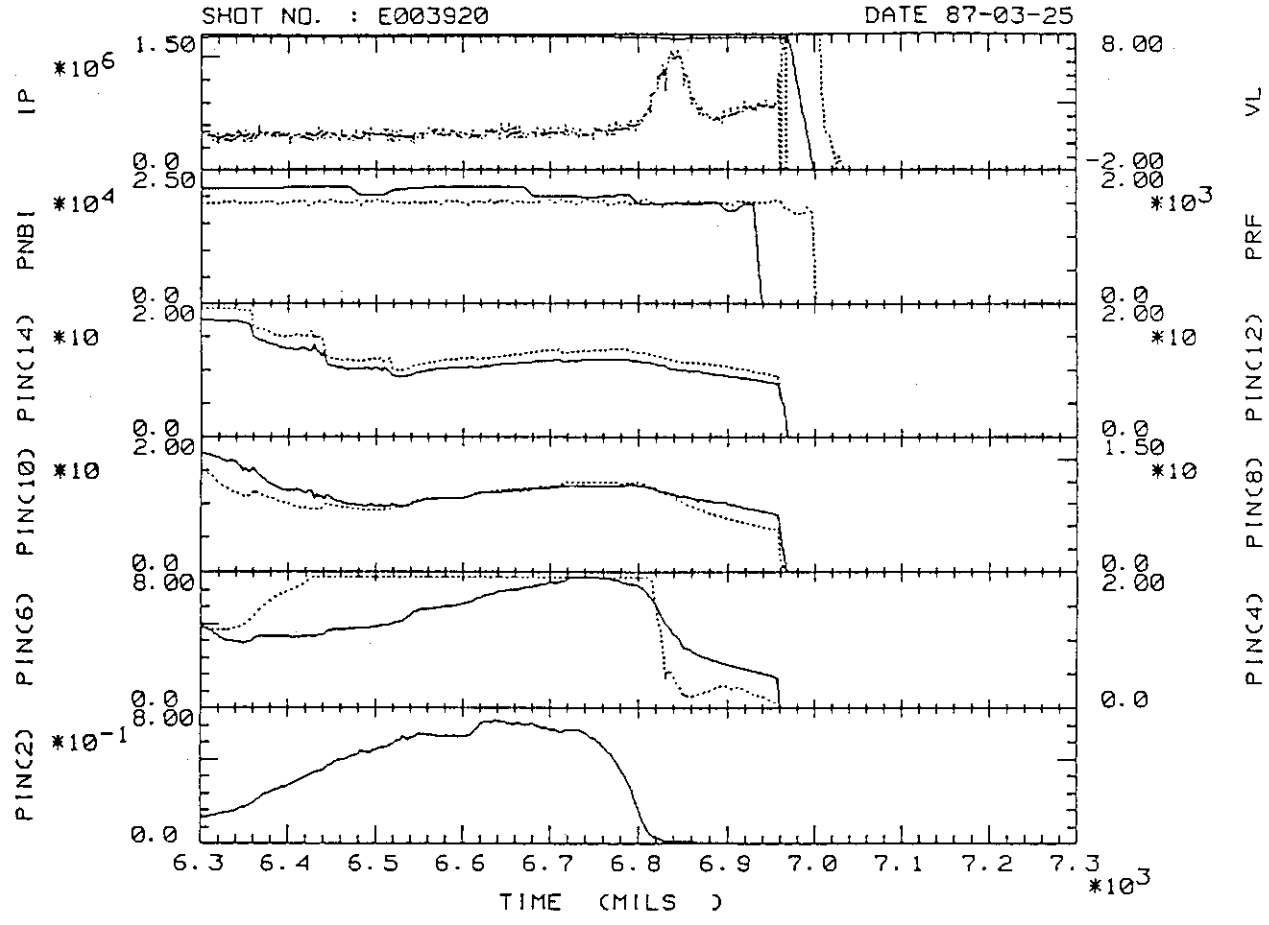

Fig.10 Expanded time evolutions of signals of a PIN diode array for a NB and RF heated plasma terminated in a disruption. Solid and dotted lines correspond to left- and right-hand signals, respectively. The top figures shows a plasma current and a loop voltage. The second ones are heating powers of Nb and RF. The PIN with a small number looks at outer portion of a plasma column and PIN(12) has a line-of-sight nearly through the plasma center.

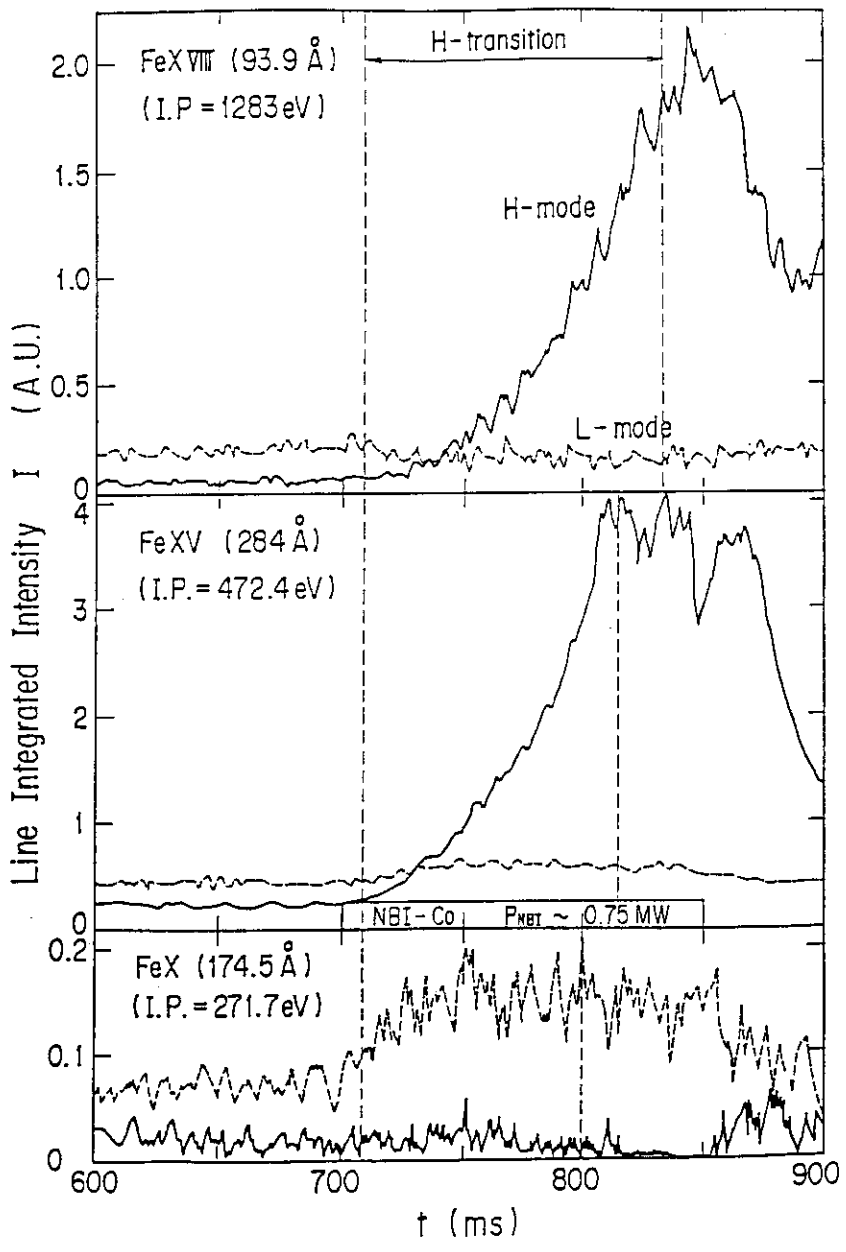

Fig. 11 Time evolution of iron line integrated intensity (FeX; λ=17.4 nm, FeXV; λ=28.4 nm, FeXVII; λ=9.4 nm) in H-(solid line) and L-mode (dash line) discharges. During H-mode phase, the emission from lower ionized ion are depressed like H_α signals, but the emissions from the higher ionized ion are increased exponentially. The increment of these ion density is not due to the increments of the impurity influx but mainly due to the improved particle confinement during H-mode phase.

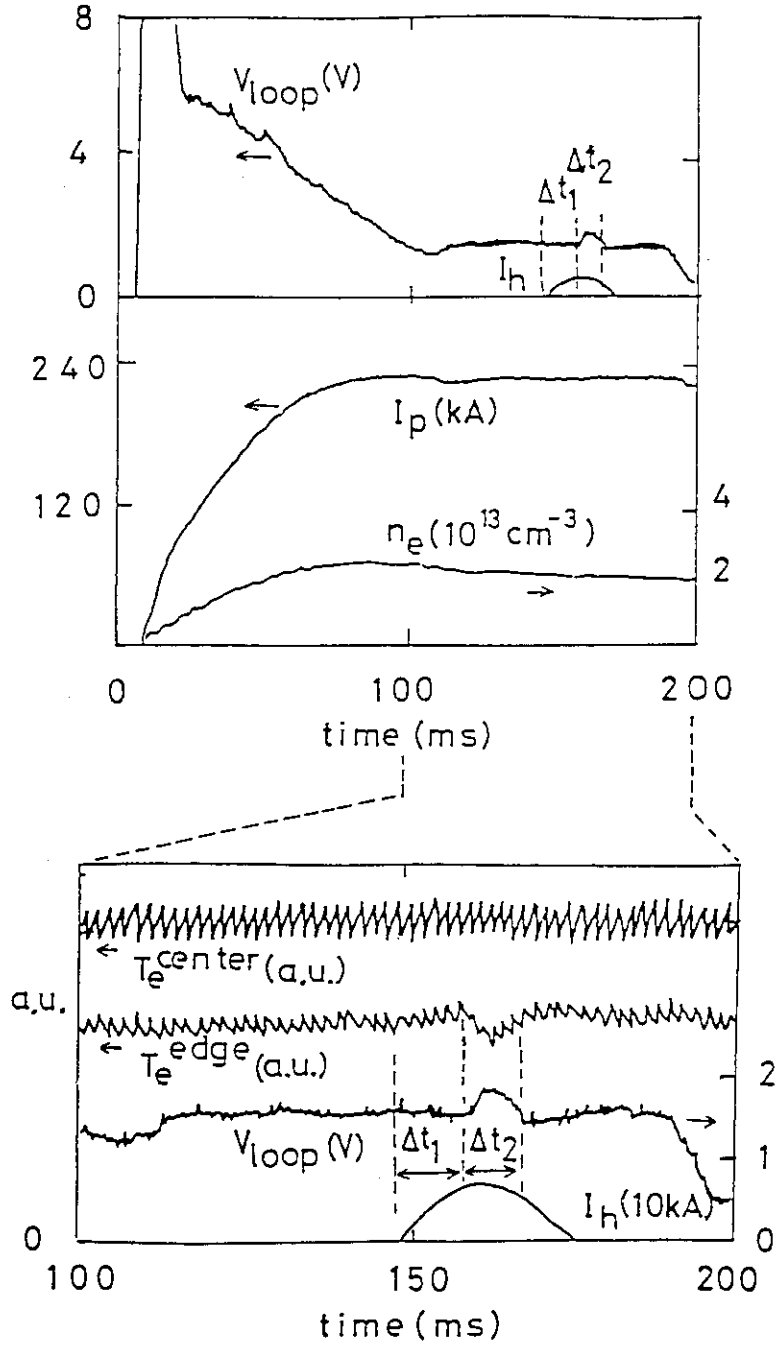

Fig. 12 Ergodic limiter experiments using m=3/n=1 local helical field perturbation by means of local modular multipole-field coils. The favourable effect of edge ergodization on the edge temperature drop is observed.

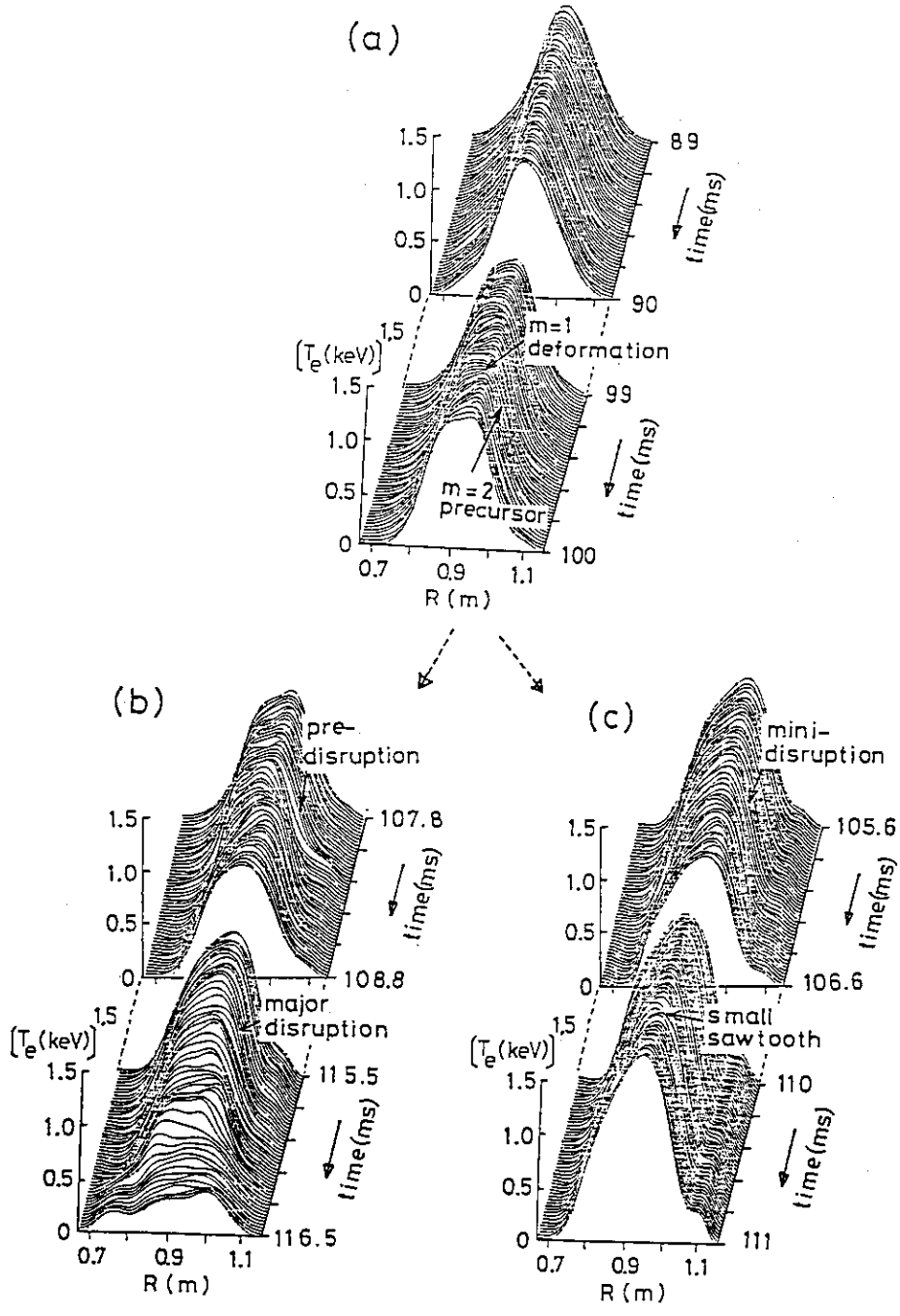

Fig. 13 Time evolution of the one-half power of the electron temperature profile $T_e^{1.5}$ (a) before helical field application, (b) without helical field application and (c) with the m=3/n=2 helical field perturvation. The stabilization is found to be attributed to the exitation of a 'mini-disruption' actively induced by $B_{h3/2}$ in advance of the calastrophic stage towards the major disruption.

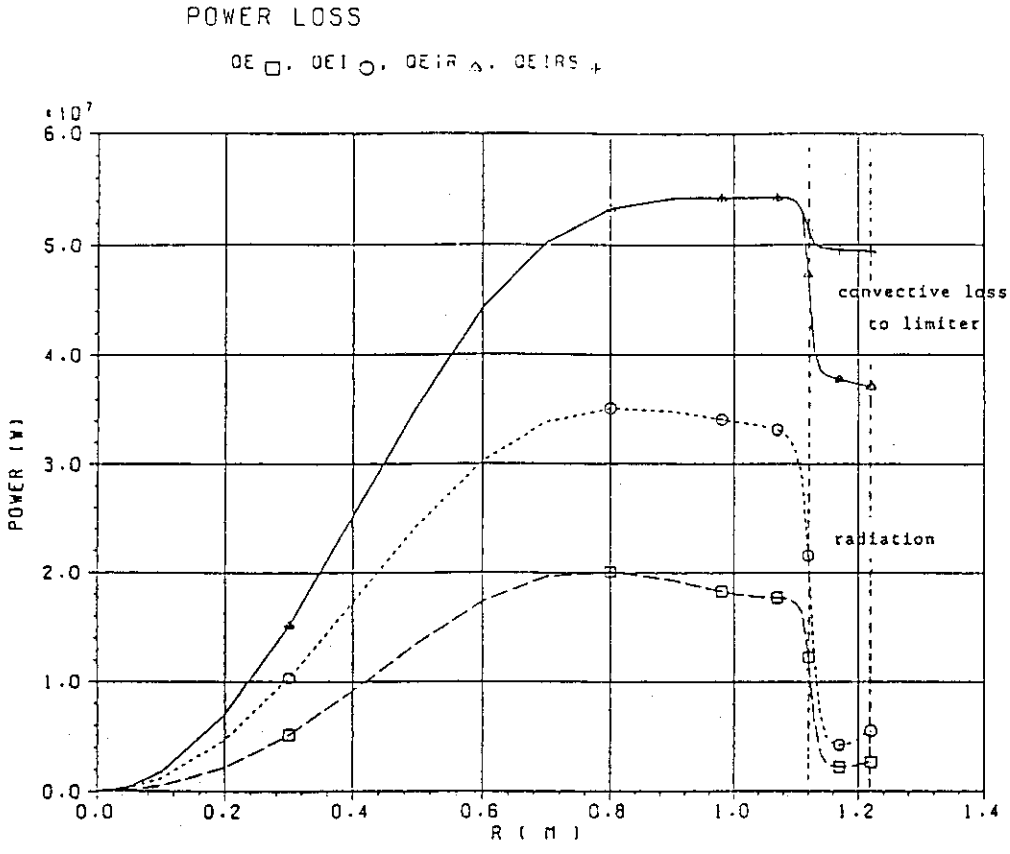

Fig. 14 Energy flow diagram obtained by self-limited impurity production mechanism. It is assumed that the anomalous diffusion coefficient in main plasma is 1.0 m^2/s and the diffusion across the field line in scrape-off layer is the Bohm diffusion. The first wall and limiter material is only carbon. Radiation power loss is 31 MW, 56% of alpha heating power, and convective heat flow to the limiter is about 10 MW.

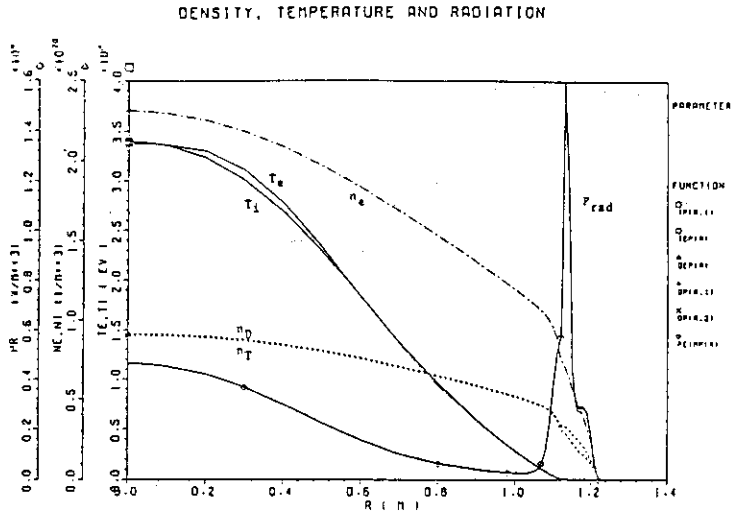

(a)

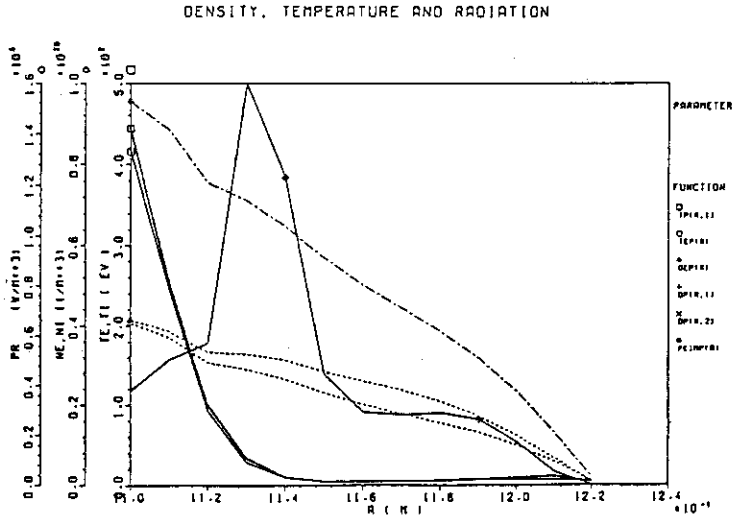

(b)

Fig. 15 (a) Density, temperature and radiation power profiles under the same self-limited impurity production condition.

(b) The expanded profiles at the region of plasma edge boundary. The carbon graphite limiter is located from R=1.12 m to R=1.22 m. The plasma edge temperature at the carbon limiter head is still about 100 eV which is seriously high temperature for physical self-sputtering.

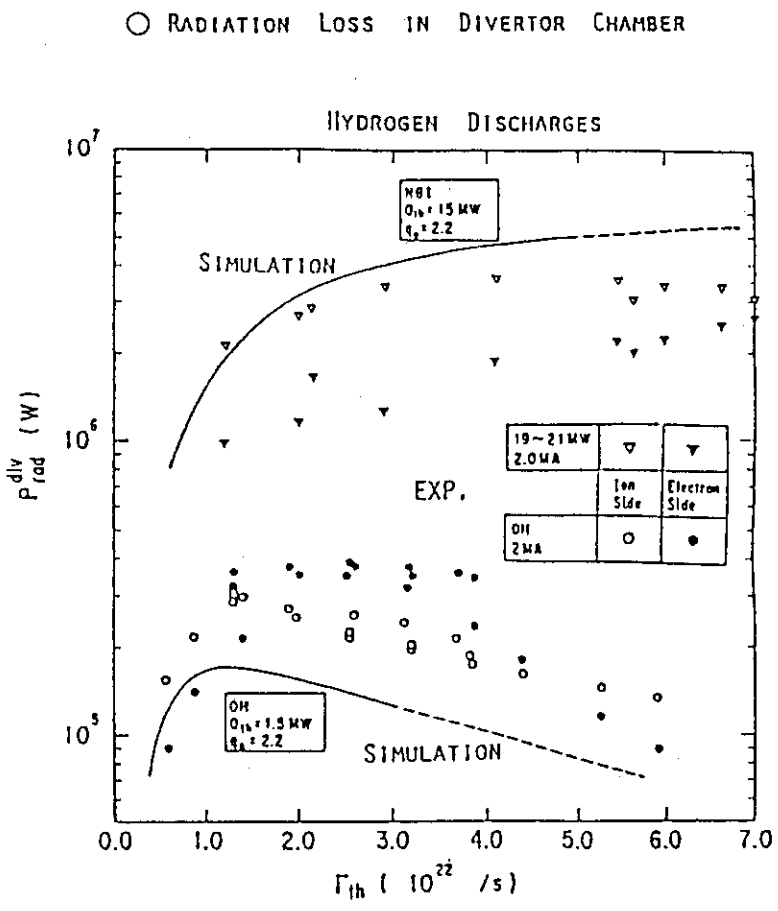

Fig. 16 Comparison between the experimental results and simulated results of radiation power in divertor chamber. In ohmically heated plasmas, the radiation power simulated by 2-D fluid model is somehow underestimated by factor of 2-3. On the other hand, the tending is opposite in NB-heated plasmas.

○ NEUTRAL PARTICLE PRESSURE

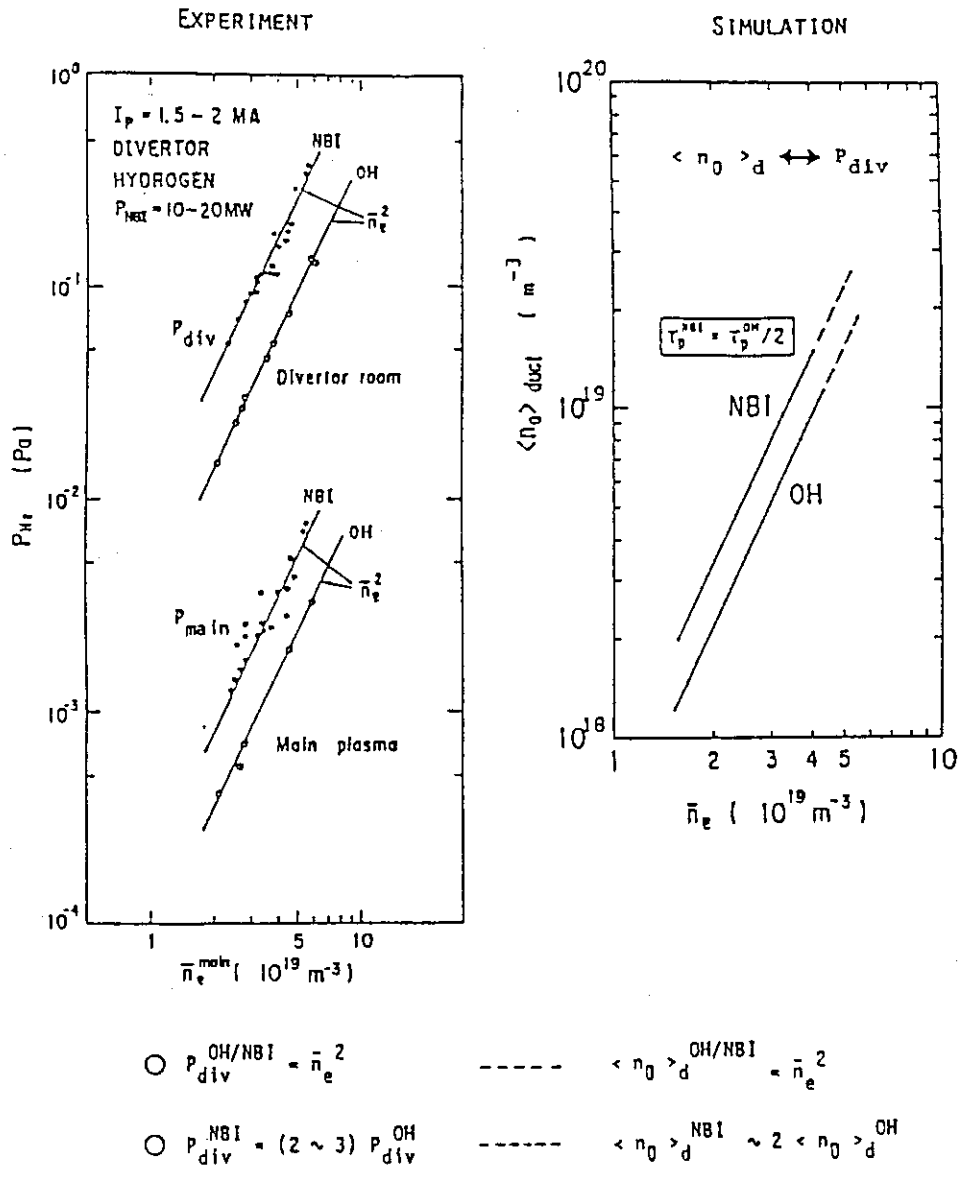

Fig. 17 Comparison between experimental results and simulated results for neutral particle pressure in divertor chamber.

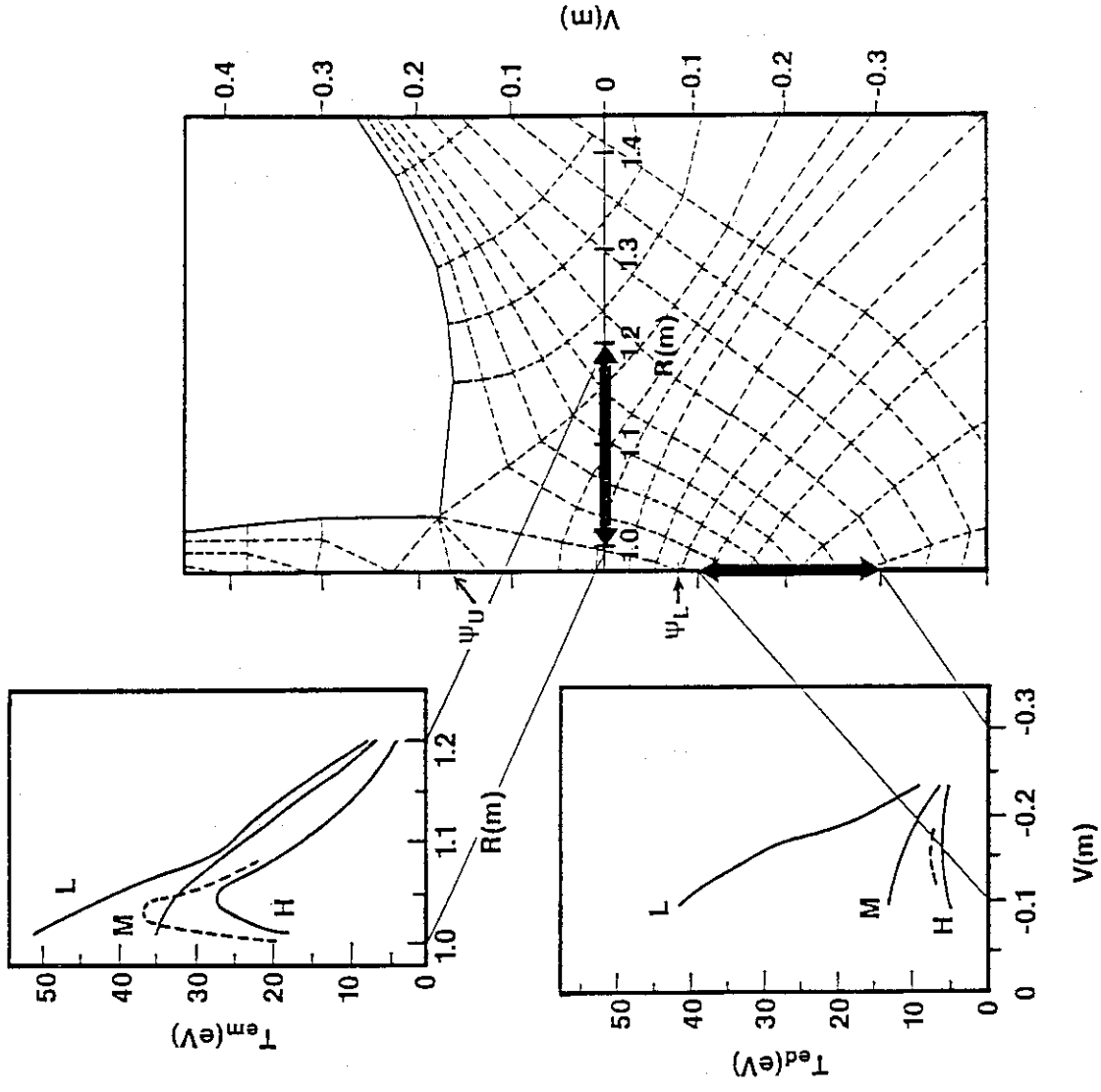

Fig. 18 Horizontal profile of the electron temperature T_{em} across the lower divertor channel (device mid-plane: V=0 m) and corresponding vertical profiles of T_{ed} on the divertor plate for each particle flux from the core plasma across the separatrix (H: $\Gamma=1.2\times10^{22}$ s^{-1}, M: $\Gamma=0.8\times10^{22}$ s^{-1}, L: $\Gamma=0.4\times10^{22}$ s^{-1}). (-----) denotes the experimental data for $\bar{n}_e$ $=3\times10^{13}$ cm^{-3}. The separatrix flux surfaces at the divertor plate (Ψ_U and Ψ_L) are also shown.

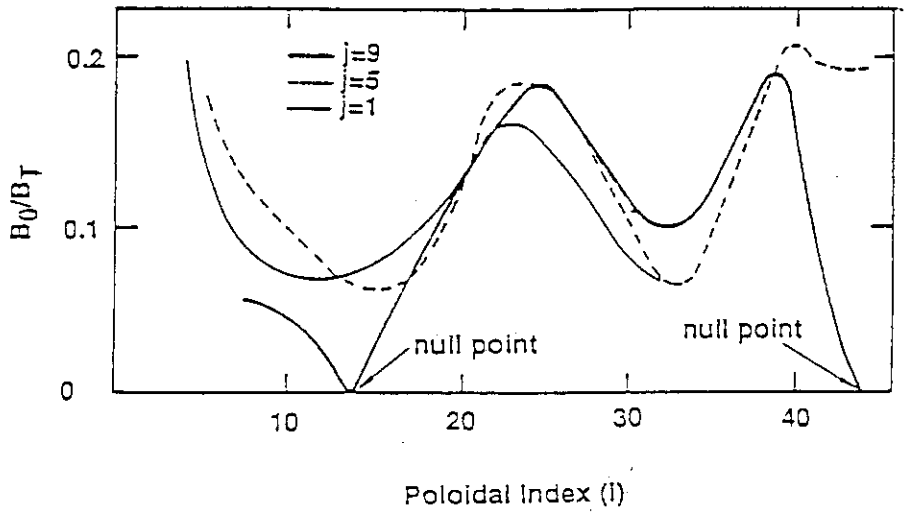

Fig. 19 The pitch angle distribution along the field lines.

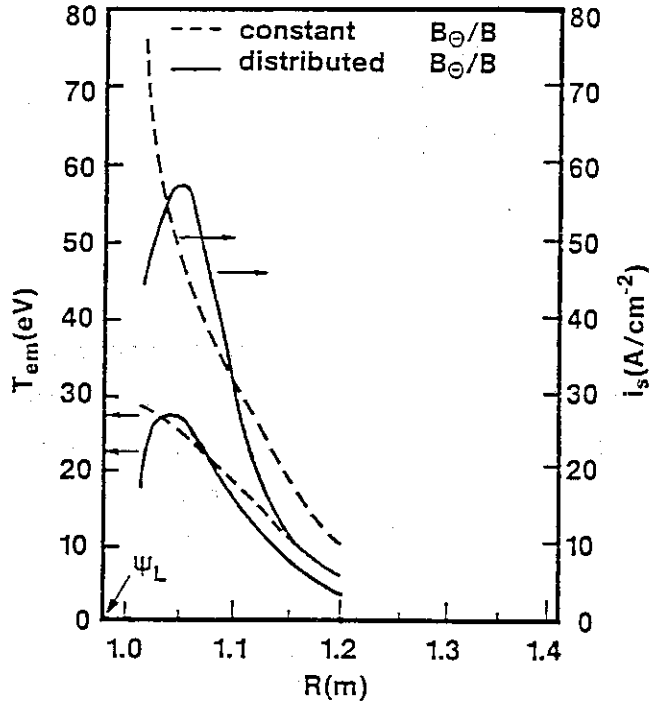

Fig. 20 Comparison of the horizontal profiles of electron temperature T_{em} and ion saturation current i_s at V=0 m (device mid-plane) with constant B_θ/B (B_θ/B=0.05) and distributed B_θ/B value for the particle flux from the core plasma of $\Gamma=1.2\times10^{22}$ s^{-1}.

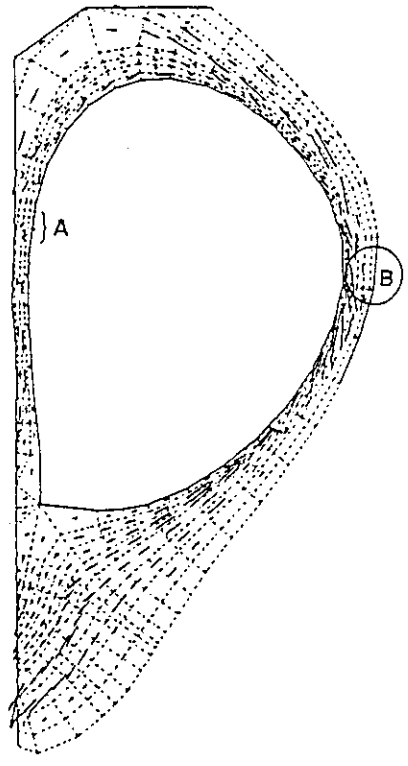

Fig. 21 Flow velocity distribution in the scrape-off layer for $\Gamma=1.2\times10^{22}$ s^{-1}. A and B show stagnation point. It is shown that the flow velocity in the poloidal direction near the null point is very small because of smaller pitch angle.

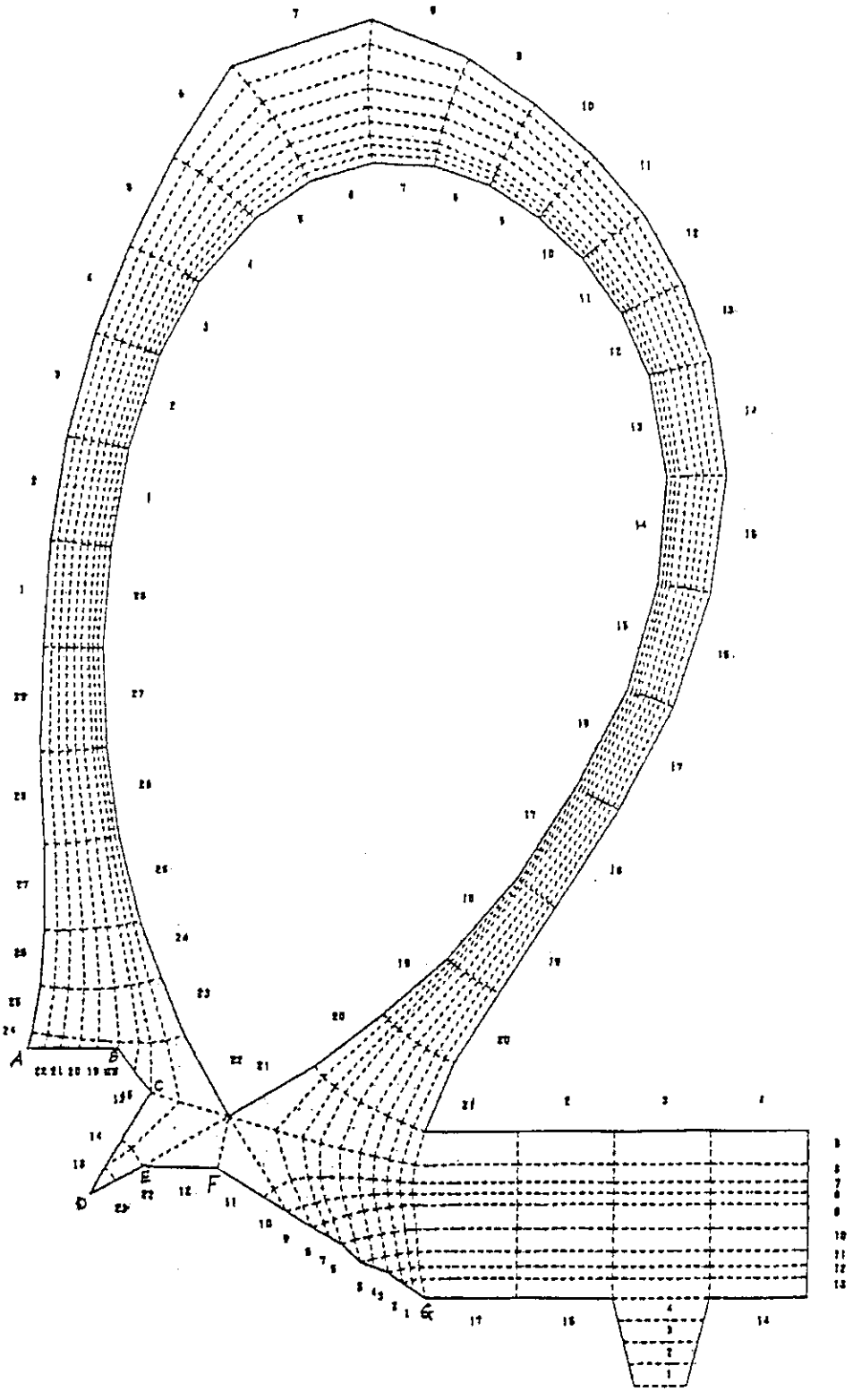

Fig. 22 Calculation model of scrape-off and divertor plasma for FER impurity control.

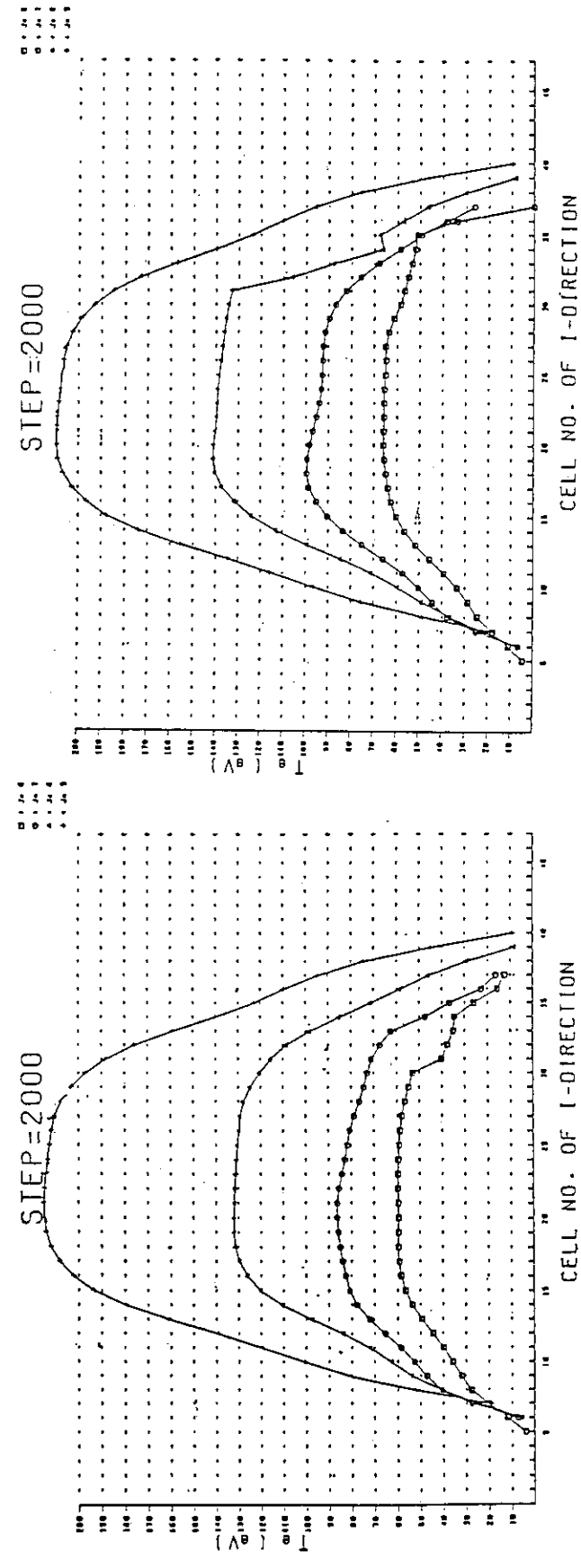

Fig. 23 Electron temperature profiles in the poloidal direction for particle flux Γ_p of 1×10^{-22} s^{-1} and 3×10^{-22} s^{-1}. Reasonable low temperature plasma in divertor region is evaluated in open diverted FER plasma under appropriate assumptions of impurity and neutral transport based on large tokamak experiments.

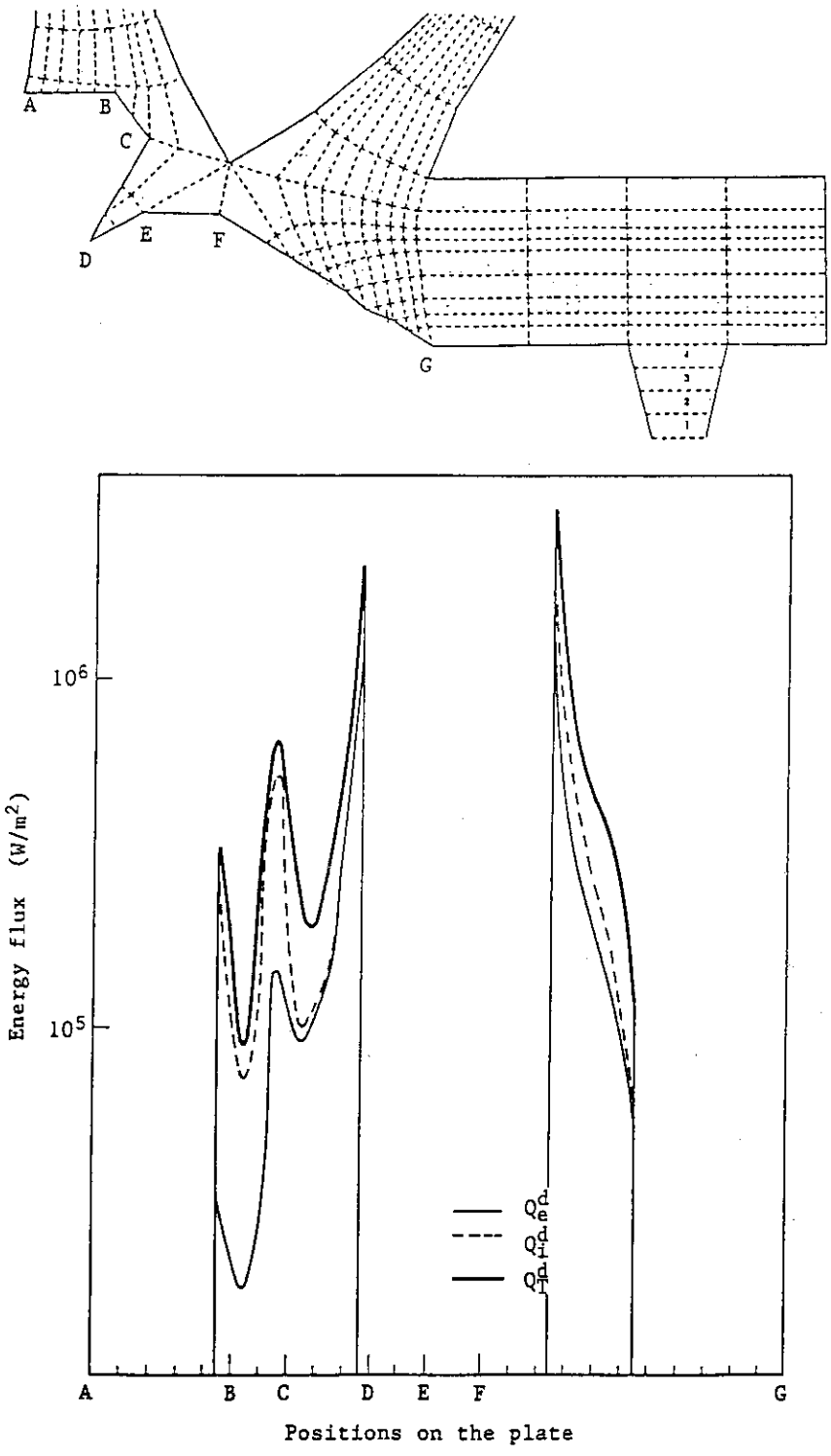

Fig. 24 Distribution of deposited energy flux Q^d on the divertor plate in case of $\Gamma_p = 1 \times 10^{22}$ s^{-1}. Total energy deposited on the inner divertor plate is almost equal to it on the outer divertor plate.

Appendixes

Appendix 2.1.1

Radiation Loss and Global Energy Balance of Ohmically Heated Divertor Discharge in JT-60 Tokamak

Y. Koide, K. Yamada, H. Yoshida, H. Nakamura, S. Niikura, S. Tsuji

Appendix 2.1.2

Impurity and MHD behavior in JT-60 Divertor Discharges

H. Takeuchi and JT-60 team

Appendix 2.1.3

Impurity Transport in Ohmically Heated JT-60 Plasma

Y. Koide, N. Akaoka, H. Takeuchi and M. Nagami

Appendix 2.2.1

Impurity Behavior during H-mode Phase in JFT-2M Tokamak

H. Ogawa

Appendix 2.3.1

Disruption Control Experiments using Local Modular Multipole-field Coils

K. Yamazaki, et al.

Appendix 3.1.1

Electric and Magnetic Structure of Edge Plasma in a Tokamak with Helical Magnetic Limiter

S. Takamura, N. Ohnishi, H. Yamada, and T. Okuda

Appendix 3.1.2

Control of Tokamak Edge Plasma by Static and Rotating Helical Magnetic Limiter

S. Takamura, H. Yamada and T. Okuda

Appendix 3.1.3

Effect of an Ergodic Magnetic Limiter on Particle and Heat Flux Control

T. Kawamura and T. Ono

Appendix 3.1.4

Resonant Helical Divertor Experiments

A. Mohri

Appendix 3.2.1

Characteristics of Radiatively Cooled Edge Plasma for Fusion Experimental Reactor - Conceptual Design Study of FY86 FER

T. Mizoguchi, M. Sugihara, S. Yamamoto, N. Fujisawa and FER design teams

Appendix 3.4.1

Helium Burial

M. Saidoh and R. Yamada

Appendix 3.4.2

Oxygen Gettering

T. Okazaki

Appendix 3.4.3

In-situ Boron Deposition

T. Abe and T. Okazaki

Appendix 4.1.1

2-D Neutral Monte-Carlo Code

K. Shimizu

Appendix 4.2.1

2-D Fluid Model Divertor-Scrape-Off Layer Code

T. Hirayama

Appendix 4.2.2

Particle Simulation of Divertor Plasma

T. Takizuka, K. Tani, M. Azumi

Appendix 4.3.1

Divertor Analysis of JT-60

H. Yoshida

Appendix 4.3.2

Development of a Two-dimensional Fluid Code and Its Application to the Doublet III

N. Ueda, M. Kasai, M. Tanaka, M. Sugihara and S. Sengoku

Appendix 4.3.3

Numerical Simulation of the FER Divertor Plasma

N. Ueda, M. Sugihara, S. Yamamoto, N. Fujisawa, and FER design teams

Appendix 4.4.1

Cold and Dense Divertor Plasma in Phase of Current Drive

S. Hitoki, M. Sugihara and S. Yamamoto

APPENDIX 2.1.1

Radiation Loss and Global Energy Balance of Ohmically Heated Divertor Discharge in JT-60 Tokamak

Y. Koide, K. Yamada*, H. Yoshida, H. Nakamura,
S. Niikura**, and S. Tsuji

Japan Atomic Energy Research Institute
Naka Fusion Research Establishment
Naka-machi, Naka-gun, Ibaraki, Japan

* On leave from Energy Research Laboratory,
Hitachi, Ltd.

** On leave from Mitsubishi Atomic Power
Industries, Inc.

1. Report on new developments in the experimental data base

— RADIATION LOSS AND GLOBAL ENERGY BALANCE OF OHMICALLY HEATED DIVERTOR DISCHARGE IN JT-60 TOKAMAK —

Yoshihiko KOIDE, Kimio YAMADA*, Hidetoshi YOSHIDA
Hiroo NAKAMURA, Setsuo NIIKURA**, Shunji TSUJI

Japan Atomic Energy Research Institute
Naka Fusion Research Establishment
Naka-machi, Naka-gun, Ibaraki, Japan

ABSTRACT

Divertor experiment in JT-60 with a small divertor chamber has been successfuly performed up to 1.6 MA discharge. Several divertor effects were experimentally confirmed as follows.

Radiation loss in main plasma saturates with the increase of plasma current and its ratio to the input power is about 20 % at 1.5 MA. The rest of input power is exhausted into the divertor chamber and a half of it is dissipated as the radiation loss.

Impurity accumulation is not observed during a few sec without internal MHD activity and gross impurity confinement time is several hundred msec.

---

* On leave from Energy Research Laboratory, Hitachi, Ltd.

**On leave from Mitsubishi Atomic Power Industries, Inc.

APPENDIX 2.1.2

Impurity and MHD Behavior in JT-60 Divertor Discharges

H. Takeuchi and JT-60 team

Japan Atomic Energy Research Institute
Naka Fusion Research Establishment
Naka-machi, Naka-gun, Ibaraki, Japan

Paper presented at the 11th International Conference on Plasma Physics and Controlled Nuclear Fusion Research, Kyoto, Japan, 13-20 Nov. 1986

IMPURITY AND MHD BEHAVIOR IN JT-60 DIVERTOR DISCHARGES

ABSTRACT

The diffusion coefficient (D_A) and the inward peaking factor (C_V) of titanium were estimated by the experimental evolution of titanium lines and the calculation result of a simulation code. D_A=1.0 m^2/s and C_V=~0 for the ohmically heated plasmas and D_A=0.6-0.8 m^2/s and C_V=0-1 for the neutral beam (NB) injection heated plasmas. No difference in titanium transport by the direction (co- or counter-) of NB injection was observed. There was no strong pinch of titanium at center in divertor discharges both with and without sawtooth oscillation.

In discharges with the ohmic and NB heating, various MHD activities were observed. The transition from single to compound sawtooth took place at a resistive diffusion time $\tau_R=\mu_0 r_I^2/\eta \geq 3.5$ sec. It was confirmed that the inversion radius observed in the wide range of q_{eff}=2.6-6 was dependent in a linear relation on $1/q_{eff}$ but independent of the density, radius, plasma current or heating power.

APPENDIX 2.1.3

Impurity Transport in Ohmically Heated JT-60 Plasma

T. Hirayama, T. Sugie, A. Sakasai, H. Kubo,
Y. Koide, N. Akaoka, H. Takeuchi and M. Nagami

Japan Atomic Energy Research Institute
Naka Fusion Research Establishment
Naka-machi, Naka-gun, Ibaraki, Japan

IMPURITY TRANSPORT IN OHMICALLY HEATED JT-60 PLASMA

Toshio HIRAYAMA, Tatsuo SUGIE, Akira SAKASAI,
Hirotaka KUBO, Yoshihiko KOIDE, Nobuo AKAOKA,
Hiroshi TAKEUCHI and Masayuki NAGAMI

Department of Large Tokamak Research
Naka Fusion Research Establishment
Japan Atomic Energy Research Institute
Naka-machi, Naka-gun, Ibaraki-ken

(Received October 11, 1986)

In the Ohmically heated plasma of JT-60, the transport of impurities has been studied by VUV and soft X-ray crystal spectroscopies, and from bolometer and soft X-ray diode signals, along with one-dimensional impurity transport code. Changing over a discharge from the limiter mode to the divertor mode, the decay of the bolometer signals was measured and the time constant was about 0.3 sec in the central chord. Temporal evolutions of T_i *XIII*(23.356Å), T_i *XX*(259.3Å) and T_i *XXI* (resonance line) were obtained in two different discharges with I_p=2*MA* which a piece of titanium was accidentally injected into. The comparison of the time behaviour of the respective lines with the simulation results by a diffusive/convective transport model shows that the anomalcus diffusion coefficient is about 1.0 m^2/s and convective inward velocity is not seen.

Keywords: Tokamak, Impurity Transport, Ohmically Heated Plasma, JT-60

APPENDIX 2.2.1

Impurity Behavior during H-mode Phase in JFT-2M Tokamak

H. Ogawa

Japan Atomic Energy Research Institute
Tokai-mura, Naka-gun, Ibaraki, Japan

2.2 JFT-2M

Impurity Behavior During H-mode Phase In JFT-2M Tokamak

by H.OGAWA

Although the energy and the particle confinement in additional heated plasma are improved in H-mode phase, the radiation losses are largely increased during burst free H-mode phase. In JFT-2M it seemed that H-mode phase is terminated by the radiation losses. These results indicates that the impurity problem is one of the most serious problem in H-mode discharge. In this note, we present the experimental results of the spectroscopic measurement in JFT-2M tokamak concerned with impurity behavior during H-mode phase.

The JFT-2M tokamak has a D-shaped vacuum vessel made of the stainless steel with 1.31 major radius and 0.415x0.595 minor radii. The fixed and movable limiters and the divertor plates are mode of graphite. Titanium gettering is used to obtain clean plasma. Two heating neutral beams(H^0) are injected near tangentially(co-and counter-injection) and the maximum power is about 2MW. The longest period of the H-mode phase is performed in the NBI heated deuterium plasma with the single null divertor configuration. In this configuration, the maximum plasma current(I_p) is 220kA and the maximum toroidal field strength is 1.5T. The obtained plasma has a D-shape with 0.28m plasma radius and its ellipticity and triangularity are about 1.43 and 0.25 respectively.

Figure 1 shows the time evolution of the iron ion line(FeX; λ=17.4nm, Ionization Potential(IP)=273eV, FeXV; λ=28.4nm, IP=487eV, FeXVIII; λ=9.3nm, IP=1.38keV) in H-(solid line) and L-mode(dash line) discharges. The magnetic configuration of these

two discharges are almost the same except that the lower movable limiter was touched the plasma in L-mode discharge. During ohmic heating(OH) phase, the emission from iron ion lines in L-mode discharge are twice as large as in H-mode discharge. This may be due to the divertor effect. During NBI heating in L-mode discharge, the emission of FeX is increased about factor two compared with OH phase but the emissions of FeXV and FeXVIII are not increased. On the other hand, in H-mode discharge the emissions of FeX is not increased but the emission of FeXV and FeXVIII are increased exponentially during H-mode phase. The same time evolutions are observed in the emissions of the titanium ion lines. These large increment of the emissions of the higher ionized metal ion lines are correlated with the large increment of the radiation losses. The radial profile of the iron ion line indicates that these large increment of the emission of higher ionized ion line during H-mode is due to the increment of the higher ionized ion density. Figure 2 shows the time evolution of the emission from the light impurity ion lines. The emissions of low ionized ions(CIV, OIV, OVI) are rapidly depressed at the H-transition which is very similar to that of the $H\alpha/D\alpha$ signals, but the emission from the higher ionized ion(CVI) is increased gradually during H-mode phase. These time evolutions are almost the same as that of the emissions from the metal impurity ions.

In summary, during H-mode phase the emissions from lower ionized ion are depressed like $H\alpha$ signals, but the emissions from the higher ionized ion are increased exponentially during H-

mode phase. The large increment of the emissions from higher ionized ion are due to the large increment of the higher ionized impurity ion densities. The impurity injection(Ar) experiment suggests that the increment of these ion density are not due to the increments of the impurity influx and mainly due to the improved particle confinement during H-mode phase.

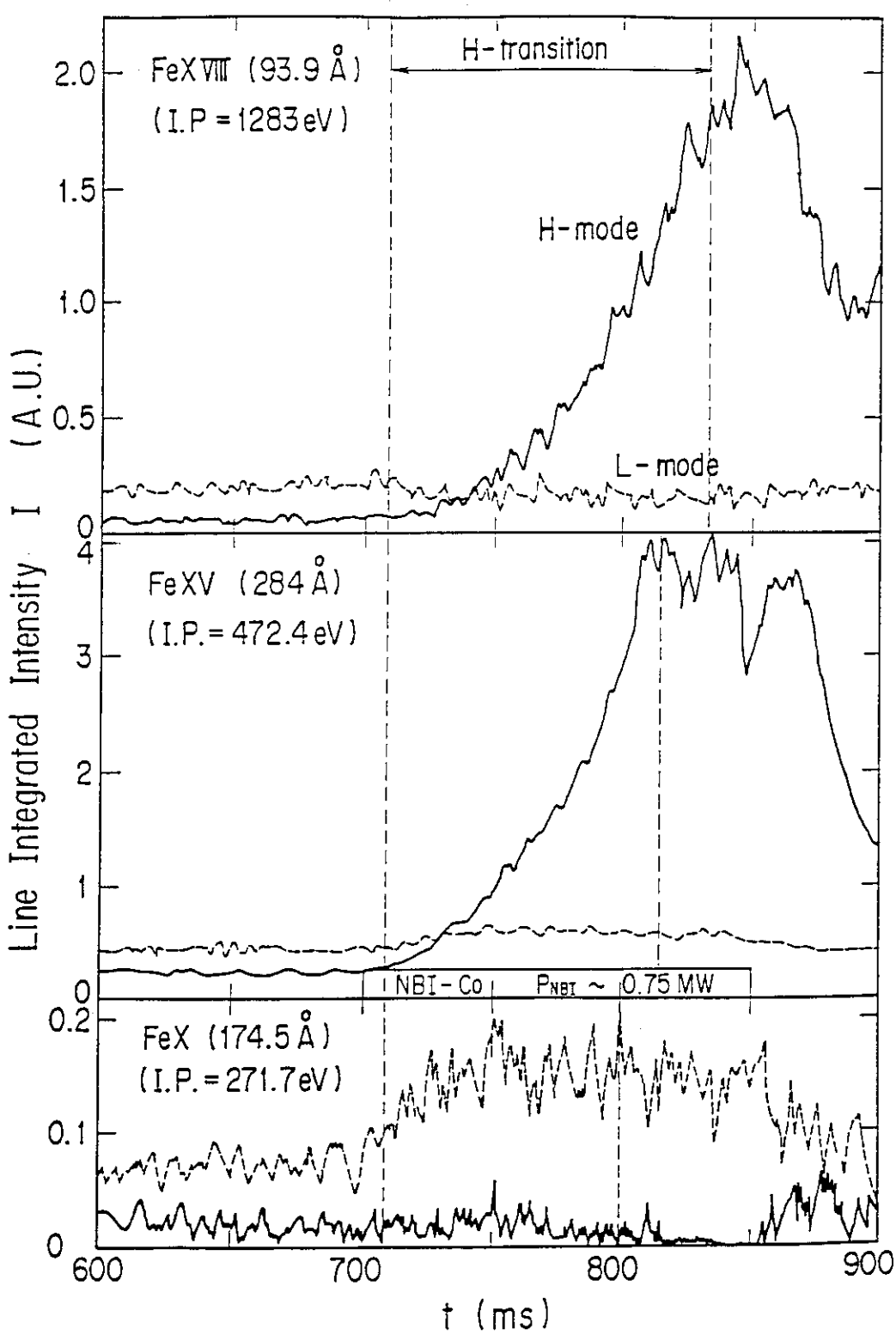

Fig. 1 Time evoluation of the iron ion line

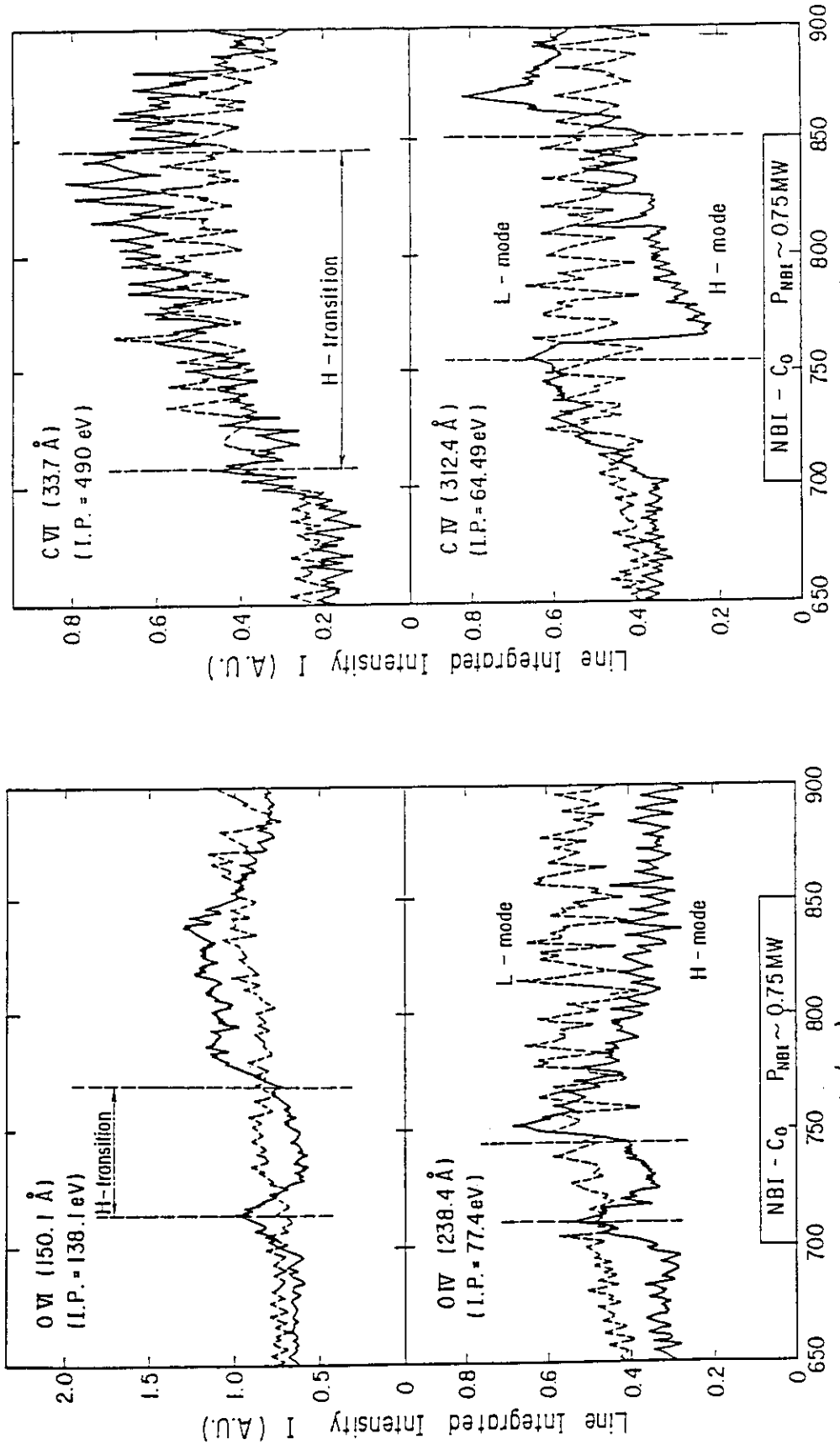

Fig. 2 The time evoluation of the emission from the lightimpurity ion lines

APPENDIX 2.3.1

Disruption Control Experiments using Local Modular Multipole-field Coils

K. Yamazaki, K. Kawahata, Y. Abe, R. Akiyama,
T. Amano, R. Ando, Y. Hamada, S. Hirokura, K. Ida,
E. Kako, O. Kaneko, Y. Kawasumi, S. Kitagawa,
T. Kuroda, K. Masai, K. Matsuoka, A. Mohri,
M. Mugishima, N. Noda, I. Ogawa, Y. Ogawa, K. Ohkubo,
Y. Oka, K. Sakurai, M. Sasao, K. Soto, K.N. Sato,
S. Tanahashi, Y. Taniguchi, K. Toi, T. Watari,

Institute of Plasma Physics
Nagoya University, Nagoya 464, Japan

Paper presented at 11th International Conference on Plasma Physics and Controlled Nuclear Fusion Research, Kyoto, Japan 13-20 Nov. 1986

Eleventh International Conference on Plasma Physics
and Controlled Nuclear Fusion Research
Kyoto, Japan, 13-20 November 1986

IAEA-CN-47/A-V-5

DISRUPTION CONTROL EXPERIMENTS USING LOCAL MODULAR MULTIPOLE-FIELD COILS

Abstract

Major disruptions are successfully suppressed in the JIPP T-IIU tokamak using compact local sets of l=3 modular multipole-field coils with m=3/n=2 dominant helical component $B_{h3/2}$. The stabilization is found to be attributed to the excitation of a 'mini-disruption' actively induced by $B_{h3/2}$ in advance of the catastrophic stage towards the major disruption. Quick but mild ergodization of m=2/n=1 magnetic islands by this mini-disruption impedes the temperature flattening, and avoids the 'two-step (pre- and major) disruption' leading to disruptive current termination. This system is easily applicable to larger tokamaks because of compact coil utilization, slow pulse application and quick stabilizing response. Using this coil system, the edge plasma control is also demonstrated by creating ergodic limiter configuration.

APPENDIX 3.1.1

Electric and Magnetic Structure of Edge Plasma in A Tokamak with Helical Magnetic Limiter

S. Takamura, N. Ohnishi, H. Yamada and T. Okuda

Department of Electrical Engineering
Nagoya University, Nagoya 464, Japan

Physics of Fluids, Vol. 30 (1987) 144

Electric and magnetic structure of edge plasma in a tokamak with helical magnetic limiter

S. Takamura, N. Ohnishi, H. Yamada, and T. Okuda

Department of Electrical Engineering,
Faculty of Engineering,
Nagoya University,
Nagoya 464, Japan

PACS numbers: 52.25.Fi, 52.40.Hf, 52.55.Fa

Abstract

A strong modification of plasma potential was observed at the plasma surface with the application of a helical field produced by a set of local helical coils. A structure of magnetic field lines was computed by a field line tracing code for a tokamak plasma. Such a field structure was examined in the experiment using electron beam probing. The potential formation and the magnetic structare are discussed referring to the scheme of an ergodic magnetic limiter.

APPENDIX 3.1.2

Control of Tokamak Edge Plasma by Static and Rotating Helical Magnetic Limiter

S. Takamura, H. Yamada and T. Okuda

Department of Electrical Engineering
Nagoya University, Nagoya 464, Japan

Paper printed in Nuclear Fusion

Control of Tokamak Edge Plasma by Static and Rotating Helical Magnetic Limiter

S. Takamura, H. Yamada, and T. Okuda

Department of Electrical Engineering,
Nagoya University, Nagoya 464, Japan

1. INTRODUCTION

Ergodic magnetic limiter (EML) has been considered in tokamaks for the purpose of impurity control owing to the uniform distribution of particle and heat fluxes to the wall along stochastic magnetic field and the resultant radiative cooled edge. This scheme has been considered innovative concept for an advanced tokamak reactor because of its mechanical simpleness compared with the usual poloidal divertors.

Experimental efforts on TEXT tokamak concerning EML have shown a reduction of metal impurity content associated with the decrease in edge electron temperature which has been confirmed by Thomson scattering. There it has been recognized that edge parameters become highly asymmetric; For example, the probe saturation current varies by more than a factor of 10 over the poloidal direction. However spatial structures of edge plasma parameters and their relation to the properties of magnetic field lines are not clear. In addition the presence of so called ergodic magnetic layer with some radial thickness has not been confirmed by numerical calculation with reasonable accuracy.

In the previous work [1] edge plasma modification, especially, plasma potential with the application of a strong helical field produced by a set of local helical coils (poloidal and toroidal mode numbers are m=10 and n=1) was

reported together with the structure of magnetic field lines computed by a field line tracing code for a simple tokamak model. In this code the structure of local helical coils was not exactly taken into account, neglecting the contribution of poloidal coil members although it was better approximation than the other work. The field structure thus obtained was examined in the experiment using electron beam probing.

In the present work the exact structure of local helical coils has been considered for obtaining mapping patterns of magnetic line of force. The connection of magnetic field line from the interior to the wall was found not to be uniform over the wall, but has a rather periodic structure, which is reflected on the particle flux to the wall. Detailed structures of edge plasma parameters have been obtained in the experiment. Such a basic study is quite important to understand edge plasma physics as well as the experiments on larger machines.

Non-uniform particle and heat fluxes to the wall has been avoided in the experiment by rotating helical magnetic field. Similar scheme has been considered as a wall lapping plasma [2]. Time lag of plasma response with respect to the rotating helical field is discussed in terms of plasma drift motions.

2. EXPERIMENTAL APPARATUS

The experiments have been performed on a small research tokamak CSTN-3 (major radius R_0=40cm, minor radius b=10cm, and limiter radius a=9cm). The vacuum vessel is made of stainless steel with the thickness of 2mm. Other characteristics of the machine is almost the same as those of CSTN-2 [1]. The plasma current I_p=1.1kA at top, the steady toroidal magnetic field $B_{\phi 0}$=875G. Eight sets of local helical coils were installed symmetrically on the torus. Each set is composed of two coils each of which has six pairs of conductors (poloidal mode number

m=6, radius r_h=10.8cm). In the case of quasi-static helical field one of two coils for each set is energyzed. The poloidal position and the current direction of each coil are chosen so that the toroidal mode number n may become one as purely as possible. On the other hand in order to drive rotating helical field both coils are energyzed by 15kHz power oscillator with 90 degrees phase difference.

3. MAGNETIC FIELD STRUCTURE

An ergodization of magnetic field lines was studied by a newly developed computer code for tracing of field lines in which the structure of local helical coils was taken into account exactly using Biot-Savart equation. Figure 1(a) shows a typical puncture plot of field lines. They start at every 5mm from r=4.5 to 9.5cm, and at every 36 degrees on the poloidal position. The toroidal turn of a field line is a hundred unless the field line intersects the wall at which the field line tracing is stopped. The overlapping of neighboring islands m=6,7,8 and 9 makes field lines stochastic at r>7cm. We note that in the area without dots near the wall the connection length of field line to the wall is very short. That is, the ergodization is broken down close to the wall, rather a periodic structure is generated. We call O point for this area. In other regions near the edge magnetic field lines go out slowly from an interior by making many toroidal turns. It is defined here as X point. The diffusion process of field lines is summarized in Fig.2, where averaged(over magnetic surface) radial excursions squared are plotted against the toroidal turn, taking the start position as a parameter. A linear dependence between these two quantities is not always found. It means that the stochastic motion observed here is not always described as an ideal diffusion although some theories employ magnetic diffusion coefficient. It is supposed to come from a quasi-coherent motion around a magnetic island,

which corresponds to "acceleration mode" in the study of chaos.

4. EXPERIMENTAL RESULTS AND DISCUSSION

4-1. Application of quasi-static field

With the application of helical field of nearly square wave with a pulse length of 300μs a drastic change in plasma potential has been detected around plasma periphery. A typical example is shown in Fig.2(b). A floating potential with respect to the vacuum chamber was measured with a Langmuir probe on the poloidal plane. A floating potential V_f is related to a plasma space potential V_s by the equation, $V_f \sim V_s - 3T_e$, for hydrogen plasma. In the present case a change in floating potential can be considered to be a change in plasma potential because no systematic change in electron temperature has been detected. A nearly concentric profile of V_f without external helical field shown in Fig.2(b-1) is strongly deformed to the profile shown in Fig.2(b-2). Let us discuss a correspondence between the puncture plot of field lines(Fig.2(a)) and the potential profile(Fig.2(b-2)). Without helical field the plasma potential is around +5 volts which is smaller than $3T_e$. When applying the helical field the plasma potential was found to go up in the area(O point) where the edge plasma contacts the wall through the field lines of short length. A rapid loss of electrons to the wall should be reduced to generate a positive plasma potential with respect to the wall, repelling electrons because of ambipolarity. Around X points the plasma potential goes down as shown in Fig.2(b-2), which may be explained as follows: Near X point magnetic field lines go out slowly. Electrons go easily along field lines. Thus interior electrons tend to flow out though not O but X point. This is the reason why the electron density increases so much near X point and decreases near O point. A recycling is not important in such a short duration of

discharge. An ion convection is not so sensitive to field lines as electrons. The difference in transport along field lines between electrons and ions gives rise to the decrease in plasma potential. It is possible that the potential at X point may be affected by the wall since a part of field lines have a chance to connect to the wall. But this is not the case for all the field lines through X point, and the collisional mean free path of bulk electrons λ_e (a few tens cm) is shorter than the field connection length. By these reasons the effect of wall does not penetrate there through ambipolarity.

Although the first purpose of EML is to distribute heat and particle flux uniformly over the wall, the measurements of ion saturation current flowing to a small plate parallel to the vacuum wall shows a strong poloidal asymmetry as is plotted in Fig.3. It shows that the plasma particles flow out through X points. This is closely related to the periodic magnetic structure observed very near the wall in the puncture plot of field lines. The density modulation thus observed results in a nonuniform wall loading. From the view point of wall erosion it should be avoided and a uniform wall loading is preferable.

4-2. Application of rotating helical field

As stated in the previous sub-section a non-uniform wall loading might bring a local erosion to the wall, which may become a serious drawback of EML scheme although other properties, like impurity shielding, may work well.

A simple way to avoid such a drawback is to rotate the helical field in the poloidal and toroidal directions. A time averaged wall loading is expected to be made uniform all over the wall although an instantaneous loading is not. A pair of local helical coil system has been employed to obtain a rotating helical field as mentioned before. The intensity of a time varying helical field decreases inside the vacuum vessel by one third compared with a static helical field owing to the

presence of metallic vacuum wall. A periodic change in particle flux has been detected as shown in Fig.4. The strongly nonuniform wall loading is now successfully replaced by poloidally more uniform time-averaged flux. In the same way a periodic change in plasma potential was also obtained. A result of phase-locked potential measurement is shown in Fig.5(a) as an equi-potential contour plot for every quarter period of oscillation. For the comparison quasi-static potential profiles corresponding to the same configuration of coil current are also shown in Fig.5(b). We can distinguish O and X points even in the case of rotating helical field. The comparison of Fig.5(a) with (b) gives a response time for plasma potential formation with respect the external helical coil current. In the above case the delay time is 33±3μs.

There are several origins which may bring a delay for potential formation. The clearest one is the field penetration time τ_1 through the metallic vacuum vessel and is given by $\tau_1=d/(2\pi f\sigma/\mu)^{1/2}$, where d is the wall thickness, μ and σ are the permeability and the conductivity of wall material. It gives $\tau_1=13\mu s$, while a magnetic probe measurement gives a value of 13±2μs very close to the former prediction. The second origin is the penetration time of field into the plasma with a static magnetic field. It is determined by the plasma conductivity due to electron-ion and electron-neutral collisions. In fact, however, is this time so short that we can not detect, that is, less than 1μs. The most physically important time is the potential formation one inside the plasma, responding to the application of helical field. Here we remind the discussion on the static case. The potential formation at X point need for electrons to be supplied from the interior to X point along stochastic magnetic fields. As inferred from Fig.3 about ten toroidal turns are necessary for the field line to have the radial excursion of around 1cm near the edge. Electron thermal velocity $v_{te}=(2T_e/m_e)^{1/2}$ is 1.32×10^8cm/s for T_e=5eV, and the time to need for some thermal

electrons to make ten turns around the torus $\tau_c=10\cdot 2\pi R_0/v_{te}$ is 19μs. The sum of τ_1 and τ_c is 32μs, which is close to the observed value. But the situation is not so simple. The delay time was found to depend on the direction of helical field rotation. The results for various conditions are summarized in TableI, where the twist of helical field coils is made so that it may have a resonance with that of helix due to plasma current. From this table it is concluded that the delay time is so short when the rotation of helical field is in the direction of electron diamagnetic drift. The diamagnetic drift motion of electrons is assumed to enhance the electron convection to poloidally moving X point in this case. In fact the electron diamagnetic drift velocity given by $v_{de}=|\nabla p/nB|$ is roughly equal to the rotation velocity v_ω at r~8cm, that is, $v_{de}=1.1\times10^5$cm/s and $v_\omega=1.5\times10^5$cm/s, where the scale length of pressure gradient is estimated to be 4cm in the experiment. When the rotation is in the direction of ion diamagnetic drift, then the drift motion of electrons is opposite to the direction of field rotation and does not enhance the electron convection to the X point. Then the electrons have to be supplied entirely through the stochastic magnetic field lines as mentiioned before.

5. CONCLUSIONS

In this paper an exact configuration of local helical coils was taken into account for the first time to obtain properties of magnetic field lines in the so called EML scheme. the first conclusion from puncture plots of field lines on a poloidal plane is that the ergodization caused by overlapping of not main and the first sideband modes but higher order sidebands mode is quite important especially in a small coil current. The second one is that the ergodization is broken down close to the wall, while a periodic structure in the poloidal direction is generated. The conclusion from the field

diffusion calculation is as follows: Even in the region where puncture points seem to be ergonized stochastic motions of field lines are not always ideal diffusion. There may be a contribution from a quasi-coherent motion around a magnetic island.

The discussion on a correspondence between a puncture plot of field lines and a modification of plasma potential profile was given. It is concluded that a potential increase around O points comes from a short connection length of field lines from wall to wall, and that a potential decrease around X points comes from a predominant electron transport along stochastic magnetic field.

The wall loading when applying static helical field was found to be extremely nonuniform along the poloidal direction. This comes from the fact that plasma particles flow out predominantly through X point. And this is also predicted from the puncture pattern of field lines near the wall, which has already mentioned before as breakdown of ergodicity.

A rotating helical field was succeeded in making a time averaged loading to the wall uniform along the poloidal and the toroidal direction. This scheme has a potential of advanced EML and should be tested in a tokamak of higher temperature.

A delay time of plasma response with respect to the coil current was discussed in terms of trivial penetration time through the wall and the electron motion corresponding to the helical configuration. In the latter the electon transport from the interior to the X points along the stochastic magnetic field determines the response time. When the rotation is in the direction of electron diamagnetic drift and the rotation velocity is comparable to the drift velocity, the diamagnetic motion of electrons accelerate the potential formation, which may come from electron supply in the poloidal direction.

In our laboratory a new machine HYBTOK-Ⅱ has been constructed for the purpose of detail study of EML. Various diagnostic techniques for edge plasma are prepared. The current objectives are the observation of electron temperature profile in the poloidal direction and the impurity shielding. In near future rotation of helical field will be tried.

References

[1] S.Takamura, N.Ohnishi, H.Yamada and T.Okuda, Phys. Fluids 30 (1987) 144.

[2] T.Kawamura, Y.Abe and T.Tazima, J. Nucl. Mater. 111&112 (1982) 268.

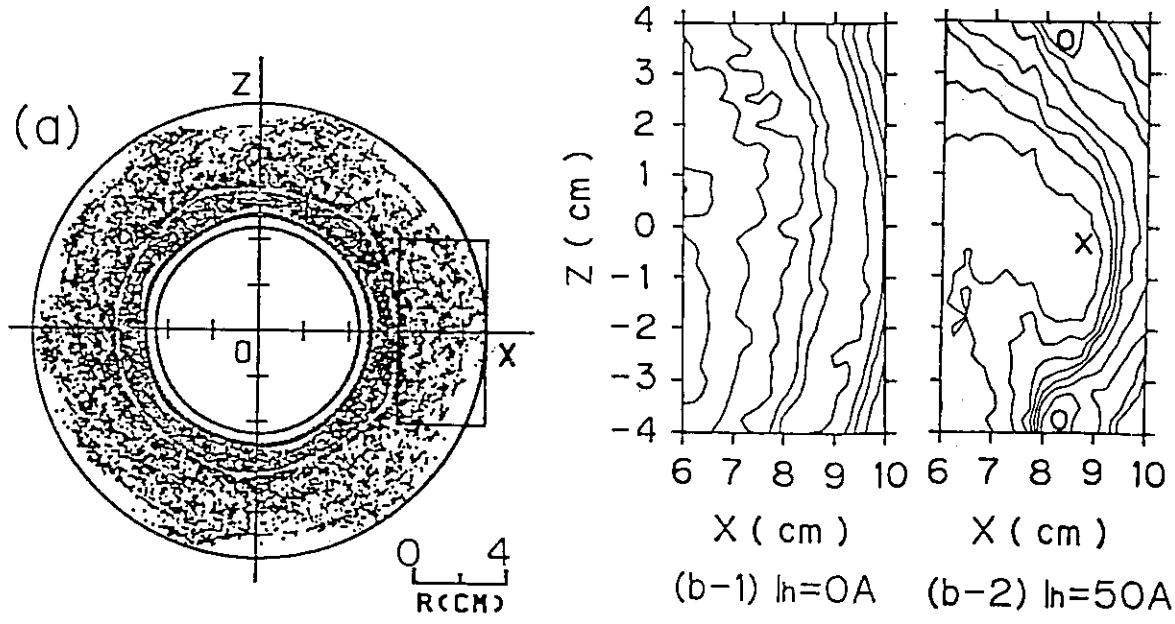

Fig. 1 Interrelation between a puncture plot of field lines(a) and a contour plot of electrostatic floating potential(b). (a) I_n=50A. Field lines are traced not only along CW direction but also CCW toroidally. (b) 2V/line. (b-1) I_n=0A, (b-2) I_n=50A.

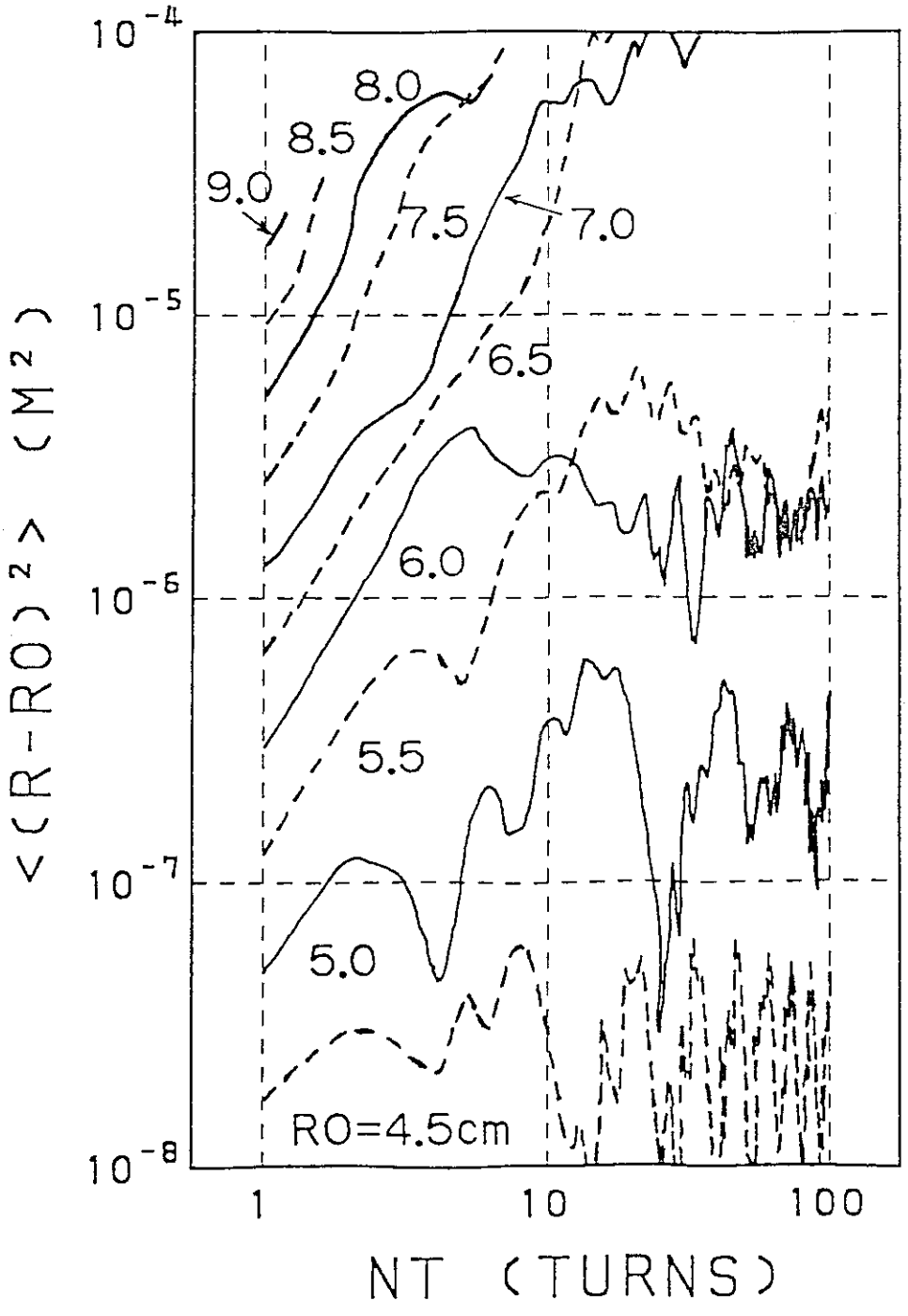

Fig.2 Magnetic diffusion processes shown by radial excursions squared of field lines with respect to the toroidal turn taking the start position as a parameter. Averaging is done for ten poloidal start positions. I_h=50A.

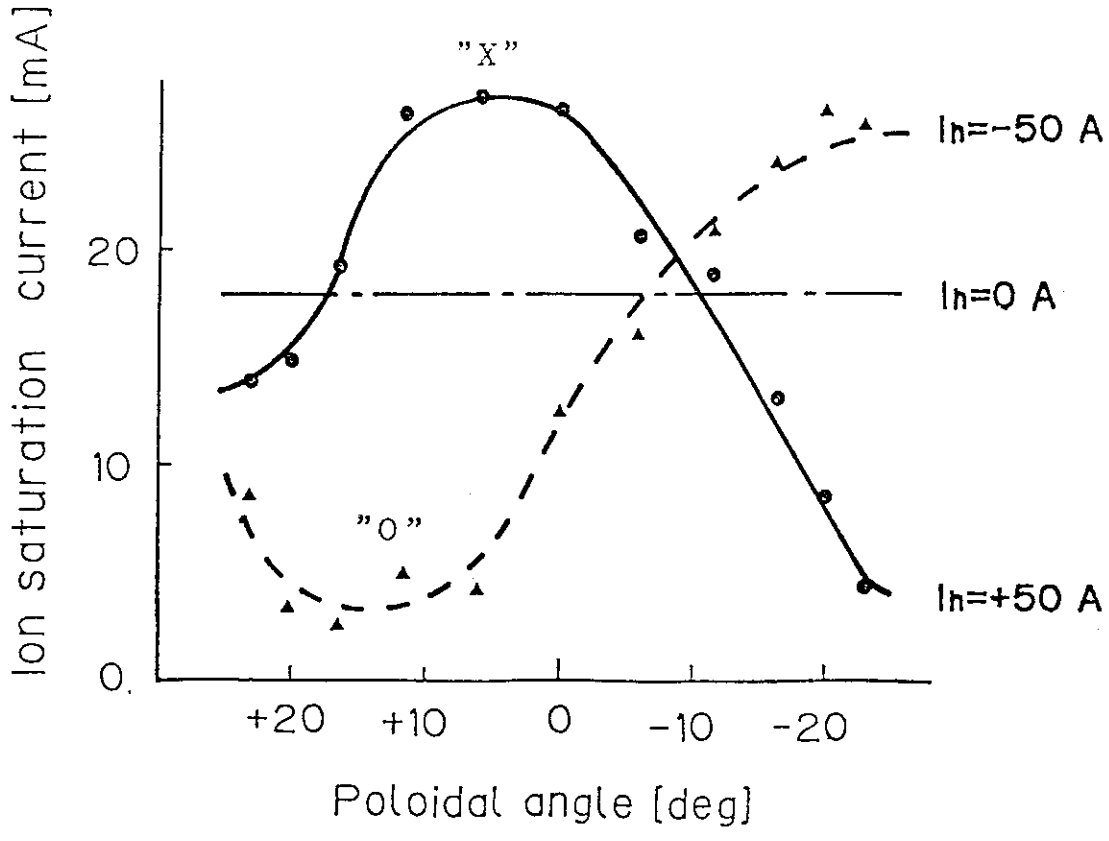

Fig.3 Poloidal profile of radial ion saturation current at r=10cm, taking the direction of helical coil current as a parameter. X and O points are inferred from Fig.1(a).

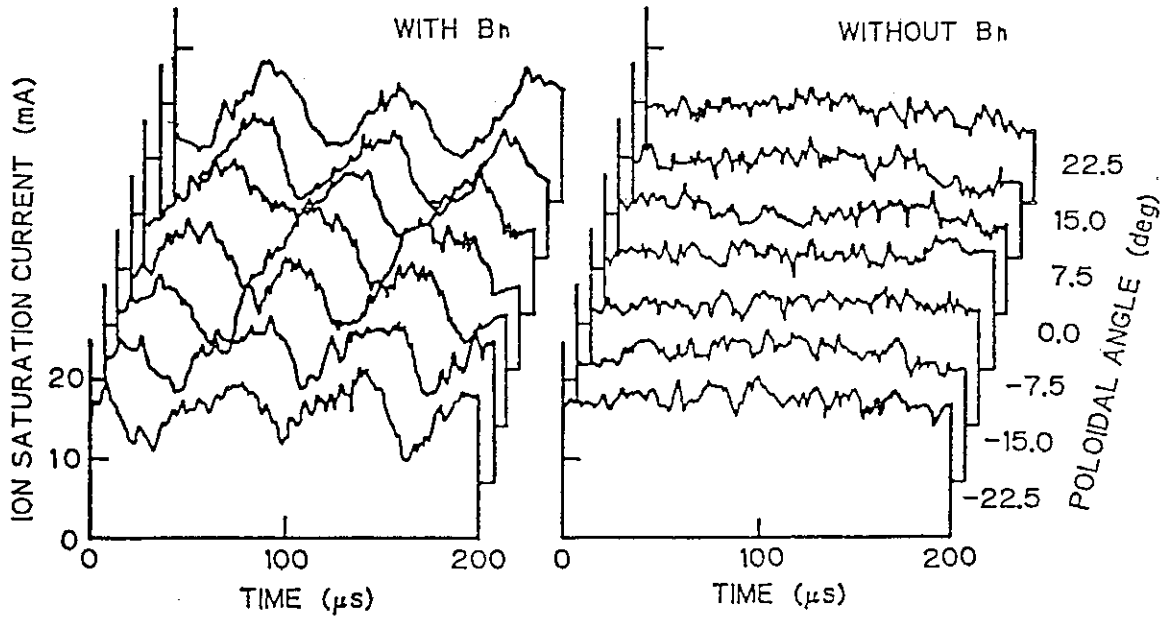

Fig.4 Time traces of radial ion saturation current at r=10cm, taking poloidal angle as a parameter with and without rotating helical field.

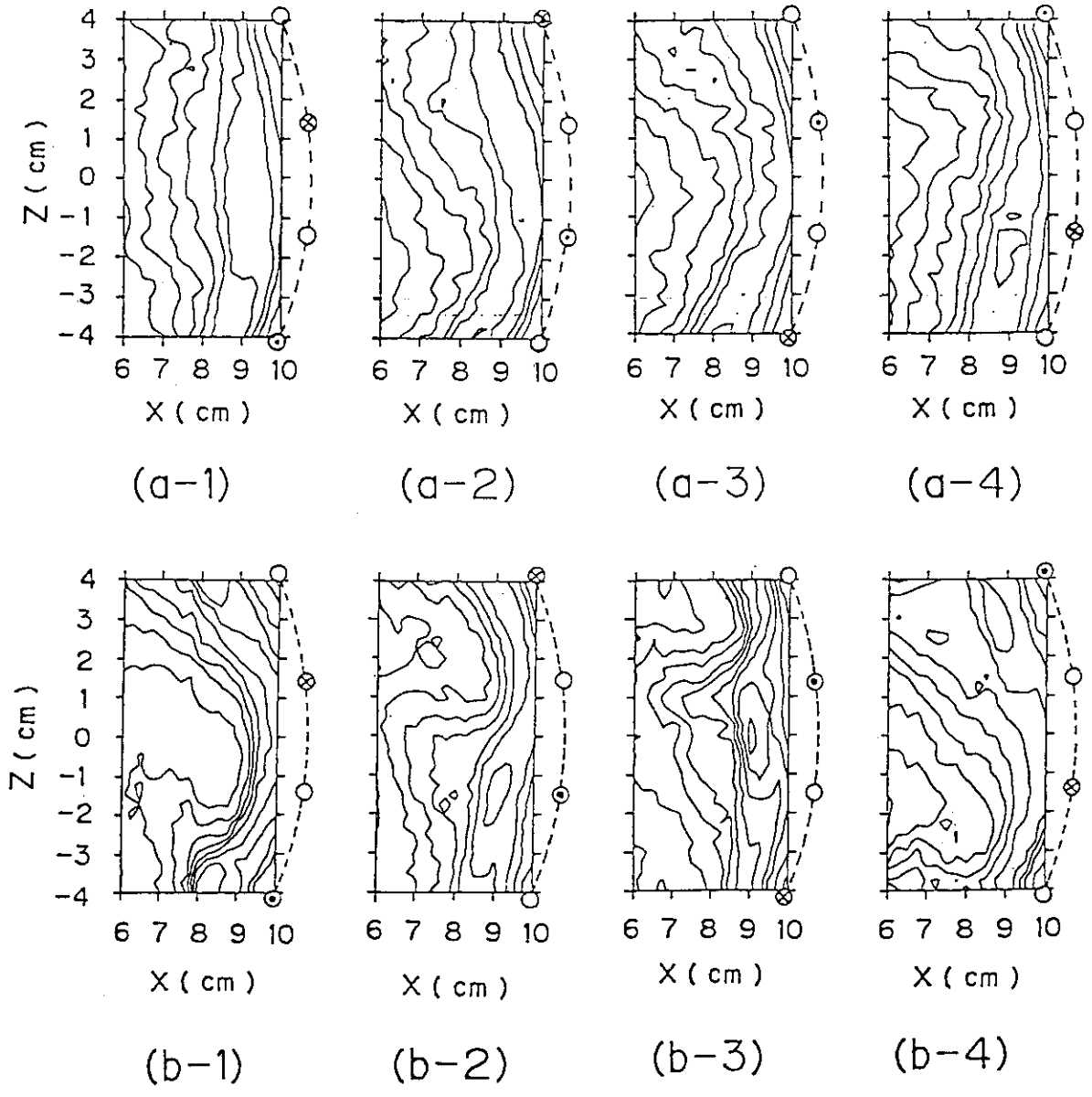

Fig.5 Two-dimensional contour plots of floating potential for rotating(a) and quasi-static(b) helical fields. 2V/line. The direction of coil current is indicated by dot or cross. Instantaneous coil current and its direction at upper plots corresponds to the configuration of coil current at lower plots respectively. Quasi-static helical coil current is 50A, and alternating one is $50A_{rms}$. B_ϕ:CCW, and I_p:CCW.

B_ϕ	I_p	Delay Time (μs)	
		Ion Diamag.	Electron Diamag.
+	+	33±3	15±5
+	-	35±5	18±3
-	+	38±8	15±10
-	-	30±5	18±10

Table 1. Response time for plasma potential with respect to the external helical coil current. Rotation of helical field is shown in terms of ion and electron diamagnetic drift. The directions of toroidal field and plasma current are indicated by + (CCW) and - (CW).

APPENDIX 3.1.3

Effect of an Ergodic Magnetic Limiter on Particle and Heat Flux Control

T. Kawamura and T. Ono*

Institute of Plasma Physics
Nagoya University, Nagoya 464, Japan

* Permanent address; Depertment of Physics
Nagoya University, Nagoya 464, Japan

Effect of an Ergodic Magnetic Limiter on Particle and Heat Flux Control+

T. Kawamura and T. Ono*

Institute of Plasma Physics, Nagoya University

Nagoya 464, Japan

Abstract

The important aspects needed for performance of an ergodic magnetic limiter are discussed. An example of distribution of magnetic diffusion coefficient calculated numerically is shown, and the characteristic nature of an ergodic scrape-off layer is pointed out. The items for innovation studies are summerized.

1. Introduction

The Ergodic Magnetic Limiter[1-6] is expected to become an alternative concept to a magnetic divertor on particle and heat flux control of a toroidal device. However the nature of the scrape-off layer produced by an ergodic magnetic limiter has not been known so much, and the effectiveness of this concept has not been proved thus far, therefore we should make an

---

+ Summary for Tokamak Innovation Study Topics (Nov. 1986)

* Permanent address; Department of Physics, Nagoya University, Nagoya 464, Japan

effort to investigate the physical characteristics of the ergodic scrape-off layer both theoretically and experimentally.

The anticipated effect of an ergodic magnetic layer is to disseminate the particle and heat flux flowing out from the main plasma uniformly all over the surface of the first wall facing the main plasma in order to reduce the wall load per unit area.

To this end the particles and heat diffusion across the magnetic field in the scrape-off layer should be as uniform as possible, therefore, it is a key issue how to produce a scrape-off layer with uniformly ergodized magnetic fields using a set of subsidiary helical coils. If this is difficult, we should prefer the concept of rotating islands proposed as a wall-lapping plasma.[7] In this note we discuss the characteristic aspects needed for performance of an ergodic magnetic limiter with respect to particle and heat flux control.

2. Diffusion in an Ergodic Magnetic Layer

In the case of a solid limiter or a magnetic divertor the magnetic field lines in the scrape-off layer are connected with the solid surface at distances of the order of a connection length of magnetic field lines. Then in such a scrape-off layer a net plasma flow along the field lines exists, therefore the depth profiles of plasma density and temperature in the scrape-off layer are approximately given by an exponential

function. On the other hand, in the case of an ergodic limiter a magnetic field line in the scrape-off layer generally reaches the wall surface after turning many times around the torus, so that there would be no remarkable net flow along the field lines.

In an ergodic magnetic scrape-off layer the particle transport is attributed mainly to the radial diffusion. The radial charged particle diffusion is considered to consist of the synthesis of the guiding center diffusion across the magnetic fields due to the classical collisions or anomalous fluctuations of the electromagnetic fields and the one due to the radial diffusion of a magnetic field line itself. The particle diffusion coefficient due to the random walk of a magnetic field line is estimated as $v_T D_m$ where $D_m = \langle(\Delta r)^2\rangle/\Delta z$ is the magnetic diffusion coefficient, Δr is a radial displacement of a wandering magnetic field line in the distance Δz along the toroidal direction, the brackets mean an ensemble average, and v_T is the parallel thermal velocity of charged particles[8].

The example of magnetic diffusion coefficient D_m calculated numerically for the case of the R-tokamak, which was designed in IPP-Nagoya, is shown in Fig. 1. In Fig.2 are shown the ion diffusion coefficients $D_E = v_T D_m$ due to the ergodic magnetic field lines for different temperatures of the scrape-off plasma together with the anomalous (Bohm) diffusion coefficient. From these calculations the radial diffusion in

the effectively ergodized magnetic field seems to be comparable with an anomalous diffusion coefficient.

3. Scrape-Off Layer Generated by an Ergodic Magnetic Limiter

Since no net plasma flow along magnetic field lines would be expected in the ergodic scrape-off layer as mentioned in Sec.2, we have different structure of the scrape-off plasma from the one of the limiter or divertor plasma. As a first point the density profile in the ergodic scrape-off plasma would be flatter than the one due to the limiter or divertor, because the net transport of particles is decided only through the radial diffusion across the magnetic fields. If we assume the uniformity of diffusion constant D_E in the ergodic scrape-off layer the density profile would reach a linear function of the scrape-off depth in the steady state and would give a different effect on the ionization of impurities released from the first wall in contrast to the density profile of an exponential function in the case of the limiter or divertor, that is, the neutral impurities released from the first wall would be ionized at points closer to the first wall, and this would enhance more the screening effect of the scrape-off layer on impurity contamination of the main plasma[9].

The heat transport in an ergodic scrape-off layer is also expected to be anomalous, therefore, the electron temperature in front of the first wall would be considerably reduced.

In the experiment with the JIPPT-IIU device, which has a set of local helical coils for an ergodic layer experiment, the decay of the edge electron temperature after a helical current operation was observed.[10] If plasma ions stay in a scrape-off layer a longer time than the energy equipartition time between ions and electrons, the energy of an ion impinging on the first wall would be reduced and the impurity release due to sputtering would also be suppressed. However, these key points should be assessed in more detail according to the realistic parameters of a toroidal device and a system of subsidiary helical coils producing an ergodic scrape-off layer.

4. Discussion

The items for innovation studies of an ergodic magnetic limiter are summerized as follows:

(a) to produce an ergodic magnetic scrape-off layer as uniformly as possible, where a magnetic diffusion coefficient D_m should be uniform in both poloidal and toroidal directions;

(b) to investigate how far a magnetic field line starting just outside the main plasma travels until it reaches the first wall. This becomes a measure to see whether the ion energy in the scrape-off layer can be reduced to the order of the electron temperature or not;

(c) to assess the first wall materials of low-Z values which

should be needed for performance of an ergodic magnetic limiter and to investigate the redeposition effect of impurities onto the first wall.

If it is difficult to realize the item (a), we would prefer the rotating islands like a proposal of a wall-lapping plasma[1,7]. The item (b) is needed to make sure the reduction of energy of an ion impinging on the first wall. If the distance of a field line starting at a point outside the main plasma to the first wall is shorter than the energy equipartition mean free path between ions and electrons, the ion temperature may not be reduced to the level of the electron temperature. The effect of an ergodic magnetic limiter should be performed only when the item (c) is associated. The problem of impurity redeposition becomes more important when we adopt the low-Z coating or the in-situ carbonization of the metallic first wall.

Since the density profile of the ergodic scrape-off plasma becomes rather flat as mentioned in Sec.3, the ionization mean free path of neutral impurities released from the first wall is short as compared with the one in the limiter or divertor case, the fact of which promotes the impurity redeposition[9]. These points should be clarified quantitatively in future work.

References

1) W. Feneberg, in 8-th Europian Conf. on Contr. Fusion and Plasma Phys. 1 (1977) 4.

2) W. Feneberg and G. Wolf, Nucl. Fusion 21 (1981) 669.

3) N. Ohyabu, Nucl. Fusion 21 (1981) 519.

4) T. Ohkawa, GA-A 16051 (1980).

5) T. Kawamura, Y. Abe and T. Tazima, J. Nucl. Mater. 93 & 94 (1980) 192.

6) T. Kawamura, IAEA-TECDOC-373 (1986) 49.

7) T. Tazima and M. Sugihara, JAERI-M 8390 (1979)

8) T. H. Stix, Nucl. Fusion 18 (1978) 353.

9) T. Kawamura, T. Ono, S. Takamura and A. Miyahara, J. Nucl. Mater. 145 & 146 (1986) in press.

10) K. Yamazaki et al., IAEA-CN-47/A-V-5, Kyoto(1986).

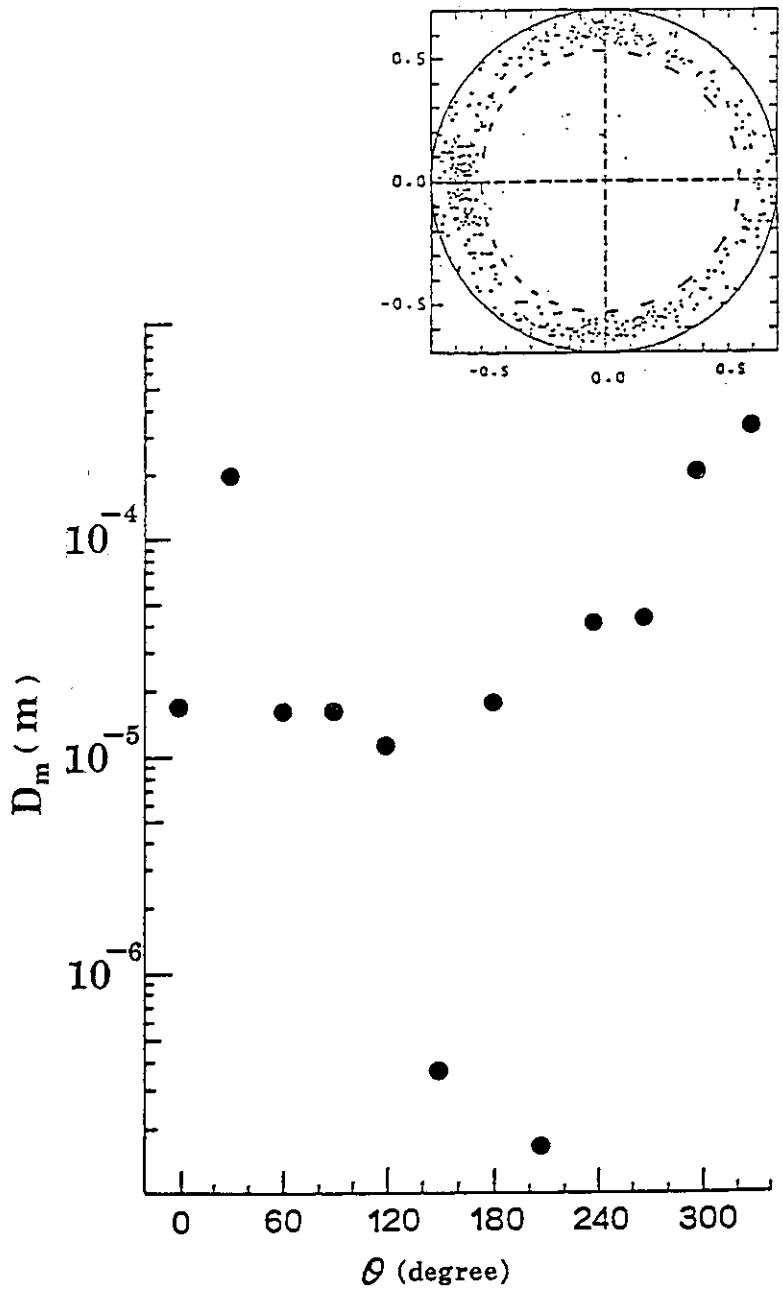

Fig. 1 Magnetic diffusion coefficient versus poloidal angle θ. The coefficient values are calculated using eq. $D_m = \langle(\Delta r)^2\rangle/\Delta z$ for the tadius r = 0.65 m, added helical field with the mode number (n, 1) = (1, 3) and the constant current I_H = 10 kA in opposite directions, and for the parameters[5] referred to the R-tokamak design(major radius R_0 = 2.1 m : minor radius of the main plasma a_p = 0.6 m : wall radius a_W = 0.7 m : toroidal field strength B_0 = 5 T : plasma current I_p = 1.5 MA).

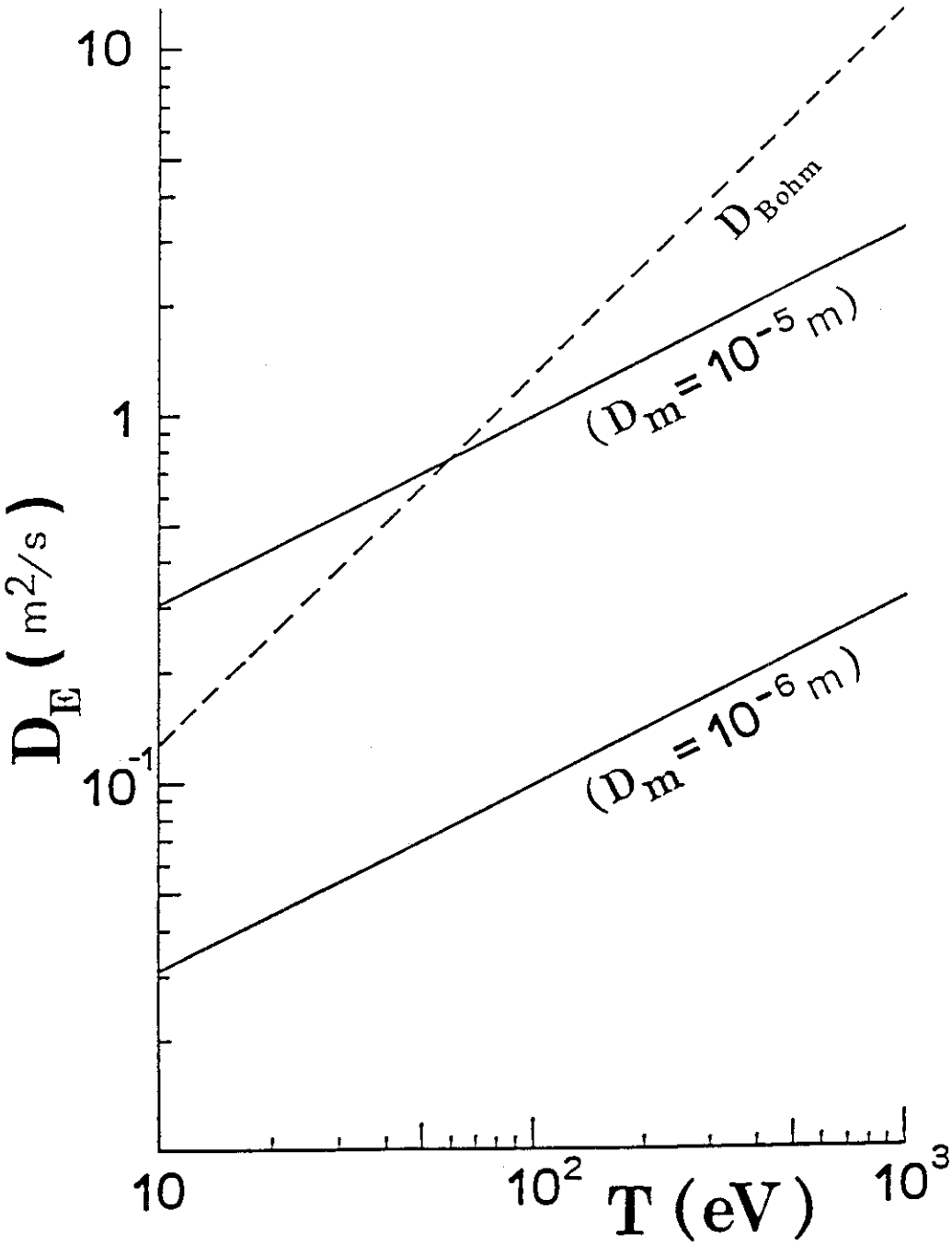

Fig. 2 Hydrogen ion diffusion coefficient versus temperature in an ergodic magnetic layer. The calculations for the coefficient are made using eq. $D_E = v_T D_m$ for appropriate values of D_m obtained. The Bohm diffusion coefficient for the magnetic field B_o = 5 T is also shown for comparison.

APPENDIX 3.1.4

Resonant Helical Divertor Experiments

A. Mohri

Institute of Plasma Physics

Nagoya University, Nagoya 464, Japan

2.3 (b)

IPP-NAGOYA

Resonant Helical Divertor Experiments

by A.MOHRI

The first resonsnt helical divertor (RHD) experiments were done in TEXT (Texas) with m=7, n=2 helical magnetic islands and a vertical scoop limiter module. Data from these studies show a reduction in the thermal loading of the leading limiter surface by as much as 50 percent and increases in the steady state particle collection efficiency of 200 percent or more. Control of the central density was demonstrated during these experiments when RHD induced effects created modifications in the edge refueling processes and enhanced the particle exhaust rate through the scoop limiter aperture.

Full scale RHD experiments have recently been initiated in JIPP T-IIU (Nagoya) as part of the helical island divertor experiment (HIDEX). This work will concentrate on evaluating the effectivness of islands for thermally shielding a pump limiter blade and will test the efficiency of particle ducting by islands during high power, auxiliary heated, plasma discharges. The JIPP T-IIU local helical coils produce m=3, n=1 magnetic islands. Helical coil currents of 5-10 kA are estimated to produce radial island widths of 1.5-2.0 centimeters. The coils are modelled in a toroidal system with a magnetic field line mapping code. The code is used to predict the width and degree of coherence of the islands for increasing helical coil current and beta poloidal. This data is used with experimental data obtained from a Langmuir probe array and two visual imaging systems (one in the visable spectral range and one in the infrared range) to measure the island properties at the pump limiter port.

A pump limiter blade design has been selected based on the mapping code data. Design refinements will continue for several months as experimental data is acquired. Presently, the entire pump limiter system, with the exception of the blade and the neutral gas duct tunnel, is in operation on JIPP T-IIU. This system is comparable in size with the ALT-I pump limiter at TEXTOR and has the capability of two point biasing with potentials of up to ± 1kV. Pump limiter operation is planned for January 1988 with full power auxiliary heated RHD tests beginning shortly thereafter. During these high power density tests implications for controlling impurities will be investigated.

Extrapolation of the TEXT and the ALT-I results indicate that it may be possible to exhaust as much as 30 percent of the particles escaping the plasma core with the JIPP T-IIU RHD system.

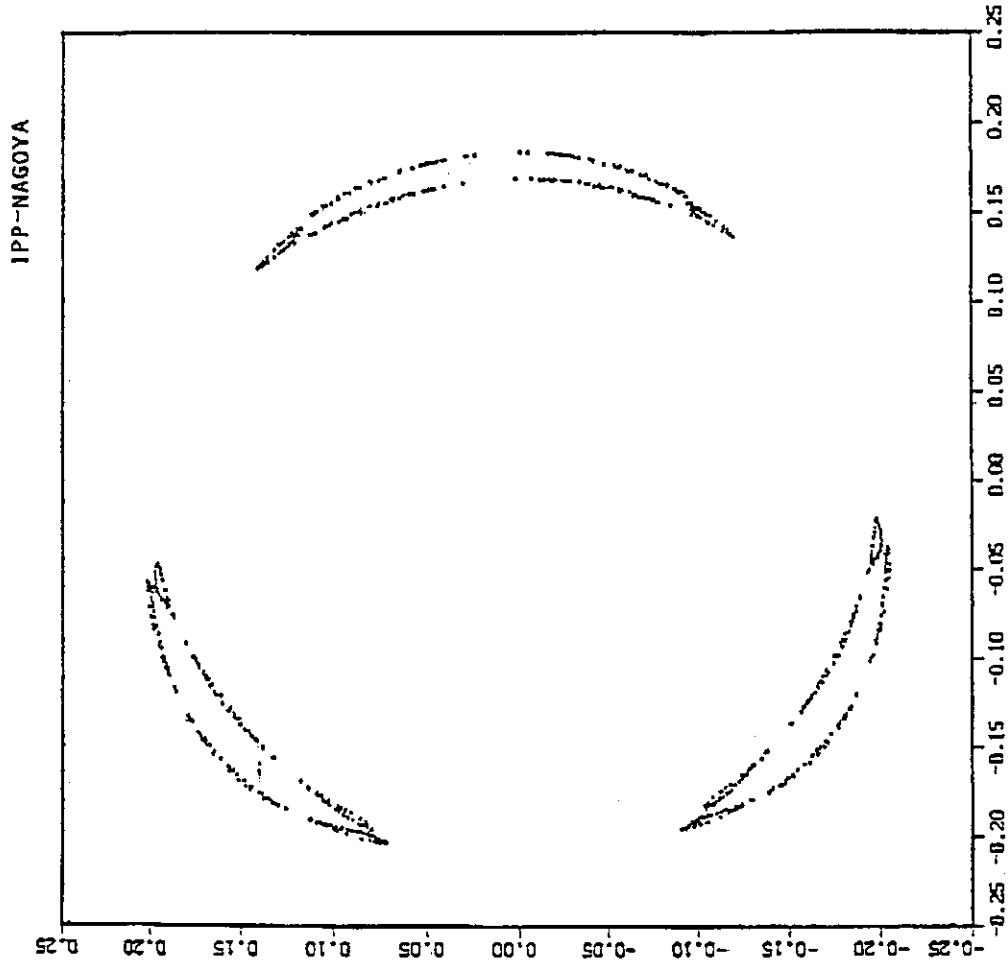

Fig. 1 Helical magnetic island formed in NTX (JIPP TIIU)

IPP-NAGOYA

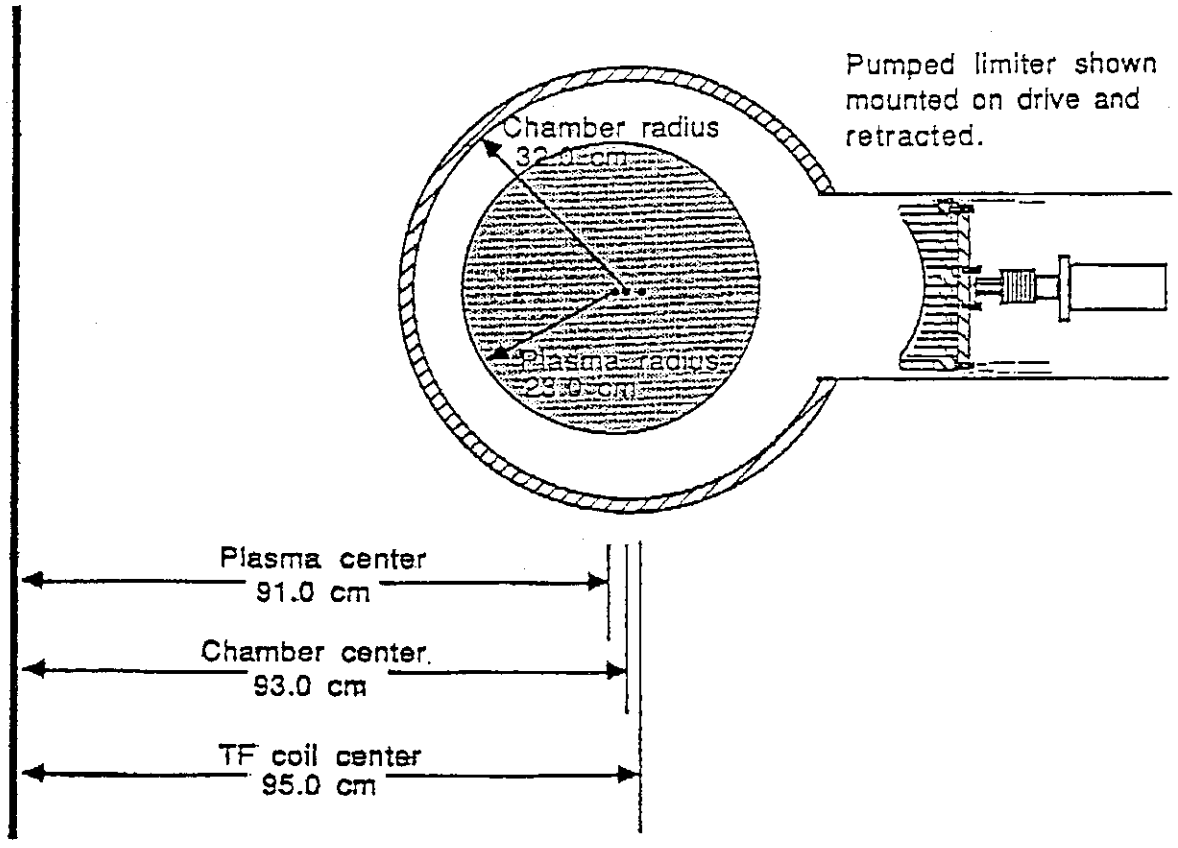

Fig. 2 HIDEX-NTX Tokamak Dimensions

APPENDIX 3.2.1

Characteristics of Radiatively Cooled Edge Plasma for Fusion Experimental Reactor - Conceptual Design Study of FY86 FER

T. Mizoguchi*, M. Sugihara, S. Yamamoto
N. Fujisawa and FER design team

Japan Atomic Energy Research Institute
Naka Fusion Research Establishment
Naka-machi, Naka-gun, Ibaraki, Japan

* On leave from Hitachi, Ltd.

Radiatively Cooled Edge

(1) Introduction

The self-limited impurity production may be achieved by means of radiative cooling at the boundary edge. In order to avoid deteriation of the global energy confinement, the energy conversion must be done in a relatively narrow portion of the edge plasma and the accumulation of impurities in the center of plasma must be prevented. The first question, in order to obtain proper conditions, is how much plasma volume is required to obtain a high enough radiation level. The width of the radiatively cooled edge layer can be expressed as $\Delta_r = P_{rad} / [f_i\ n_e^2\ L\ 4\pi^2\ R\ a\ \kappa]$, where n_e is the electron density, f_i is the impurity concentration, L is the emissivity of the impurity, R is the plasma major radius, a is the plasma minor radius and κ is the elongation. The required Δ_r is estimated about 18-35 cm for $f_i \sim 0.01$-0.02 in case of $n_e \sim 5 \times 10^{13}$ cm^{-3}, $L \sim 6 \times 10^{-25}$ w·cm^3, $R \sim 5$ m, $a \sim 1.2$ m, $\kappa \sim 1.6$ and $P_{rad} = 200$ MW. However, the emissivity of the impurity should be much larger if proper diffusive/convective transport is applied instead of corona equilibrium model. Thus such a wide layer of Δ_r may not be neccessary.

The second question is what type of plasma transport is required to form an attractive cooled edge. As it discussed at the next section the anomalous diffusion coefficient of impurities is about (0.4-2.0) m^2/s in medium size and large size tokamak devices including JET and JT-60. However, the property of convective inward flow velocity is not clear. Furthermore transport of scrape-off plasma is not known. In this study, we assume that diffusion property in the scrape-off is a Bohm-like diffusion such as $D^A = D^A_\kappa = \chi_e = \chi_i = D_B$ or $D_B/2$, where D_B is the Bohm diffusion coefficient.

APPENDIX 3.4.1

Helium Burial

M. Saidoh and R. Yamada

APPENDIX 3.4.2

Oxygen Gettering

T. Okazaki*

APPENDIX 3.4.3

In-situ Boron Deposition

T. Abe and T. Okazaki*

Japan Atomic Energy Research Institute
Naka Fusion Research Establishment
Naka-machi, Naka-gun, Ibaraki, Japan

* Energy Research Laboratory, Hitachi, Ltd.

Helium burial

- Required Work for Helium-Pumping by In-Situ Metal Deposition -

M. Saidoh and R. Yamada (JAERI)

Helium ash exhaust is one of the most important problems in D-T fusion tokamak reactors, so that many methods have been proposed for this purpose. The use of a helium retention wall as a helium-pumping means seems to be attractive because no vacuum ducts or pumps are needed. An improved system of this concept has been proposed in which helium is removed in-situ by trapping in freshly deposited metal surface layers of a limiter or divertor (1).

Available data, however, are extremely limited and important parameters used for the design study so far are estimated values based on extrapolation from limited experimental data and from theoretical arguments. Therefore key required work for this concept are experimental work related on materials to obtain necessary values. The experiments should be carried out by using deposited materials because no information on the properties of deposited materials relevant to helium-pumping is practically available. The data base of materials required are: (1) helium saturation trapping levels; (2) helium release versus temperature; (3) self-sputtering yield; and (4) thermophysical and mechanical properties of deposited materials containing trapped helium.

Further design work should also be continued.

References

(1) J. N. Brooks and R. F. Mattas, J. Nucl. Mater. 121 (1984) 392

Oxygen Gettering

T. Okazaki (Hitachi, Ltd)

The active removal of oxygen from plasma is one of the important issues in the present fusion facilities. In-situ oxygen gettering may be an effective method to reduce the oxygen level.

In the next generation fusion reactors such as INTOR or the commercial reactor, impurity exhaust system will be installed. The impurities such as oxygen are continuously pumped out through the system during the operation. Therefore, the amount of the impurities such as oxygen is decreased. This point is different from that of the present fusion facilities which do not always have such exhaust system of impurities. In the sense, the in-situ oxygen gettering method will not be necessarily needed to reduce the impurities from the plasma.

In-situ Boron Deposition

T. Abe, T. Okazaki* (JAERI, Hitachi, Ltd*)

In the fusion reactor, it is necessary to alleviate the problems associated with first wall design such as surface erosion and impurity production. The in-situ Boron coating of the first wall seems to be attractive method because deposited Boron films are made at low deposition temperatures, compared with those of carbon, and it makes the local deposition easier.

Available data, however, are limited and hence it is necessary to have experimental study of the material property on the diborane decomposition rate, erosion rate of Boron layer during the start-up phase and the mechanical stability of the Boron layer during the DT burn phase.

Unfortunately, diborane gas used in the Boron layer deposition is extremely toxic and experimental study on the Boron coating, mentioned above, is not planned in our country.

APPENDIX 4.2.1

2-D Fluid Model Divertor-Scrape-Off Layer Code

T. Hirayama

Japan Atomic Energy Research Institute
Naka Fusion Research Establishment
Naka-machi, Naka-gun, Ibaraki, Japan

3. Refinement to the model being implemented

3.1 2-D Fluid Model Divertor-Scrape Off Layer Code

T. Hirayama (JAERI)

The region including the scrape-off plasma, the periphery of the main plasma and the divertor plasma is analyzed by the two-dimensional fluid code.

The outline of the code is described as follows. The assumptions used in the code are:

(i) the rectangular toroidal coordinates (ψ, θ, ζ) is used with the toroidal axisymmetry ($\partial/\partial\zeta = 0$),

(ii) the charge neutrality is kept,

(iii) the radial flow velocity u_ψ is composed of the classical and anomalous terms,

(iv) the plasma equilibrium is also given.

The basic equations are following,

• Continuous equation

$$\frac{\partial n_a}{\partial t} + g^{-1/2}\left[\frac{\partial}{\partial\psi}\left(n_a u_\psi |\nabla\psi| g^{1/2}\right) + \frac{\partial}{\partial\theta}\left(n_a u_\theta |\nabla\theta| g^{1/2}\right)\right] = S_a \qquad (1)$$

• Momentum balance equation

$$\frac{\partial u_{/\!/}}{\partial t} + \left[u_\psi |\nabla\psi| \frac{\partial u_{/\!/}}{\partial\psi} + u_\theta |\nabla\theta| \frac{\partial u_{/\!/}}{\partial\theta}\right]$$

$$= -\frac{1}{\Sigma m_a n_a}\left[\frac{B_\theta}{B}|\nabla\theta| \frac{\partial}{\partial\theta}\Sigma P_a - \Sigma F^{vis}_{/\!/,a}\right.$$

$$\left. + \Sigma R_{/\!/,a} - \Sigma m_a S_a u_{/\!/}\right] \qquad (2)$$

(species: a = e and H)

• Ion heat balance equation

$$\frac{3}{2}\frac{\partial P_a}{\partial t} + \frac{5}{2} g^{-\frac{1}{2}} \left[\frac{\partial}{\partial \psi} \left(P_a u_\psi \, |\nabla\psi| \, g^{+\frac{1}{2}} \right) + \frac{\partial}{\partial \theta} \left(P_a u_\theta |\nabla\theta| \, g^{\frac{1}{2}} \right) \right]$$

$$= - g^{\frac{1}{2}} \left[\frac{\partial}{\partial \psi} \left(q^a_\psi \, |\nabla\psi| \, g^{\frac{1}{2}} \right) + \frac{\partial}{\partial \theta} \left(q^a_\theta \, |\nabla\theta| \, g^{\frac{1}{2}} \right) \right]$$

$$+ u_\psi \frac{\partial P_a}{\partial \psi} |\nabla\psi| + u_\theta \frac{\partial P_a}{\partial \theta} |\nabla\theta|$$

$$+ Q_a + W_a^{vis} + \left(S_{Ea} - u_a \cdot R_a + \frac{m_a}{2} u_a^2 S_a \right) \qquad (3)$$

• Electron heat balance equation

$$\frac{3}{2}\frac{\partial P_e}{\partial t} + \frac{5}{2} g^{-\frac{1}{2}} \left[\frac{\partial}{\partial \psi} \left(P_e u_\psi \, |\nabla\psi| \, g^{+\frac{1}{2}} \right) + \frac{\partial}{\partial \theta} \left(P_e u_\theta \, |\nabla\theta| \, g^{\frac{1}{2}} \right) \right]$$

$$= - g^{-\frac{1}{2}} \left[\frac{\partial}{\partial \psi} \left(q^e_\psi \, |\nabla\psi| \, g^{+\frac{1}{2}} \right) + \frac{\partial}{\partial \theta} \left(q^e_\theta \, |\nabla\theta| \, g^{\frac{1}{2}} \right) \right]$$

$$+ u_\psi \frac{\partial P_e}{\partial \psi} |\nabla\psi| + u_\theta \frac{\partial P_e}{\partial \theta} |\nabla\theta|$$

$$- \Sigma Q_a + F_e \cdot j/e \, n_e + \left(S_{Ee} - u_e \cdot R_e \right) \qquad (4)$$

These equations are solved by the finite elements method in the real plasma equilibrium and real geometry. Main analytical object of this code is JT-60 in JAERI and the code can also be applied to the next generation fusion reactor such as FER and INTOR.

This code is under development and will be completed at the end of March. The coupling between this code and the two-dimensional neutral Monte-Carlo code will be done until the end of this year. Furthermore this code has the plan to be extended to (a) the analysis of the limiter discharge mode and (b) the coupling of this code and the two-dimensional Monte-Carlo impurity code.

APPENDIX 4.1.1

2-D Neutral Monte-Carlo Code

K. Shimizu

Japan Atomic Energy Research Institute
Naka Fusion Research Establishment
Naka-machi, Naka-gun, Ibaraki, Japan

2-D Neutral Monte-Carlo Code

K. Shimizu (JAERI)

Neutral influences the particle and energy balance, and play an important role on sputtering impurity and the charge exchange loss of neutral beam injection. The information of neutral density profile is necessary for the analysis of H_α mesurement and charge exchange spectrum. In order to study neutral particle behaviour including the effects of asymmetric source and divertor configuration, the two dimensional neutral transport code has been developed using the Monte-Carlo techniques. The equilibrium obtained from the magnetic fitting code is used. Plasma parameter, such as density and temperature, are functions of poloidal flux function ψ and are taken from the experimental data.

The code can handle any number of hydrogen species and two type of neutral sources are modeld. Recycling of the limiter or wall, gas puffing sources and neutral backflow from divertor region are edge source. The other is volume source which is produced by recombination and beam neutral. The plasma is divided by flux surfaces and the plasma parameter are piecewise homogeneous in these zones. The sample particles are lunched at the boundary for recycling and gas puffing neutrals and from the interior of the plasma for volume sources. They are traced by considering the ionization and charge exchange processes in each zones. When the particles hits the wall, they are backscattered considring the particle and energy reflection coefficients as described in ref. (1). The surface which is prescribed by some poloidal flux function ψ_W is used as the wall at present. The algorithm uses the path length estimater method. The precise computations of time the sample particle spend in each zones are time consuming calculation. In order to save the computer time, the integration of the particle path is done with constant step size Δl, which must be less than the distance between zones ΔR. This method is very efficient and make it easy to treat varied configuration.

Source biasing, suppression of absorption and splitting with Russian roulette are used to reduce the statistical variance.

Using this code we analyzed the neutral transport in the divertor configuration (E642) in which the crearance δ_{30} was changed during discharge, where δ_{30} is the distance between the separatrix and toroidal limiter placed at 30 degree off the midplane. Intensity of H_α from divertor decreased as δ_{30} in the experiment. Figure 1 shows the 2 dimensional distribution of neutral density. We supposed that the ion recycled mainly at the 30 degree limiter. The fraction of ionization in the scrape off region is 0.21 for δ_{30}=4cm and 0.12 for 2 cm. This quantity is proportional to the particle influx into divertor , and hence H_α intensity from divertor. So the result is consistent with the experimental data.

1) Y. SEKI, Y. SHIMOMURA, K. MAKI, M. AZUMI and T. TAKIZUKA, Nucl. Fusion 20 (1980) 1213.

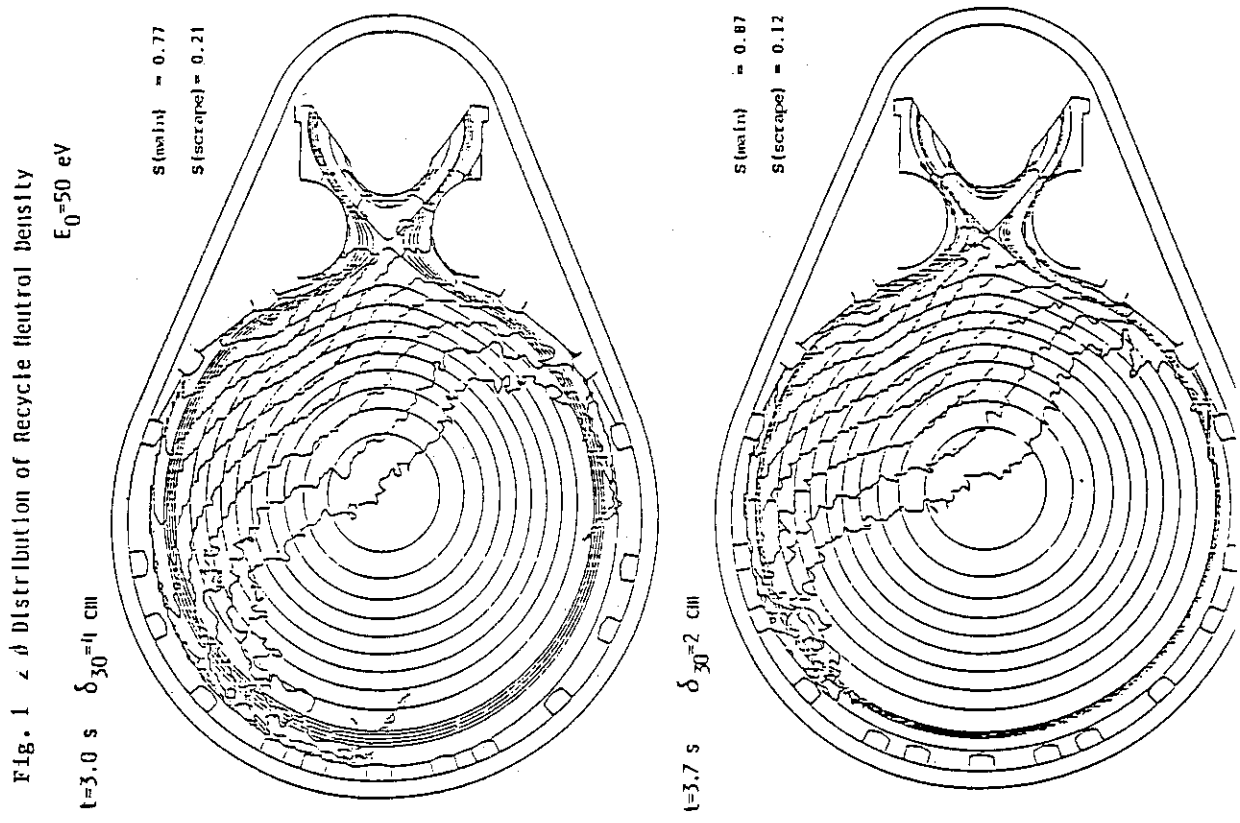

Fig. 1 ν Distribution of Recycle Neutral Density E_0=50 eV δ_{30}=1 cm δ_{30}=2 cm

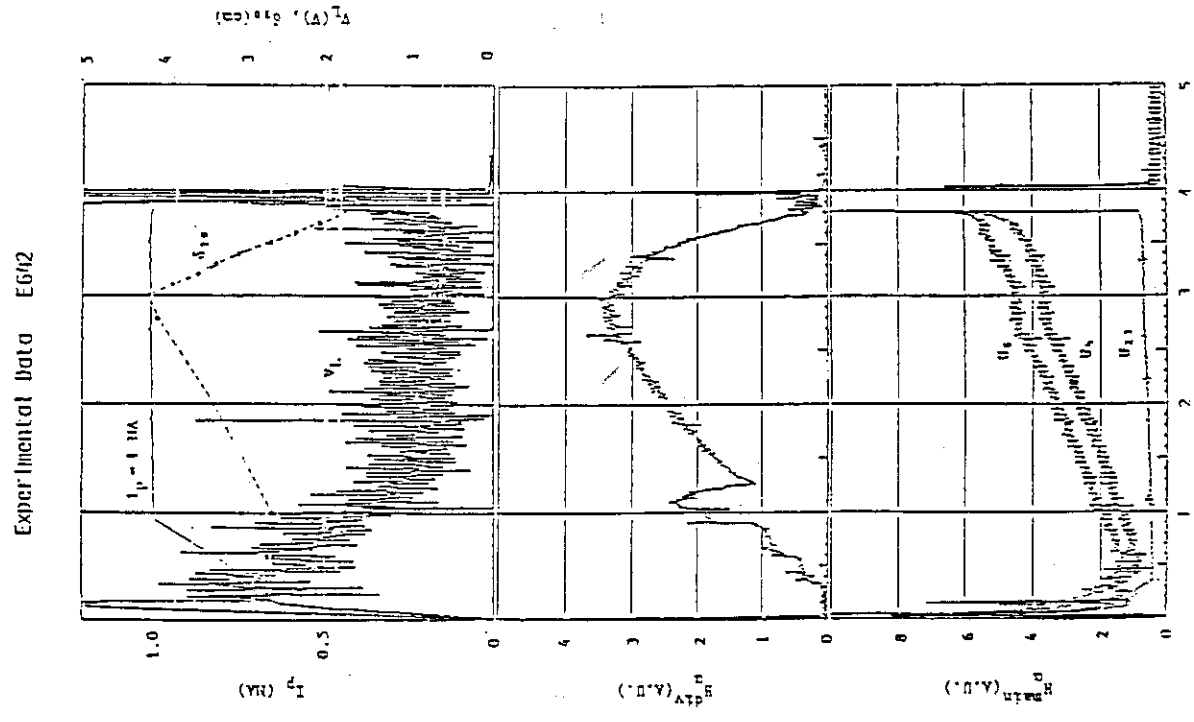

Halo Neutral

PLASMA PARAMETERS

B_T = 4.5 T

I_p = 2.7 MA

E_B = 75.0 KeV

$P_E : P_{E/2} : P_{E/3}$ = 0.6 : 0.3 : 0.1

n_{e0} = 10.0×10^{13} cm^{-3}

T_{e0} = 10.0 KeV

τ_p = 0.2 sec

E_0 = 50.0 eV

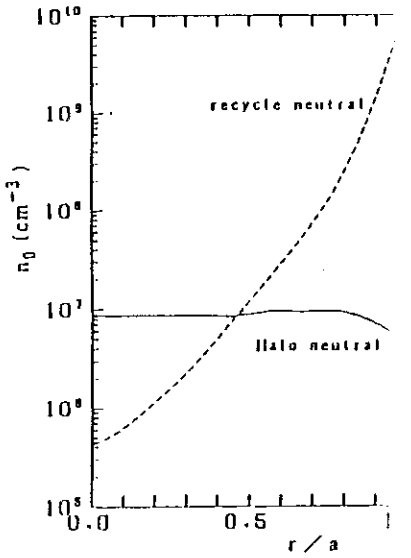

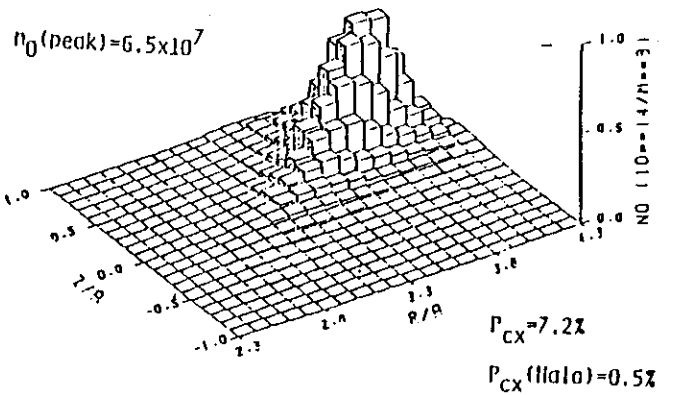

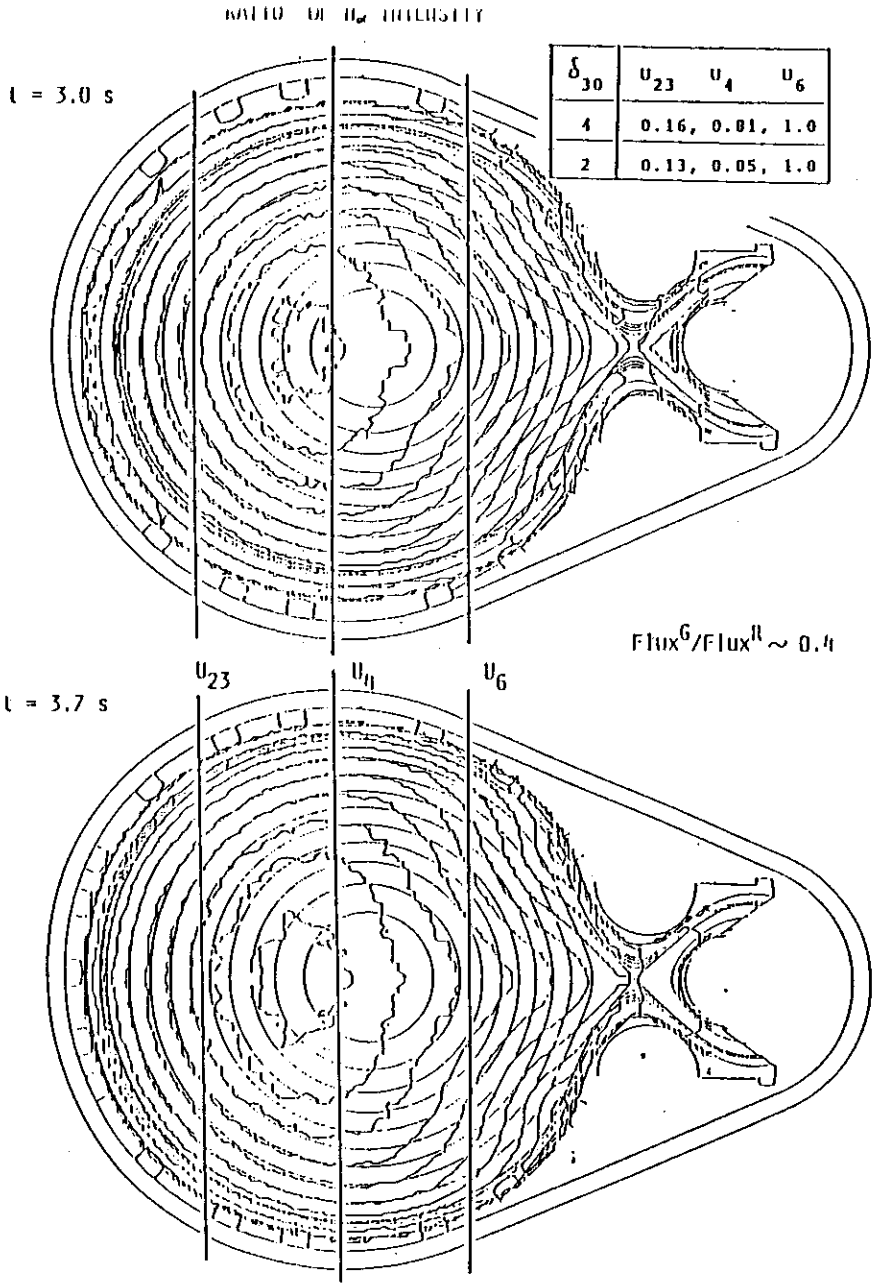

2-D NEUTRAL TRANSPORT CODE

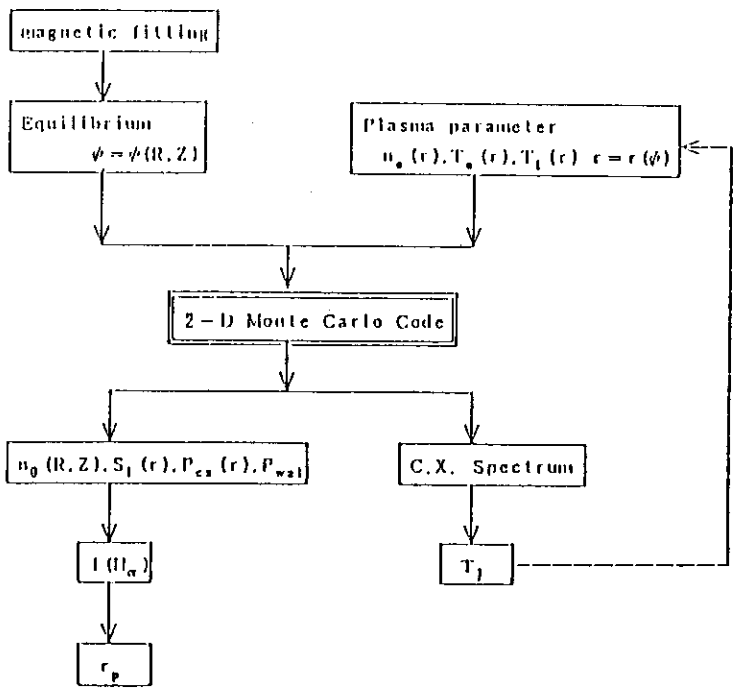

MODEL

- source

  recycle, Gass-puff, NBI

  reflection

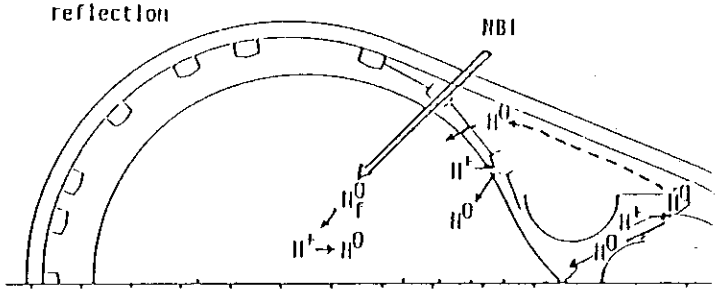

- Geometry $\psi = \psi(R,Z)$ Equilibrium
- Wall $\psi = \psi_W$ ---- real wall geometry
- Plasma Parameter

  $n_e(\vec{r}) = n(\psi)$, $T_e(\vec{r}) = T_e(\psi)$, $T_i(\vec{r}) = T_i(\psi)$
- Method

  source biasing

  survival biasing

  path integral with constand path length ($\Delta\ell$)

Comparison with AURORA code

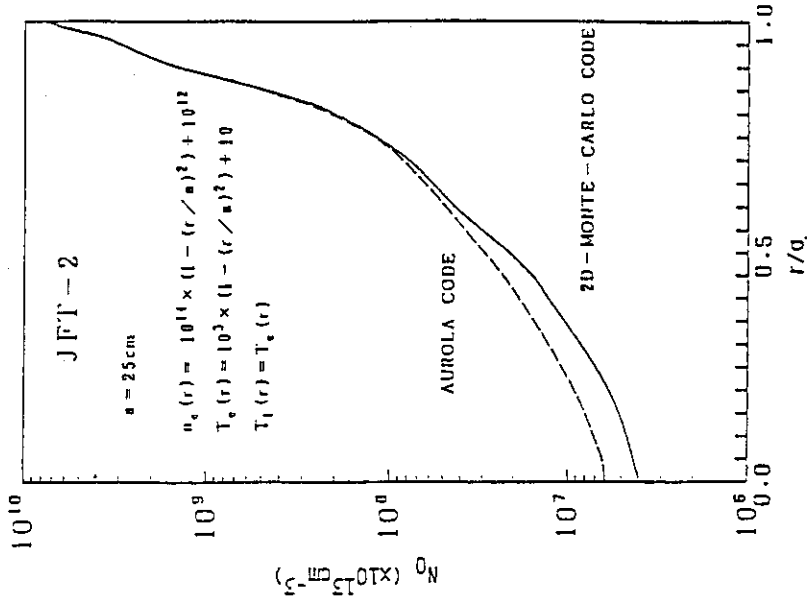

FLOW CHART

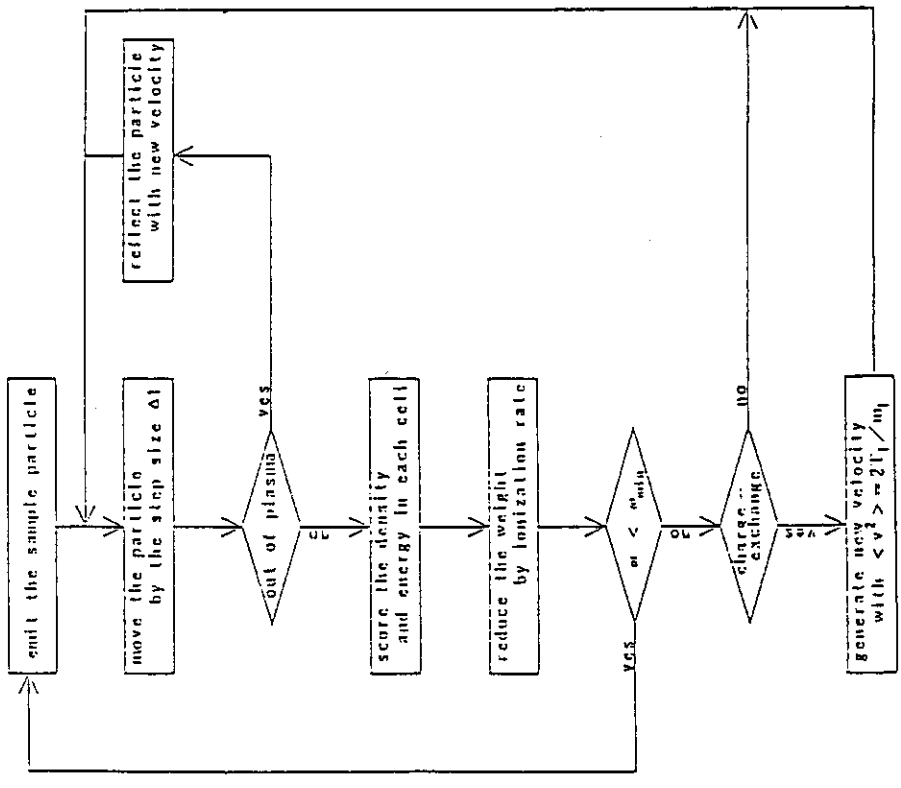

APPENDIX 4.2.2

Particle Simulation of Divertor Plasma

T. Takizuka, K. Tani and M. Azumi

Japan Atomic Energy Research Institute
Naka Energy Research Establishment
Naka-machi, Naka-gun, Ibaraki, Japan

Paper presented at U.S.-Japan Workshop on Advanced Plasma Modelling, 24 - 27 Sep. (1985)
IIP Research Report

Proceeding of U.S-Japan Workshop on Advanced
Plasma Modelling, 24 - 27 Sep. (1985),
IPP Research Report

Particle Simulation of Divertor Plasma

T. Takizuka, K. Tani, M. Azumi
Japan Atomic Energy Research Institute
Tokai, Naka, Ibaraki 319-11, Japan

Abstract Characteristics of divertor plasma are studied by using a one-dimensional electrostatic particle code with a binary collision model. Effects of recycling particles near the divertor plate are introduced. Heat flow is investigated in detail, and the estimation of ion heat conduction from the temperature gradient is found unaccurate when particles are highly recycled near the plate.

APPENDIX 4.3.1

Divertor Analysis of JT-60

H. Yoshida

Japan Atomic Energy Research Institute
Naka Fusion Research Establishment
Naka-machi, Naka-gun, Ibaraki, Japan

Paper presented at TRIRARTITE IEA meeting
Naka, Japan 21 - 22 Nov. 1986

List of Participants
Comparison Exp. DATA & ANALYSIS
(TRIPARTITE IEA MEETING)
Nov. 21-22, 1986 at Naka Fusion Research Establishment, JAERI

2.2 Divertor Analysis of JT-60

Presented by

H. YOSHIDA

Contents

Tripartite IEA Meeting

Naka, Nov.21-22,1986

Introduction

I would talk about " Divertor Analysis of JT-60 ".
Divertor function of heat removal, particle recycling control and impurity control have been successfully obtained in JT-60. In this meeting, the experimetal results of divertor discharges concernig heat removal and particle control are discussed, and compared with the simulation results. Firstly, the characteristics of divertor plasma, especially the global power balance and the radiative cooling in the divertor chamber, are presented. Secondly, the simulation model to interpret the behavior of divertor plasma is introduced. Thirdly, the characteristics of divertor plasma are compared between experimental data and simulation results. Finally, the summary and near future plan are prsented.

APPENDIX 4.3.2

Development of a Two-Dimensional Fluid Code and its Application to the Doublet III Divertor Experiment

N. Ueda*, M. Kasai*, M. Tanaka**,
M. Sugihara and S. Sengoku

Japan Atomic Energy Research Institute
Naka Fusion Research Establishment
Naka-machi, Naka-gun, Ibaraki, Japan

* Mitsubechi Atomic Power Industries, Inc.
** Century Research Center Corporation

Paper submitted to Nuclear Fusion

JAERI-memo 62-245

4. DESIGN STUDIES

4.1 DEVELOPMENT OF A TWO-DOMENSIONAL FLUID CODE AND ITS APPLICATION TO THE DOUBLET III DIVERTOR EXPERIMENT

N. UEDA, M. KASAI
Mitsubishi Atomic Power Industries, Inc.
4-1, Shibakouen 2-chome,
Minato-ku, Tokyo, Japan

M. TANAKA
Century Research Center Corporation
Chuo-ku, Tokyo, Japan

M. SUGIHARA, S. SENGOKU
Japan Atomic Energy Research Institute
Tokai, Ibaraki, Japan

ABSTRACT

A two-dimensional time dependent fluid code has been developed for transport processes in the edge plasma in a tokamak, coupled with Monte-Carlo method for neutral gas behavior. The code employs Particle In Cell method for numerical solution of fluid equations and can easily treat the free boundary of a radially diffusing plasma. Simulation of the D-III divertor experiment has been performed with this code, and it has been confirmed that the radial profiles of temperature and density in the scrapeoff and divertor regions can be simulated fairly well.

APPENDIX 4.3.3

Numerical Simulation of the FER Divertor Plasma

N. Ueda*, M. Sugihara, S. Yamamoto

F. Fujisawa and FER design team

Japan Atomic Energy Research Institute
Naka Fusion Research Establishment
Naka-machi, Naka-gun, Ibaraki, Japan

* Mitsubishi Atomic Power Industries, Inc.

Numerical Simulation of the FER divertor plasma

by N. Ueda

In the simulation of reactor size plasma, it is important to include the behavior of impurities which arise from the sputtering vaporization of the structural material by heat concentration and so on. The mathematical model of the behavior of impurity ion in charge state Z consists of the momentum conservation equation and the equation of continuity. The equation are written as follows*,

for x impurity ion

$$\rho_x\left(\frac{\partial}{\partial t} + \vec{V}_x\cdot\nabla\right)\vec{V}_x = -\nabla P_x + \vec{F}_x + \vec{R}_x + S_p^x - S_p^x - S_n^x \vec{V}_x \ ,$$

$$\vec{F}_x = q_x\vec{E} + q_x(\vec{V}_x \times \vec{B}) \ ,$$

$$\vec{E} = -\nabla P_e/en_e \ ,$$

$$\vec{R} = -\rho_x(\vec{V} - \vec{V}_x)/\tau_x - \frac{\rho_x}{m_x}\left[\alpha_x\nabla(kT_e) + \beta_x\nabla(kT_i)\right] \ ,$$

$$\alpha_x = 0.71\ Z^2 \ ,$$

$$\beta_x = -3\cdot\frac{1-\mu-5\sqrt{2}\ z^2\cdot(1.1\mu^{2.5} - 0.35\mu^{1.5})}{2.6 - 2\mu + 5.4\mu^2} \ ,$$

$$\mu = m_x/(m + m_x) \ ,$$

where S_p, S_n, $S_E^{i,e}$, $E_s^{i,e}$ and τ_x denote following meanings,

S_n : source term in mass conservation equation

S_p : momentum source term

$S_E^{i,e}$: energy source $\pm\begin{cases} Q^{ei} - Q_{cx} \\ Q^{ei} + Q_{rad} \end{cases}$

$E_s^{i,e}$: $E_s = \frac{3}{2}\frac{kT}{m} + \frac{1}{2}\vec{V}\cdot\vec{V}$

τ_x : spitzer slowing down time

Temperature of impurity ion is assumed to be equal to that of fuel ion without solving the energy conservation equation.

The applicability of the code in relation to the combination of the ion species is summarized in Fig. 1. The code can treat four cases ((a) ~ (d)) shown in the figure.

In Fig. 2, calculational mesh for FER reactor is shown. In the

* use Neuhauser's impurity flow equations

figure, the segments $\overline{AB}$, $\overline{BC}$, $\overline{CD}$, $\overline{DE}$, $\overline{EF}$ and $\overline{FG}$ correspond to the divertor plate and the sheath criterion is assumed at the place.

Calculational conditions used are as follows,

$$Q_T = Q_e + Q_i = 60 \text{ MW} \quad ,$$

$$\Gamma_p = 1 \times 10^{22} s^{-1},\ 3 \times 10^{22}\ s^{-1} \quad ,$$

$$\Gamma_{He}^{2+} = \Gamma_p \times 0.05 \quad ,$$

respectively.

In Fig. 3, T_e profiles for particle fluxes of 1×10^{22} s^{-1} and 3×10^{22} s^{-1} are shown. The maximum temperature in the scrapeoff layer is approximately 210 eV at the j=8 flux tube. The e-folding length of T_e is nearly cm T_e decreases to approximately 20 eV at the divertor plate.

Density profile is shown in Fig. 4. Near the plate, $n_e \simeq 2 \times 10^{14}$ cm^{-3} for $\Gamma_p = 1 \times 10^{22}$ s^{-1} and $n_e \simeq 6 \times 10^{14}$ cm^{-3} for $\Gamma_p = 3 \times 10^{22}$ s^{-1} respectively. So we can see very high density build up near the divertor plate. The density around the boundary of the core plasma is roughly 7×10^{12} cm^{-3} for $\Gamma_p = 1 \times 10^{22}$ s^{-1} and 1×10^{14} cm^{-3} for $\Gamma_p = 3 \times 10^{22}$ s^{-1}.

In Fig. 5, flow velocity of the fuel ion in the poloidal plane shown. The flow in the j=9 flux tube which locates nearest to the boundary of the core plasma in the inboard side scrapeoff layer disrects to the upper stream.

In Fig.6, flow velocity in the poloidal plane for H_e^{1+} is shown. H_e^{1+} of the j=9 flux tube in the inboard side scrapeoff layer also go upstream. The spatial distribution of H_e^{1+} is comparatively uniform in the poloidal direction (i.e. not localized at the divertor region) such as fuel ions.

In Fig. 7 and Fig. 8, time evolution of the total mass and energy contained in the system is shown. From this figure we can see that after the 1200 step, mass and energy in the system do not change so distinctly. These results indicate the steady state is achieved after the step.

In Fig. 9, we show the energy flow into the divertor plate. The peak value at the outside and inside divertor plate is 310 W cm^{-2} and 220 W cm^{-2} respectively. As leaving from the flux tube j=9 which locates nearest to the separatrix to j=5 flux tube, Q_e^d and Q_i^d decreases rapidly

and monotonically in the outside divertor. On the other hand, the second and third peaks appears in the inside divertor because of complicated shapes of the plate. In the estimation of the deposited energy flux, it is to be noticed that ionization energy loss should count in the sum. In this case of $\Gamma_p = 1 \times 10^{22}$ s^{-1} and $Q_T = 60$ MW, the ionization energy loss is approximately 0.89 MW in the unit toroidal length.

Particle flux to the divertor plate Γ^d is shown in Fig. 10. The positions of the peak values also exist at the j=9 flux tube.

4. ACKNOWLEDGEMENTS

The authors are very grateful to Drs. T. Takizuka, K. Shimizu and members of FER plasma design team of JAERI for their fruitful discussions.

It is a pleasure to acknowedge the support of Drs. S. Tamura (JAERI), N. Asami (Mitsubishi Heavy Industries, Ltd.), T. Miura (Century Research Center Corporation) and M. Nishikawa (Mitsubishi) Atomic Power Industries, Inc.)

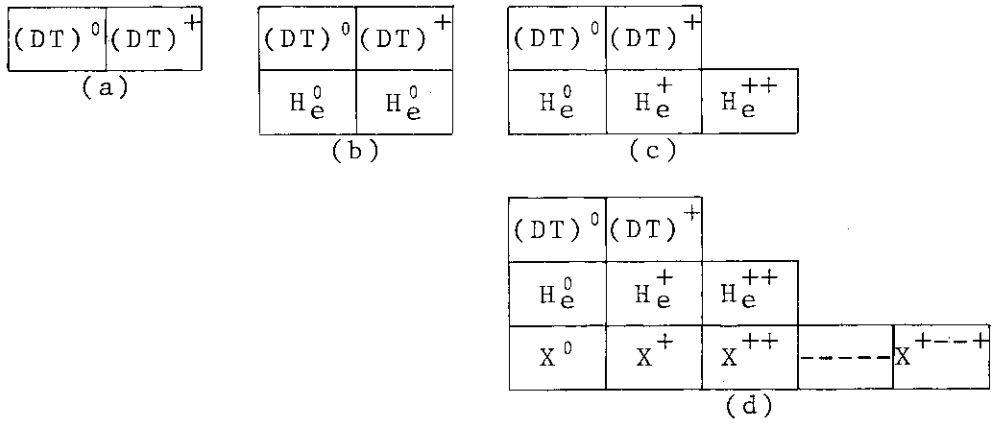

Fig. 1 Combination of the paticle species included in the code. X denotes the impurity ion.

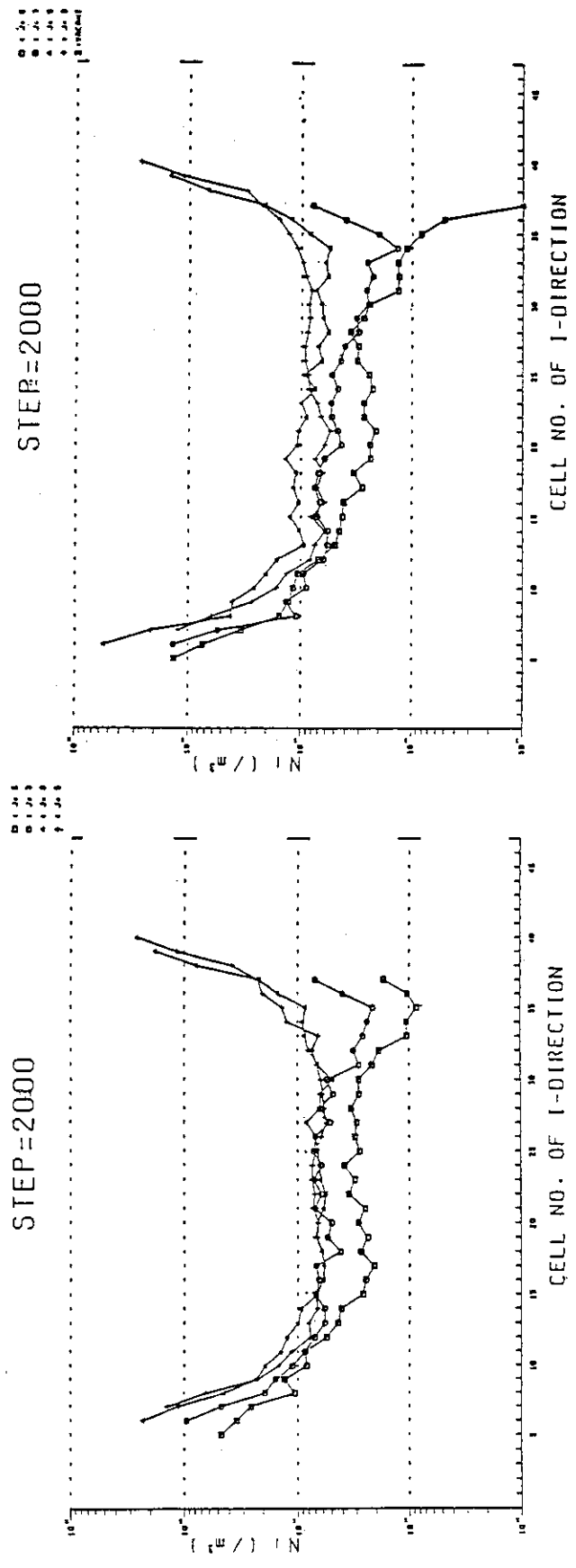

Fig.4 Density profiles in the poloidal direction for particle flux Γ_p of $1.\times10^{22}s^{-1}$ and $3.\times10^{22}s^{-1}$.

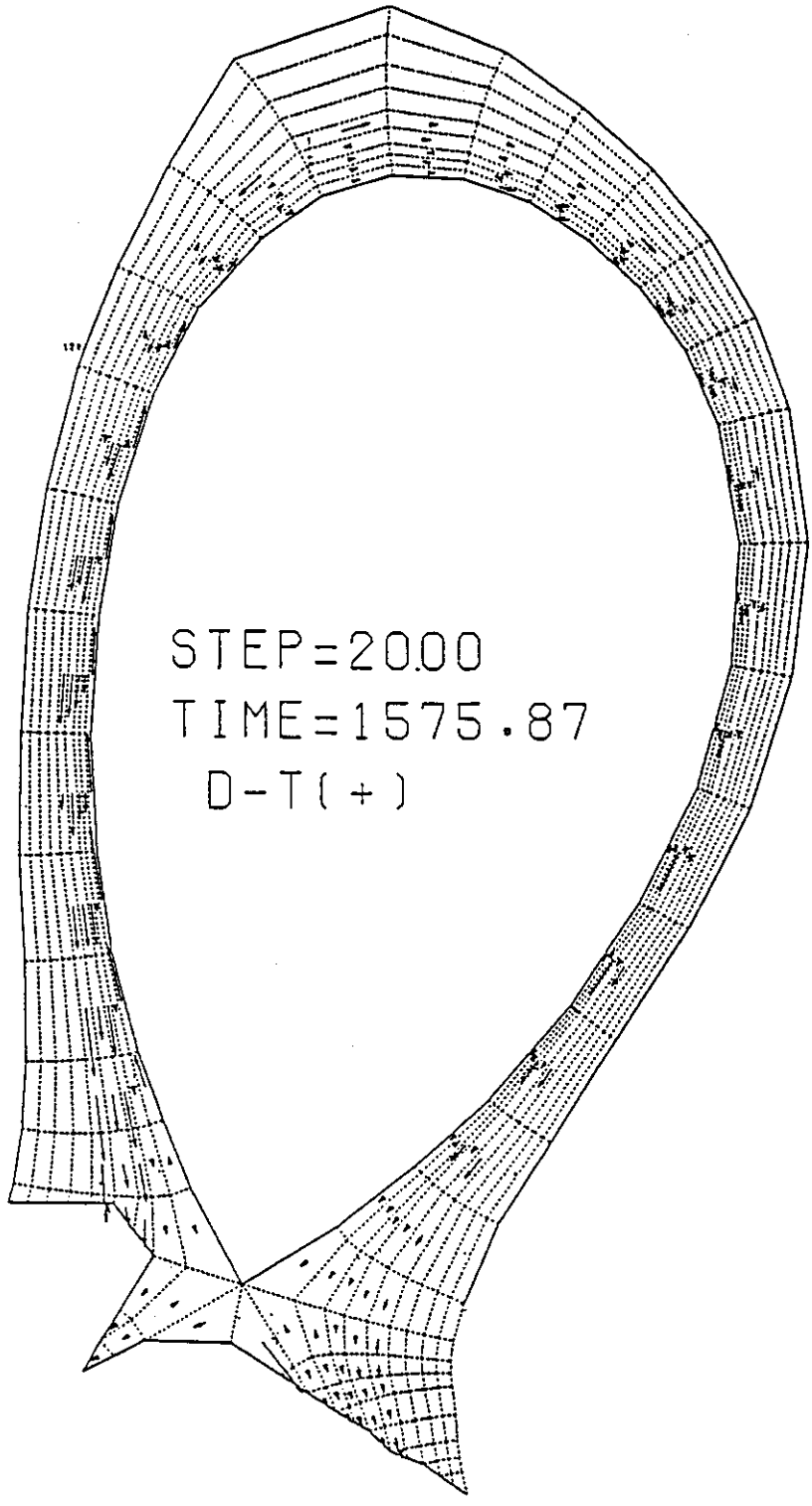

Fig.5-(a) Flow velosity of the fuel ion for Γ_p = 1.x10^{22}s^{-1}.

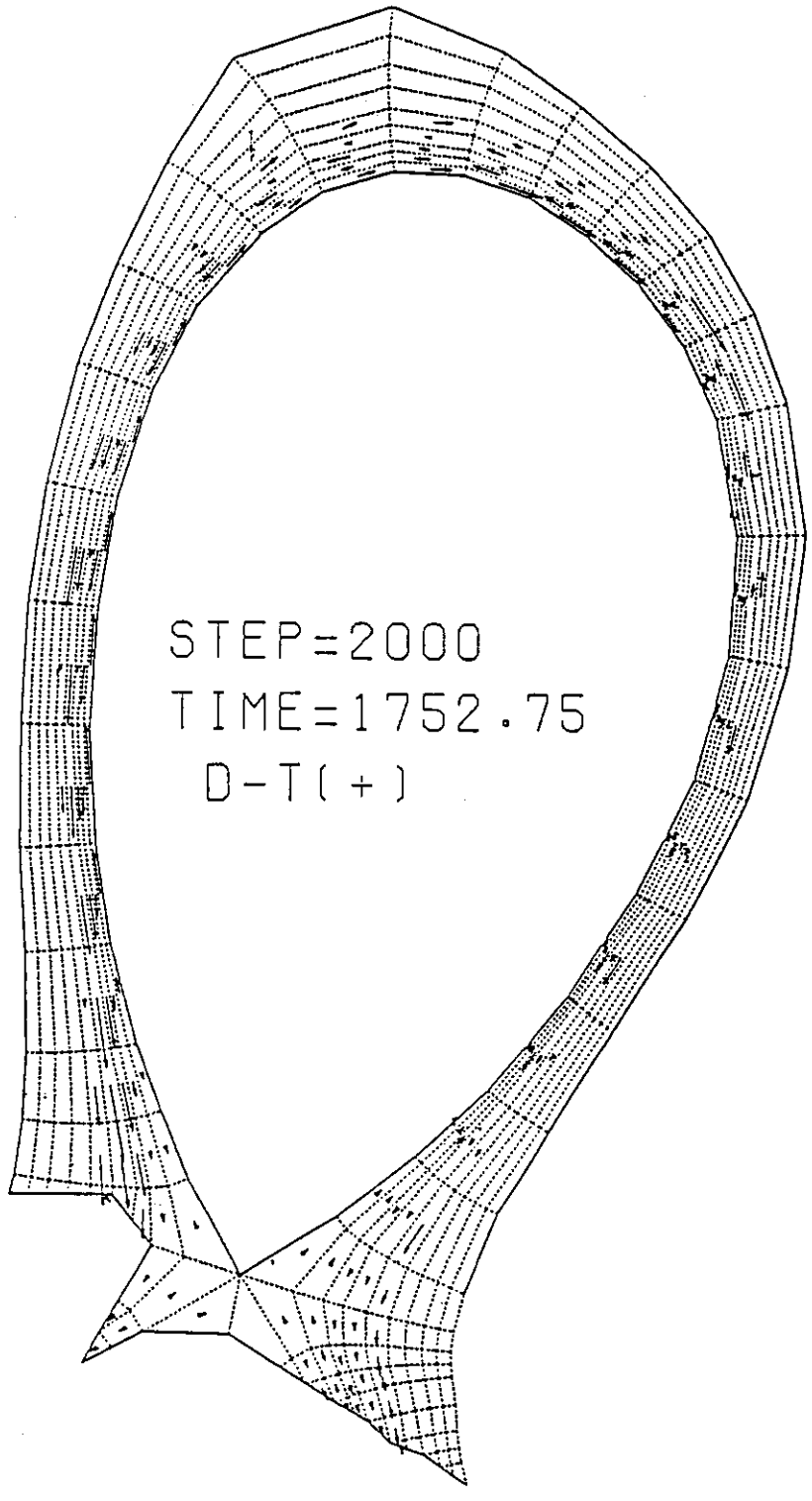

Fig.5-(b) Flow velosity of the fuel ion for $\Gamma_p = 3.x10^{22}s^{-1}$.

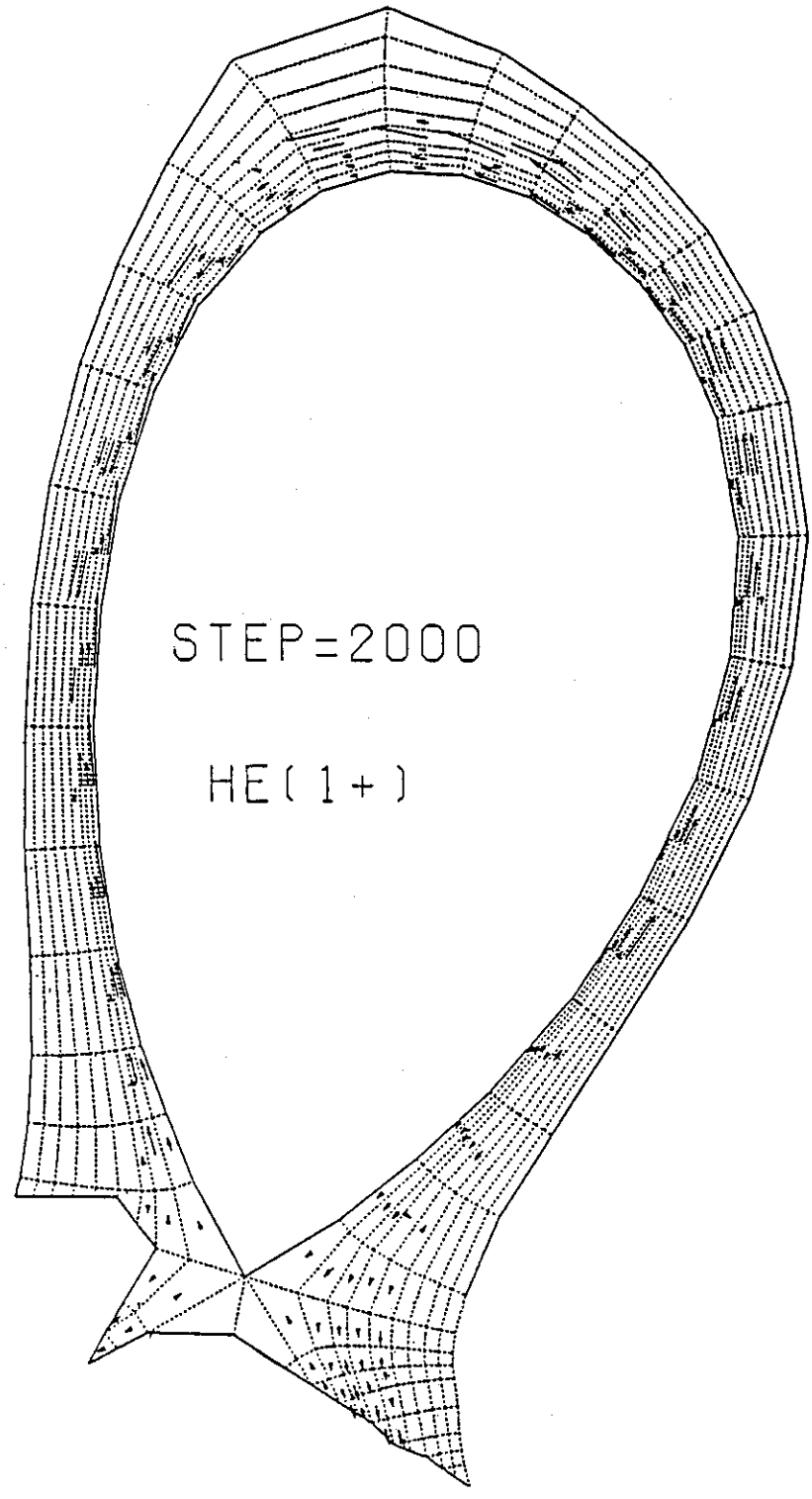

Fig.6-(a) Flow velosity of He^{1+} for $\Gamma_p = 1.x10^{22}s^{-1}$.

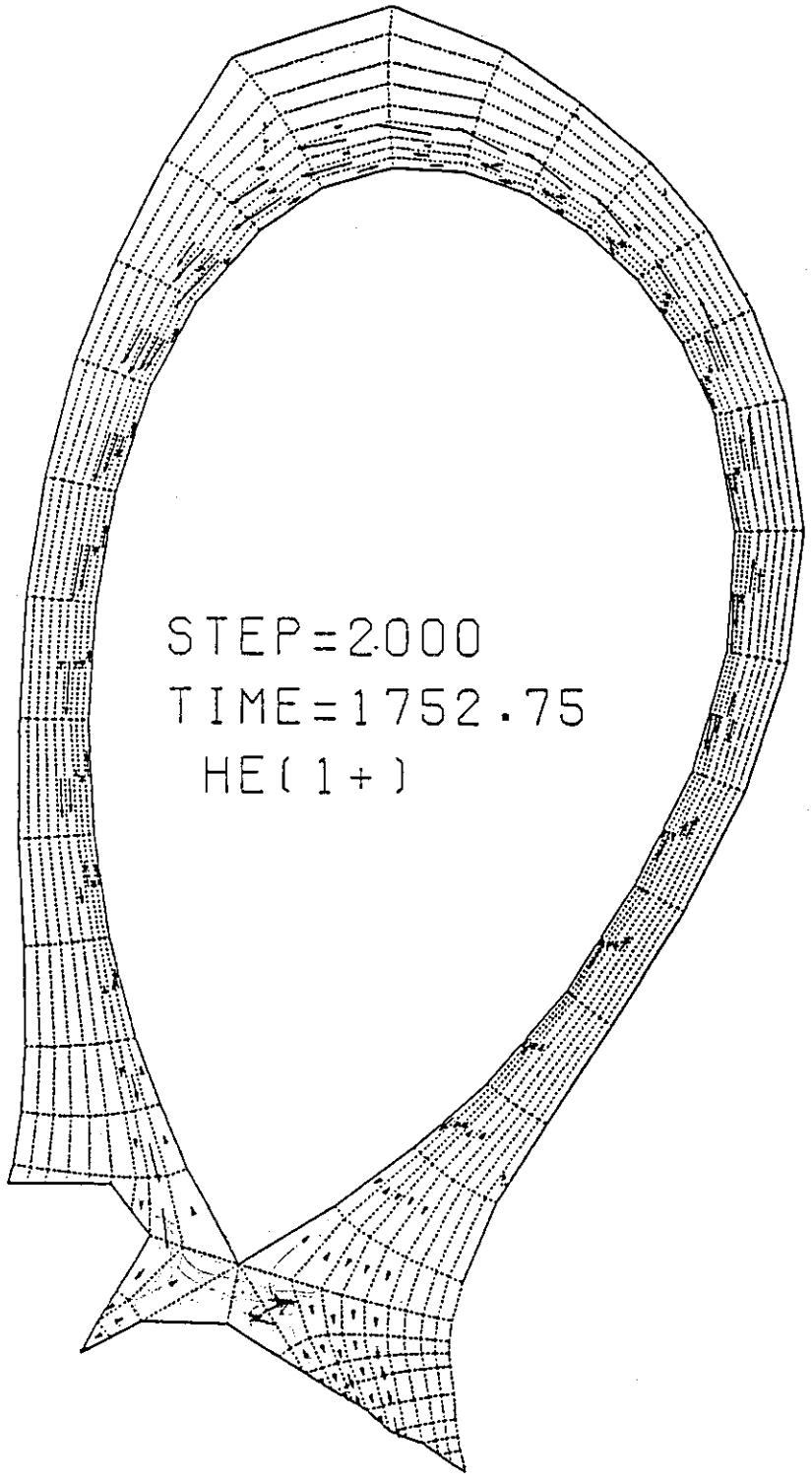

Fig.6-(b) Flow velosity of He^{1+} for $\Gamma_p = 3.x10^{22}s^{-1}$.

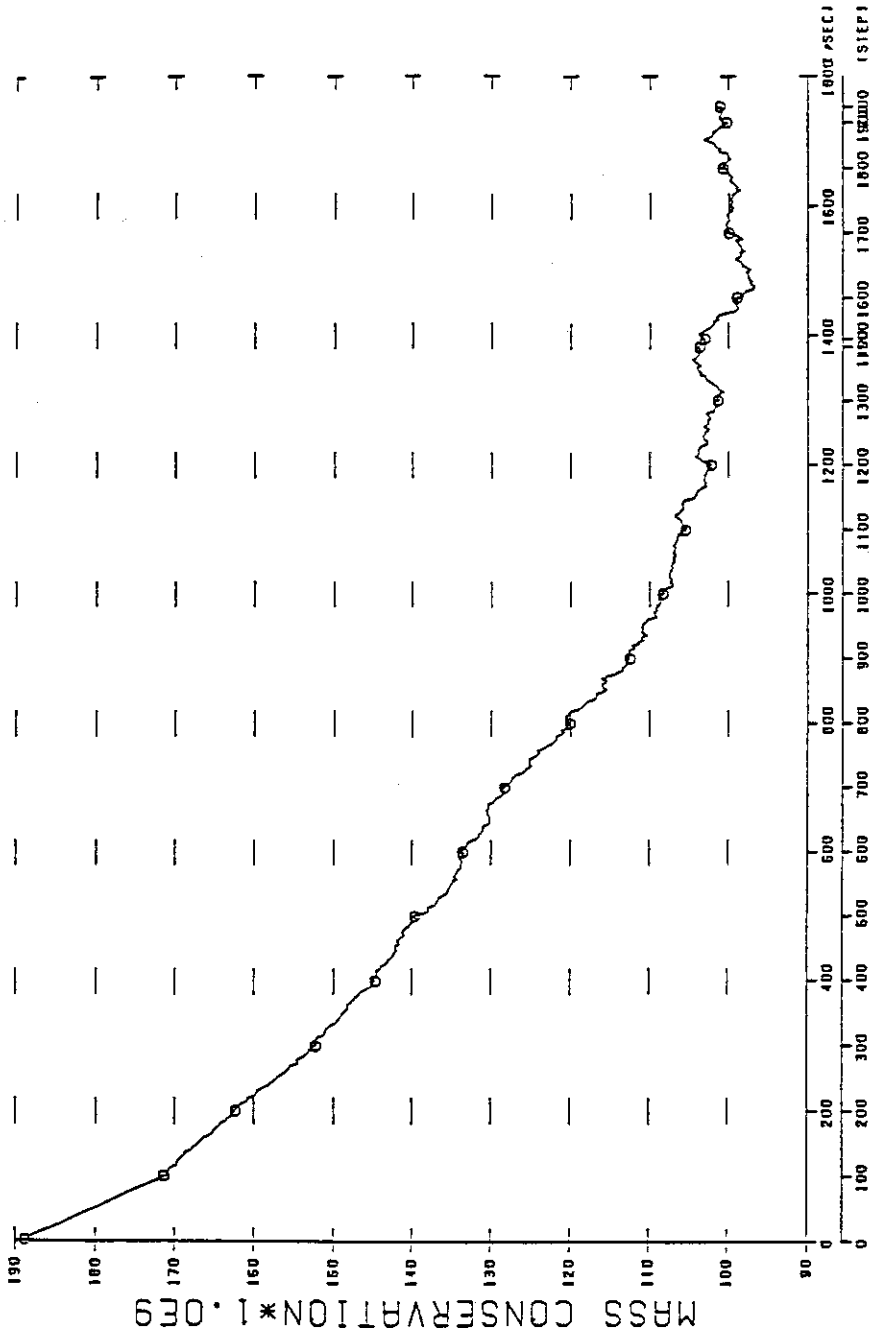

Fig.7 Time evolution of the total mass in the system

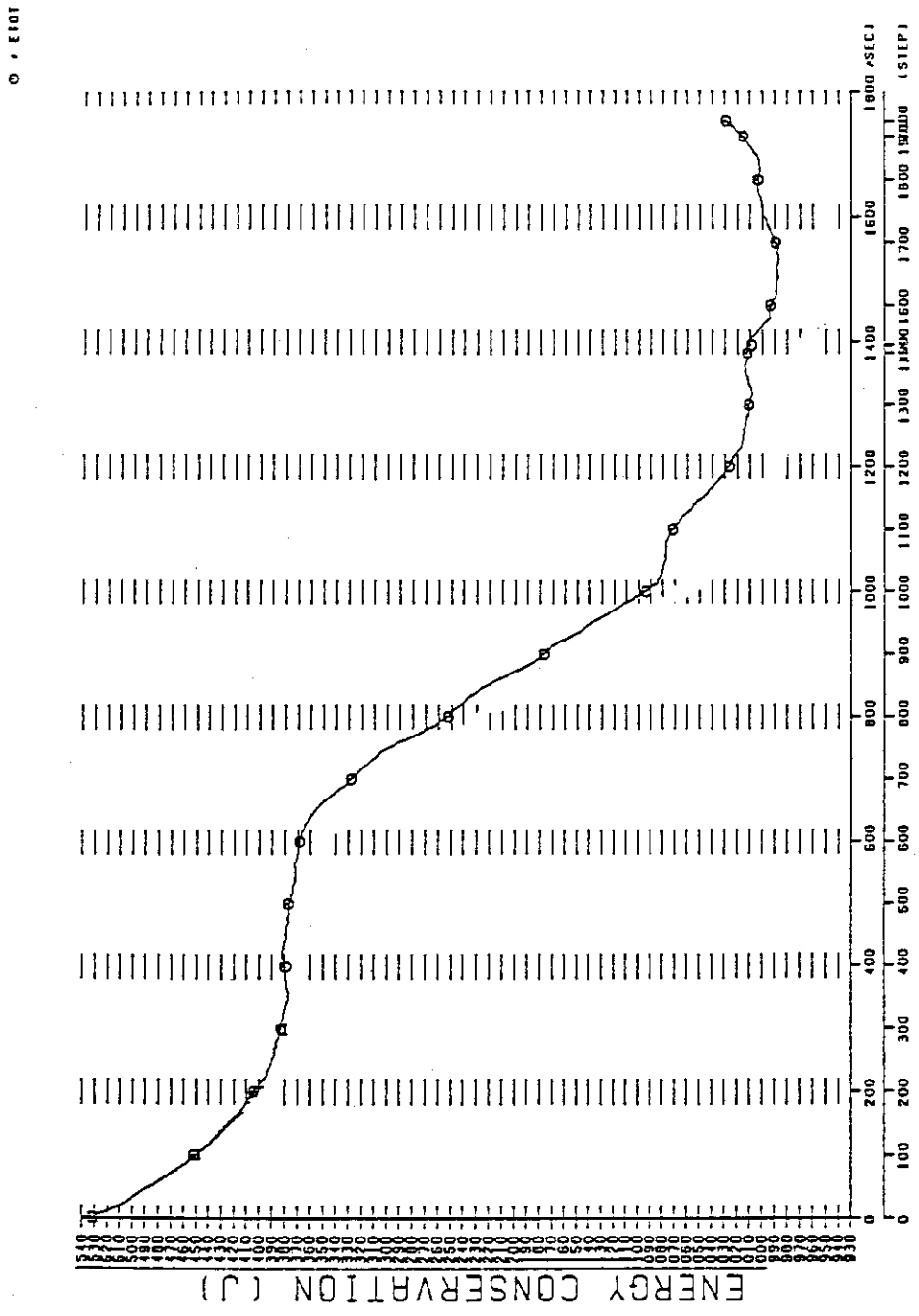

Fig.8 Time evolution of the total energy in the system.

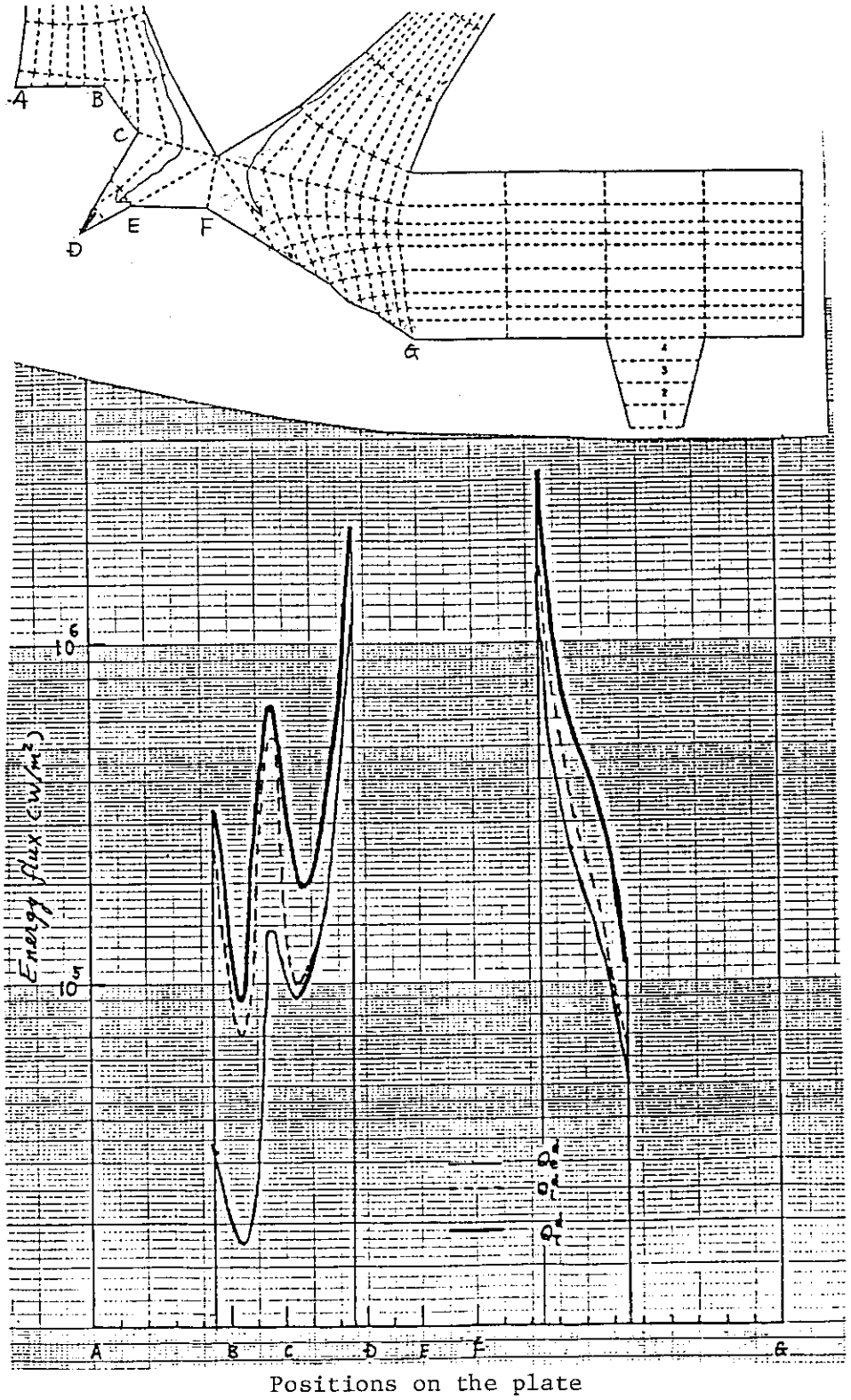

Fig.9 Distribution of deposited energy flux Q^d on the divertir plate ($\Gamma_p = 1.x10^{22} s^{-s}$).

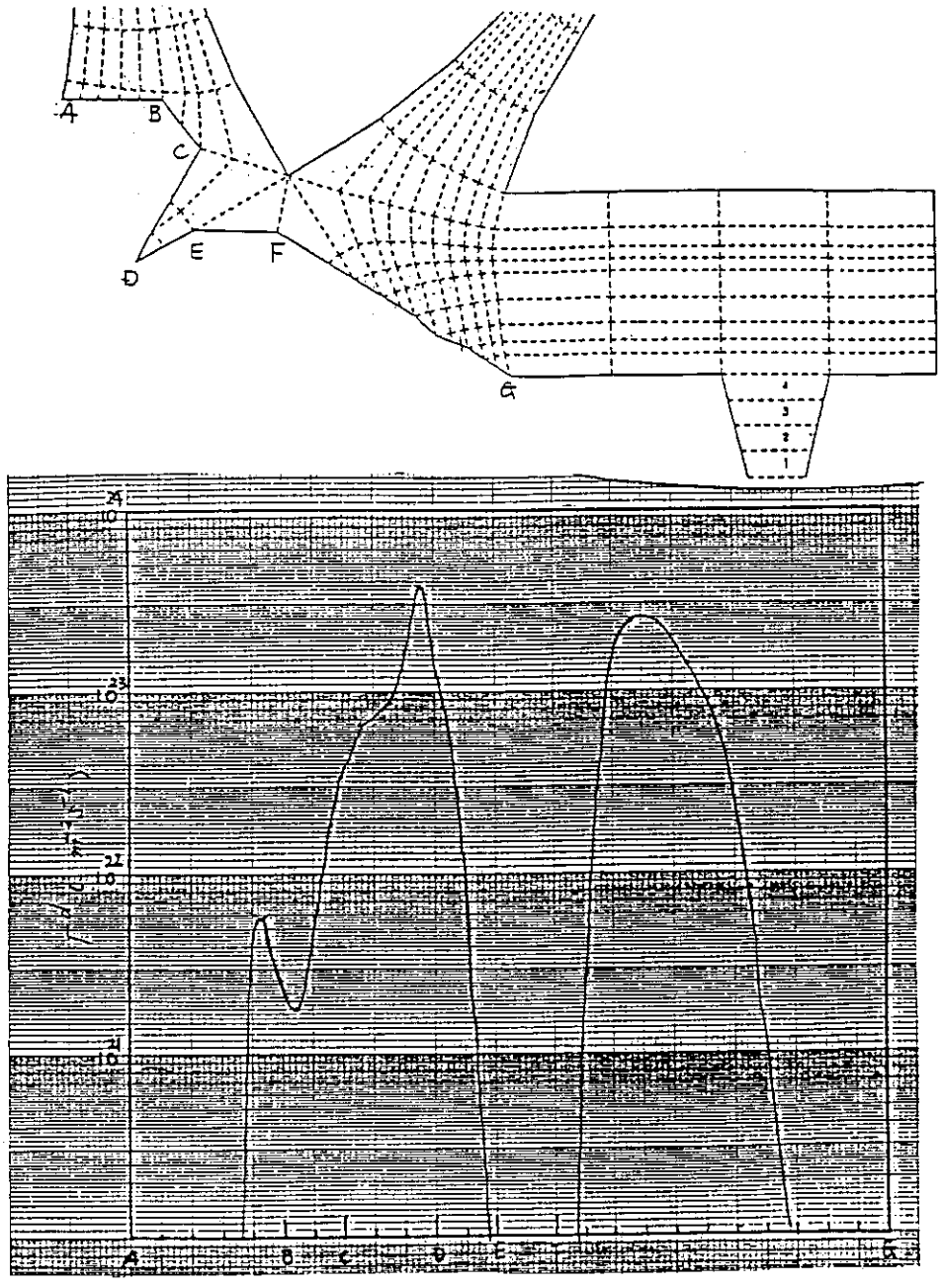

Fig.10 Distribution of deposited particle flux Γ^d on the divertor plate ($\Gamma_p = 1.\times10^{22} s^{-1}$).

APPENDIX 4.4.2

Cold and Dense Divertor Plasma in Phase of Current Drive

S. Hitoki*, M. Sugihara and S. Yamamoto

Japan Atomic Energy Research Institute
Naka Fusion Research Establishment
Naka-machi, Naka-gun, Ibaraki, Japan

* Present address: Mitsubishi Electric Corp.
Marunouchi, Chiyoda-ku, Tokyo, Japan

Paper submitted to Journal of Japanese Applied Physics

Submitted to Journal of Japanese Applied Physics.

4.3 Cold and Dense Divertor Plasma in Phase of Current Drive

Formation of Cold and Dense Divertor Plasma during Phases of Non-Inductive Current Ramp-up and Recharging in Tokamak Fusion Reactor

Shigehisa HIROKI*, Masayoshi SUGIHARA, and Shin YAMAMOTO

Naka Fusion Research Establishment,

Japan aAtomic Energy Research Institute

Naka-machi, Naka-gun, Ibaraki-ken

Abstract

Possibility of the formation of cold and dense divertor plasma during non-inductive current ramp-up and recharging phases in Tokamaks is investigated. Temperature of 30-50eV is obtained near the neutralizer plate for a reasonable absorbed power (20MW in FER) in the phase of current drive by LHRF wave (lower hybrid wave). Above temperature is obtained under a restriction on the value of efficiency of current drive determined by the experiments of JT-60. For a higher absorbed power of 30MW, the temperature near the plate can be reduced to about 15eV. According to the experiments done in JT-60 and others, the driving efficiency might go over the restricted value

---

* On leave from Mitsubishi Electric Corp., Marunouchi, Chiyoda-ku, Tokyo 100.

$\eta_{20}=R(m)I_{rf}(A)n_e(10^{20}m^{-3})/P_{rf}(W)=0.3$ by increasing the average main plasma temperature. For $\eta_{20}>0.3$, the temperature near the plate is reduced below 10eV in the phase of current drive. Related parameters are also determined for obtaining the cold and dense divertor plasma. Current drive by NBI (neutral beam injection) is also investigated.